

University of Southern Queensland

Faculty of Health, Engineering and Sciences

Simulation of Carbon Dioxide Dispersion Using
Computational Fluid Dynamics

A dissertation submitted by

Jamal Hallajian

in fulfillment of the requirements of

ENP4111 Professional Engineer Research Project

towards the degree of

Bachelor of Engineering (Honours) (Mechanical)

Submitted: November, 2024

This page intentionally left blank

University of Southern Queensland

Faculty of Health, Engineering and Sciences

ENP4111 Dissertation Project

Limitations of Use

The Council of the University of Southern Queensland, its Faculty of Health, Engineering and Science, and the staff of the University of Southern Queensland, do not accept any responsibility for the truth, accuracy or completeness of material contained within or associated with this dissertation.

Persons using all or any part of this material do so at their own risk, and not at the risk of the Council of the University of Southern Queensland, its Faculty of Health, Engineering and Science or the staff of the University of Southern Queensland.


This dissertation reports an educational exercise and has no purpose or validity beyond this exercise. The sole purpose of this dissertation project is to contribute to the overall education within the student's chosen degree program. This document, the associated hardware, software, drawings, and other material set out in the associated appendices should not be used for any other purpose: if they are so used, it is entirely at the risk of the user.

CERTIFICATION

I certify that the ideas, designs and experimental work, results, analyses and conclusions set out in this dissertation are entirely my own effort, except where otherwise indicated and acknowledged.

I further certify that the work is original and has not been previously submitted for assessment in any other course or institution, except where specifically stated.

Student Name: Jamal Hallajian

Student number: 

Signature



Date

04/11/2024

ABSTRACT

As the global community direct its focus on mitigating climate change, Carbon Dioxide emissions due to their contribution to global warming have gained significant attention. To address this issue, one of the main strategies that is in place is Carbon Capture, Utilisation, and Storage (CCUS). A critical part of this process is transportation of CO₂ for which pipelines are used owing to their efficiency, vast coverage, capacity and reliability. Although the hazards associated with CO₂ specially when it is subjected to changes in operating conditions needs extensive investigations into how it behaves and the risks associated with that. This research intends to thoroughly study and analyse the impact of these operating conditions on the dispersion behaviour of CO₂ in the event of a pipeline leak or rupture. Using software simulations with the focus on Computational Fluid Dynamics (CFD) accompanied by real-life incident or existing experimental data this research aims to determine hazardous distances for a range of operating conditions. The expected outcome is a set of developed safety guidelines and operational recommendations. This is to ensure the well-being of communities that live near CO₂ pipelines and guiding the infrastructure towards sustainability and net-zero carbon emissions.

ACKNOWLEDGEMENTS

I would like to express my appreciation to my supervisors, Dr. Khalid Saleh, and Dr. Guillaume Michal, for their support, mentorship, and valuable guidance throughout the course of my research. Their insights and encouragement were instrumental in shaping the direction of my research project. I am particularly grateful for their patience in helping me with the challenges I encountered.

I would also like to extend my appreciation to Dr. Xiong Liu for sharing his expertise in CO₂ dispersion. His prompt and patient responses to my questions were invaluable, particularly as I delved into the complexities of gas dispersion modelling of CO₂ jets and release scenarios.

Finally, I would like to extend my gratitude to Richard Young for his support in helping me access and learn USQ's HPC resource for the simulation work. His patience and assistance in developing script files has been deeply appreciated.

TABLE OF CONTENTS

CHAPTER	PAGE
ABSTRACT	5
ACKNOWLEDGEMENTS	6
TABLE OF CONTENTS	7
LIST OF TABLES	11
LIST OF FIGURES	12
NOMENCLATURE	15
GLOSSARY	16
CHAPTER 1: INTRODUCTION.....	17
1.1 Background / Justification:	17
1.2 Aims, Objectives and Research Question/s:	18
1.2.1 Specific Objectives:	19
1.2.2 Expected Outcomes:	19
1.3 Outline of suggested research methodology:.....	19
1.3.1 Experiments and studies to be conducted.....	19
1.3.2 How data will be analysed.....	20
1.3.3 How to interpret the analysis	21
1.3.4 Expected outcomes:	21
1.3.5 Research contribution:	22
CHAPTER 2: BACKGROUND AND LITERATURE REVIEW	23

2.1	OVERVIEW OF Equation of states (EOS)	23
2.1.1	Ideal Gas Equation of State (EOS)	23
2.1.2	Peng Robinson (PR) Equation of State (EOS)	24
2.1.3	GERGE-2008 Equation of State (EOS)	25
2.1.4	Comparison of equation of states	27
2.2	Characteristics of Pure CO ₂ and CO ₂ Mixtures	29
2.3	CO ₂ Phases	30
2.4	CO ₂ Decompression	32
2.5	Decompression Models	39
2.6	CO ₂ Phase Change During Decompression	43
2.7	Computational Flow Dynamics (CFD) Dispersion Models	45
2.8	Summary	46
CHAPTER 3: METHODOLOGY		48
3.1	Two-dimensional (2D) simulation of CO ₂ jet using peng-robinson (PR) Equation of state (EOS)	48
3.1.1	Model Assumptions	50
3.1.2	Creating the 2D geometry	50
3.1.3	Boundary Conditions	53
3.1.4	Mesh Details	56
3.1.5	Solver Type and Solution settings	57
3.1.6	Equation of State implementation	63

3.1.7	Miscellaneous Settings	65
3.2	CO ₂ dispersion analysis in a complex environment.....	70
3.2.1	Model Assumptions.....	70
3.2.2	Purpose and Functionality of the Domain	71
3.2.3	Boundary Conditions for the 3D Simulation.....	72
3.2.4	Mesh Details	81
3.2.5	Solver Type and Solution settings.....	82
3.2.6	Equation of State implementation	86
3.2.7	Miscellaneous Settings	88
CHAPTER 4: RESULT AND DISCUSSION		92
4.1	Two-dimensional (2D) simulation of CO ₂ jet using peng-robinson EOS	92
4.1.1.	Velocity Profile Along the Axis	92
4.1.2.	Temperature Distribution Around Nozzle Outlet.....	93
4.1.3.	Pressure Distribution Around Nozzle Outlet.....	94
4.1.4.	Velocity Distribution Around Nozzle Outlet and Mach Disk	96
4.1.5.	Mach Number	98
4.1.6.	Distribution of CO ₂ in the domain.....	100
4.2	CO ₂ dispersion analysis in a complex environment.....	102
4.2.1	CO ₂ Concentration Over Time at 10 m ³ /h	102
4.2.2	CO ₂ Concentration Over Time at 12 m ³ /h	105
CHAPTER 5: CONCLUSIONS AND FUTURE WORK		110

5.1	simulation of CO ₂ jet using peng-robinson EOS	110
5.2	CO ₂ dispersion analysis in a complex environment.....	113
REFERENCES		116

LIST OF TABLES

Table 1 –Boundary conditions.....	81
-----------------------------------	----

LIST OF FIGURES

Figure 1 – Illustration of the 210 Possible Binary Combinations resulting from the 21 Components of Natural Gas included in the GERG-2008 equation of state (Kunz & Wagner 2012).....	26
Figure 2 – phase diagram of CO ₂ and its various phases across a range of pressures and temperatures.....	32
Figure 3 – ductile fracture and decompression waves (Botros et al. 2004).....	33
Figure 4 – diagram of the BCM model (Liu et al. 2018).....	34
Figure 5 – saturated line of pure CO ₂ and phase envelopes of CO ₂ mixtures (Liu et al. 2018)	36
Figure 6 – schematic of the pipeline loop and the overall experiment setup (Ahmad et al. 2015).....	37
Figure 7 - CO ₂ PipeHaz project, a high-velocity CO ₂ jet resulting from a complete rupture release test (Woolley, Fairweather, Wareing, Falle, et al. 2014).	38
Figure 8 – CO ₂ PIPETRANS joint industry project, test assembly (Guo et al. 2021)	39
Figure 9 - gas decompression behavior for the assessment of ductile fracture propagation (Botros et al. 2004).	41
Figure 10 – average speed of decompression wave, PR EOS, SW EOS and Experimental data (Flechas et al. 2020).....	42
Figure 11 – Decompression wave speed from experiment vs modelling data (Botros et al. 2007).....	43
Figure 12- Various leak cases and their pressure-enthalpy paths (Hill et al. 2011).	44
Figure 13 – Comparison of velocity profiles between CFD simulation and experimental data.	52

Figure 14 – Details of the 2D computational domain.	53
Figure 15 – Meshing configuration around the nozzle outlet.....	53
Figure 16 - Computational domain setup for the CO ₂ jet simulation.....	54
Figure 17 – ANSYS Fluent model settings for inlet boundary condition.	55
Figure 18 – ANSYS Fluent model settings for Wall boundary condition.	56
Figure 19 – Meshing around the inlet and nozzle.	57
Figure 20 – ANSYS Fluent Solution Methods settings.....	60
Figure 21 - ANSYS Fluent Viscous Model settings for k-epsilon.....	63
Figure 22 – Properties of CO ₂ in ANSYS Fluent.....	64
Figure 23 - ANSYS Fluent Residual Monitors.	65
Figure 24 – Initialization settings in ANSYS Fluent.....	66
Figure 25 - ANSYS Fluent, patching the inlet conditions.....	67
Figure 26 – ANSYS Fluent, run calculation settings.	68
Figure 27 –Convergence behavior of various flow variables during the simulation.	69
Figure 28 - Computational domain for CO ₂ dispersion simulation.....	72
Figure 29 - Model settings for CO ₂ inlet boundary condition.	75
Figure 30 – UDF script to define a power-law velocity profile for wind.....	77
Figure 31 - Model settings for Air inlet boundary condition.	78
Figure 32 - Model settings for Wall boundary condition.	79
Figure 33 - Model settings for outlet boundary condition.....	80
Figure 34 – mesh details for the 3D dispersion model.....	82
Figure 35 – ANSYS Fluent Solution Methods settings.....	84
Figure 36 - Viscous Model properties for k-omega.	86
Figure 37 – properties of CO ₂ in Ansys Fluent	87
Figure 38 - ANSYS Fluent Residual Monitors.	88

Figure 39 – Initialization settings in ANSYS Fluent.....	89
Figure 40 - ANSYS Fluent, patching the inlet conditions.....	90
Figure 41 – ANSYS Fluent, run calculation settings.	91
Figure 42 – Prediction of velocity along the axis of CO ₂ jet.....	93
Figure 43 - Temperature contour plot of CO ₂ jet flow.	94
Figure 44 - Pressure contour plot of CO ₂ jet	96
Figure 45 - Velocity contour plot of the CO ₂ jet flow at outlet and downstream of nozzle.	98
Figure 46 - Mach number contour plot.....	99
Figure 47- shadowgraph image alongside the simulated velocity.....	100
Figure 48 – CO ₂ mass fraction distribution plot.....	101
Figure 49 – CO ₂ concentration over time at the given coordinates and 12m ³ /h flowrate.	103
Figure 50 - Contour plot showing the dispersion of CO ₂ mass fraction at 10 m ³ /h flowrate, with emphasis on 1% concentration level.	104
Figure 51 - CO ₂ concentration over time at the given coordinates and 12m ³ /h flowrate..	106
Figure 52 - Contour plot showing the dispersion of CO ₂ mass fraction at 12 m ³ /h flowrate, with emphasis on 1% concentration level.	107
Figure 53 - Iso-surface visualization of CO ₂ showing the release point, CO ₂ envelope, consequence distance, and wind direction.....	109

NOMENCLATURE

CO₂: Carbon dioxide

ppm: Parts per million

CCS: Carbon capture and storage

NGCC: Natural gas combined cycle

CFD: Computational fluid dynamics

EOS: Equation of State

PR EOS: Peng–Robinson Equation of State

GERG: European Gas Research Group

BTCM: Battelle Two-Curve Model

QRAs: Quantitative Risk Assessments

CAD: Computer-Aided Design

FVM: Finite Volume Method

RNG: Renormalization Group

k- ϵ : k-Epsilon Model

GLOSSARY

Expansion Wave: Also known as a decompression wave, it initiates and propagates in both directions along a gas pipeline away from the rupture location.

Choked Flow: When the flow becomes choked, it reaches sonic speed at the exit point due to a significant initial pressure drop.

Transient Flow: Flow conditions that change with time, as opposed to steady-state flow which remains constant.

CFD Software: Computational Fluid Dynamics software used for simulating fluid flow and solving governing equations.

Meshing: The process of dividing a physical domain into small elements (mesh) to facilitate numerical analysis.

Spatial Discretization: The process of dividing the computational domain into small control volumes for solving equations.

Turbulence Model: Mathematical representation of turbulence in fluid flow simulations, such as the k- ϵ model.

CHAPTER 1: INTRODUCTION

1.1 BACKGROUND / JUSTIFICATION:

In the recent years, the researchers' attention has been attracted by the accelerating threat of global warming, due to a sharp increase in CO₂ levels. Specifically, the concentrations have increased from around 340 ppm in 1980 to 421 ppm by 2022. This shift proves the urgency and significance of addressing climate change (Hekmatmehr et al. 2024).

One of the technologies used to mitigate the impact of emissions produced by fossil fuels is carbon capture and storage (CCS) technique. The CCS process involves storing the carbon dioxide (CO₂) captured at large industrial sources such as fossil fuelled electricity generation plants and factories into saline aquifers also known as geologic formations. This will prevent CO₂ from entering the atmosphere (Vianello et al. 2012). Soepyan et al. in a study proposed a natural gas combined cycle (NGCC) power plant equipped with a hybrid CCS system designed to achieve efficient capture and continuous transition between varying operational loads. The research highlights the potential profitability and environmental advantages of implementing advanced CCS technologies in the natural gas power generation sector (Soepyan et al. 2024).

A critical component of CCS is the transportation of CO₂ through pipelines from capture points to geologically pre-determined locations for subsequent processing steps such as sequestration or enhanced hydrocarbon recovery. One of the most effective methods for transportation of large quantities of CO₂ between the points of capture and storage facilities is using pipelines. Pipelines allow a stable flow of CO₂ captured from continuous operations like fossil fuel power plants (Onyebuchi et al. 2018). One of the disadvantages of using pipelines is leaks and catastrophic failures, specifically those related to propagating or

unstable fractures, leading to a rapid and massive release of CO₂ supply. In the event of pipeline rupture and accidental release of CO₂ the environment, people, and animals around the point of discharge are at great risk. There is a risk of cryogenic burns and breathing dry ice in addition to loss of consciousness or asphyxiation (Luo et al. 2024).

Accurately assessing the hazardous distances of CO₂ and the impact of pipeline operating conditions such as flowrate in the CO₂ release distance is critical. Modelling techniques such as computational fluid dynamics (CFD) provide accurate assessments of various release scenarios. Through the analysis results together with experimental findings we can put the required safety procedures in place and ensure emergency response plans are in place in the event of an accidental CO₂ release. Additionally, this process helps in ensuring that communities are not located in close proximity of high pressure CO₂ pipelines (Li et al. 2023).

1.2 AIMS, OBJECTIVES AND RESEARCH QUESTION/S:

The primary aim of this research is to accurately assess hazardous distances and the impact of pipeline operating conditions on CO₂ release, using advanced modelling techniques such as computational fluid dynamics (CFD). While utilizing pipelines for CO₂ transport offers several advantages, it is critical to identify the risks involved in the accidental release of CO₂ into the atmosphere. Through analysis results, the report aims to ensure the implementation of the necessary precautions and contingency plans for mitigating the risks associated with accidental CO₂ releases. Additionally, the report aims to contribute to community safety by addressing the proximity of CO₂ pipelines to residential areas.

1.2.1 Specific Objectives:

- Evaluate hazardous distances correlating to various operating conditions.
- Utilize Computational Fluid Dynamics (CFD) to assess various CO₂ release scenarios.
- Compare the analysis results with existing experimental data.

1.2.2 Expected Outcomes:

Identify safe separation distance from high pressure CO₂ pipelines under different scenarios and gain an insight into the dispersion patterns and behaviours.

The utilisation of CFD will contribute valuable data to the broader industry knowledge.

The outcomes will serve as a basis for formulating scenario-specific guidelines for the safe operation and management of CO₂ release incidents.

The outcomes will contribute to the optimisation of emergency response plans.

1.3 OUTLINE OF SUGGESTED RESEARCH METHODOLOGY:

Given the importance of understanding CO₂ hazardous distances, a methodological approach needs to be undertaken for the success of this research.

1.3.1 Experiments and studies to be conducted

The primary approach of this research will involve extensive software-based simulations, using Computational Fluid Dynamics (CFD). Ansys Fluent software will be utilised to replicate and analyse scenarios related to accidental release of CO₂ into the atmosphere following by a pipeline leak. This choice is driven by several advantages. Firstly, it allows me to explore a range of pipeline operating conditions, including variations release

flowrates, which can be updated in the software environment. Secondly, CFD simulations allow to model complex fluid behaviour, such as turbulence, with a high degree of accuracy. Additionally, this approach allows us to predict and compute hazardous distances associated with different sets of parameters, and this will assist with improving the current safety rules and regulations.

In terms of measurements, two flowrates from low to high will be applied to the model. Additional variables such as pipeline material, pressure and temperature can also be incorporated to the model considering the time constraints. At every simulation run, the concentration of CO₂ in the domain will be measured at sensors located downwind of the release point. In case of anomalies or unexpected behaviours during the simulations, these will be noted for further analysis and finding the root cause.

In addition to the simulations, real-world data from the past studies or incidents related to CO₂ releases or pipeline leaks will be sourced. This data will provide a realistic target against which the simulated data can be verified.

1.3.2 How data will be analysed

After running the CFD simulations, the first step is to obtain the relevant data from the simulation output files. Ansys Fluent can generate output files containing a wide range of data, including flow velocities, pressures, temperatures, concentration of CO₂ in air and other variables. The data may need to be formatted, organised, or filtered to obtain meaningful datasets for analysis.

Using Excel the simulation results will be visualised. This is important for gaining an understanding of fluid flow patterns and variations of CO₂ concentration in the air. The simulation results will then be compared with experimental data obtained from other studies,

to validate the accuracy of the CFD model. This comparison will confirm that the simulation result is consistent with real world data.

Changes will be made to model parameters such as boundary conditions, turbulence models, solution methods, time step size and mesh resolution to understand how they affect the simulation results. This will help to identify important parameters and how they impact the outcome.

1.3.3 How to interpret the analysis

I will be running the simulation several times and compare the results each time to ensure the analysis has reached a stable state and that further iterations will not change the results significantly. Furthermore, based on the analysis results, I will be able to understand the nature of the relationship between the intensity of the leak and CO₂ hazardous distances and any particular conditions that present the highest risk in the expansion of CO₂ distances.

After reviewing the analysis results, I will conduct a preliminary evaluation of the hazardous distances and concentration of CO₂ at a distance and validate the results using experimental data.

1.3.4 Expected outcomes:

- Produce a 2D simulation model that is able to capture the key flow structures of the CO₂ jet at the release point, including the Mach disc.
- Produce a 3D simulation model that allows for realistic scenario, simulating how CO₂ interacts with its environments, including factors like wind and ground effects.
- Validate the 2D and 3D simulations using existing experimental data.

- The utilization of CFD will contribute valuable data to the broader industry knowledge.
- The outcomes will serve as a basis for preparing scenario-specific guidelines for the safe operation and management of CO₂ release incidents.
- The outcomes will contribute to the optimisation of emergency response plans.

1.3.5 Research contribution:

This research is intended to provide a detail understanding of the behaviour of CO₂ when mixed with ambient air and how pipeline operating conditions effect safety and design. While previous studies have investigated CO₂ transportation in a general sense this research will look at specific factors such as intensity of the leak and environmental conditions and their impact on the dispersion, generating a particular knowledge in this field.

The research will have a positive impact on the society by improving our understanding of the risks associated with CO₂ transportation and reducing those risks. By understanding and determining the safe distances around CO₂ pipelines, this research will contribute to the safety of the communities living around CO₂ pipelines.

This study will open the pathway for future research work in this area. By identifying the relationship between flowrate and environmental conditions and their effects on CO₂ behaviour during dispersion (result from a hole or rupture) this research is likely to be the foundation for further research and experimental activities in this field and as a result more stringent rules in the pipeline design standards and improvements in the safety monitoring systems.

CHAPTER 2: BACKGROUND AND LITERATURE REVIEW

2.1 OVERVIEW OF EQUATION OF STATES (EOS)

An Equation of State (EOS) is a mathematical relationship that explains the connection between the physical properties of a fluid, such as pressure, volume, and temperature. These equations play a key role in identifying and predicting the behaviour of gases, liquids, and solids under various conditions. The primary purpose of an Equation of State is to provide a systematic and quantitative framework for showing the thermodynamic properties of a substance, and this enables us to make predictions about its behaviour in different environments (Shalom et al. 2002).

The accuracy of these models is crucial for designing components like pipelines, separators, vessels, and rotating equipment in carbon capture, as deviations from experimental data can lead to uncertainties, which impacts both capital and operating costs. There is currently a need for further experimental measurements, especially for mixtures with more than five components and the existence of "exotic" compounds that are found in carbon capture, for example heavier hydrocarbons and amines (Vitali et al. 2023).

2.1.1 Ideal Gas Equation of State (EOS)

Under standard pressure and temperature conditions, many single-component fluids like CO₂ exhibit a linear relationship involving pressure, volume and temperature as outlined by the ideal gas law.

$$Pv_m = RT \quad (2.1)$$

Here, v_m represents the molar volume, P represents standard pressure, R represents the universal gas constant and T is temperature (Taylor & Cohen 1990) . However, this linear

relationship between pressure, volume, and temperature is no longer applicable at higher pressures or lower temperatures. In these cases, the ideal gas law needs additional terms to accurately describe real gas behaviour (Böttcher et al. 2012).

To account for these limitations, scientists have developed several EOS that can accurately describe the behaviour of fluids under various conditions, including different phases and mixtures. In the following sections we will explore two additional Equation of State (EOS) relevant to CO₂ followed by a comparison of their applications.

2.1.2 Peng Robinson (PR) Equation of State (EOS)

Amongst all existing equations of state, Peng–Robinson EOS is defined as a simple equation that is very popular in the oil and gas industry. This classic model can effectively describe the correlation between temperature, pressure and composition of phases in single-component as well as multi-component systems. Using the PR EOS means we only require acentric factor and some key properties. However, it needs to be noted that this EOS can only be used only in systems where pure substances are present. Also, for calculating mixture properties, it requires the application of suitable mixing rules. While the Peng–Robinson EOS proves satisfactory for gas-phase scenarios, its accuracy reduces when dealing with gas pressures lower than the triple point and liquid phases (Abdulkadirova et al. 2010). The presentation of the Peng–Robinson EOS is as follows (Dilay & Heidemann 1986).

$$P = \frac{RT}{v - b} - \frac{d\delta}{v(v + b) + b(v - b)} \quad (2. 2)$$

In equation (2. 2) v represents specific volume and R represents the gas constant. The coefficients b and d and δ are determined from critical pressure and temperature and are given by the following equations.

$$d = 0.45724 \frac{(RT_c)^2}{P_c} \quad (2. 3)$$

$$b = 0.07780 \frac{RT_c}{P_c} \quad (2. 4)$$

$$\delta = [1 + (0.37464 + 1.54226\omega - 0.26992\omega^2)] \left(1 - \sqrt{\frac{T}{T_c}} \right) \quad (2. 5)$$

Where P_c is the critical pressure, T_c is the critical temperature, and ω is the acentric factor.

2.1.3 GERGE-2008 Equation of State (EOS)

In process engineering, development of accurate EOS for natural gas mixtures is a critical step. These EOS models play a key role in optimising processing equipment and gas pipeline systems. Their application helps to minimise over-design, which leads to more economic and efficient systems. The GERG-2008 EOS draws upon a robust foundation of experimental data on thermodynamic properties for 21 key natural gas elements. This data ensures the model is accurate in representing the behaviour of natural gas mixtures (Rowland et al. 2016). The 21 components include nitrogen, carbon dioxide, methane, and several hydrocarbons and extends from ethane to n-decane. Additionally, GERG-2008 accounts for hydrogen, carbon monoxide, water, oxygen, hydrogen sulphide, argon, and helium. Figure 1 illustrates the 210 binary combinations that can arise resulting from the 21 components present in natural gas mixtures included in the GERG-2008 equation of state (Kunz & Wagner 2012).

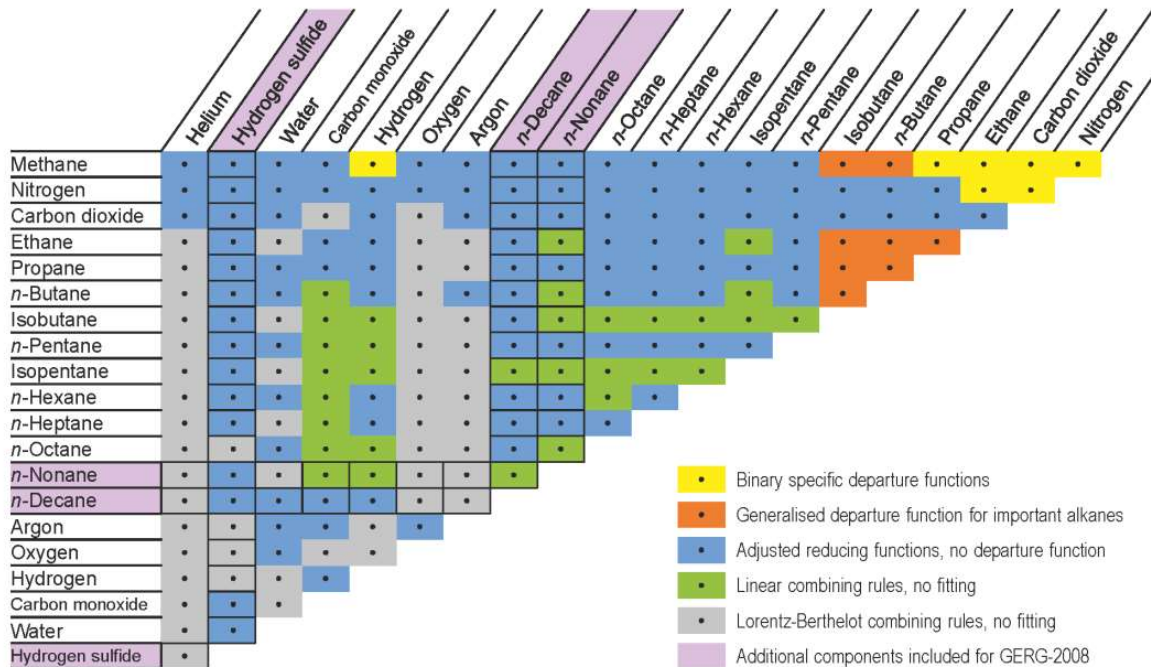


Figure 1 – Illustration of the 210 Possible Binary Combinations resulting from the 21 Components of Natural Gas included in the GERG-2008 equation of state (Kunz & Wagner 2012).

The GERG-2008 model is valid for the entire 210 natural gas compositions and covers all thermodynamic phases. This includes gas phase, liquid phase, supercritical, and vapor–liquid equilibrium states not only involving pure gasses but also for a mixture of the mentioned components. The standard application range extends from pressures up to 35 MPa and temperatures varying between 90K and 450K (Kunz & Wagner 2012).

The advantage of this EOS is that the mentioned temperature and pressure range coincides with the region where very accurate data from experiments for thermal and caloric properties of natural gas exist. GERG-2008 can be further extended for use at pressures going as high as 70 MPa and temperatures ranging from 60 K to 700 K.

The detailed formulation of GERG-2008, enables its application in various engineering fields. These applications include the entire natural gas value chain, including processing,

pipeline and shipping transportation, storage, liquefaction, and separation processes of gas components (Kunz & Wagner 2012). The numerical presentation of this EOS is as follows.

$$\alpha(\delta, \tau, \bar{x}) = \alpha^o(\rho, T, \bar{x}) + \alpha^r(\delta, \tau, \bar{x}) \quad (2.6)$$

In this equation α^o denotes the ideal gas properties and it depends on the mixture temperature T , density ρ and molar composition \bar{x} in accordance with the below expression.

$$\alpha^o(\rho, T, \bar{x}) = \sum_{i=1}^N x_i [\alpha_{oi}^o(\rho, T) + \ln x_i] \quad (2.7)$$

The additional term (α_r) in the equation accounts for the Helmholtz free energy of the mixture. This term is determined using the following expression.

$$\alpha^r(\delta, \tau, \bar{x}) = \sum_{i=1}^N x_i \alpha_{oi}^r(\delta, \tau) + \sum_{i=1}^{N-1} \sum_{j=i+1}^N x_i x_j F_{ij} \alpha_{ij}^r(\delta, \tau) \quad (2.8)$$

In the above expression τ is the inverse reduced mixture temperature and δ represents the reduced density of the mixture and, are calculated using the following equations. N signifies the total number of components in a given mixture (Rowland et al. 2016).

$$\delta = \frac{\rho}{\rho_r(\bar{x})} \quad \text{and} \quad \tau = \frac{T_r(\bar{x})}{T} \quad (2.9)$$

2.1.4 Comparison of equation of states

Choosing the right equation of state (EOS) for a fluid is critical, as it describes the relationship between pressure, volume, and temperature. This comparison focuses on three EOS including Peng-Robinson (PR), GERG-2008, and the Ideal Gas equation of state. The

PR and Ideal Gas equation of state models were specifically used in the 2D and 3D simulations conducted in this study.

Peng-Robinson (PR) EOS is a simpler, cubic equation that facilitates easier solution methods compared to GERG-2008 EOS. However, its accuracy is limited to single-component systems such as pure CO₂ or certain multi-component systems at standard pressures and temperatures. Additionally, the PR EOS is most efficient for gases and vapours, where density is low. For more complex mixtures, additional mixing rules are needed, which can add complexity. In this study, PR EOS is selected for the simulation of 2D CO₂ jet, due to its well-documented precision in modelling the vapor-liquid equilibrium of various gases (Li & Yan 2009). This EOS offers a balance between computational efficiency and accuracy for gas-phase systems like CO₂. In ANSYS Fluent, the PR EOS is available as a built-in thermodynamic model for real-gas behaviour.

The Ideal Gas EOS, was applied in the 3D simulation, where CO₂ is expected to remain within the ideal gas region. The ideal gas model assumes that the gas behaviour remains linear under all conditions, thereby simplifying calculations. Although it is less accurate for high pressure systems, it provides a reliable approximation for gases under standard conditions. This assumption also reduces computational costs for larger simulations like the 3D simulation.

GERG-2008 EOS is a more complex model specifically designed for natural gas mixtures. It utilises experimental data for various components and their interactions, which makes it highly accurate across a wider range of pressures, temperatures, and fluid phases (liquid, gas, supercritical). Although, the high accuracy result leads to the increased cost of computational power needed to solve it. Although GERG-2008 was not used in this study,

it remains valuable for complex natural gas mixtures and scenarios that demand high accuracy across various fluid phases.

In summary, the PR EOS was a good choice for simpler CO₂ scenarios, as used in the 2D simulation, while the Ideal Gas EOS provided a simpler, computationally efficient solution for the 3D simulation. GERG-2008, although not used in this study, is best for when dealing with complex natural gas mixtures and conditions requiring high accuracy across different fluid phases.

2.2 CHARACTERISTICS OF PURE CO₂ AND CO₂ MIXTURES

CO₂ is odorless, colourless gas and not flammable. Each atom of CO₂ contains two atoms of Oxygen and one atom of Carbon bonded together. CO₂ due to having greater density than air it tends to settle in valleys and lower grounds which leads to the risk of suffocation. In a CO₂ plume and when the CO₂ temperature is lower than the atmosphere around the plume water vapour present in the air condenses into small droplets, however it is difficult to differentiate between these droplets and CO₂ particles.

Figure 2 presents the phase diagram of pure CO₂. The phase diagram illustrates the states in which CO₂ exists (solid, liquid, and gas) and the transitions between these states.

Key features of the CO₂ phase diagram are as follows;

- The triple point of CO₂ is the condition where all its phases including solid, liquid, and gas exist in equilibrium. For CO₂, this occurs at the temperature of -56.6°C (216.8 K) and a pressure of 0.5 MPa. When comparing with many other gases, the critical point of CO₂ occurs at reasonably high pressures. A property that needs to be taken into account in the design and operation of pipelines and storage systems.

Infrastructure must be built to withstand these high pressures to safely transport and store CO₂, particularly in applications such as carbon capture and storage (CCS).

- The critical point of CO₂ occurs at a critical temperature of 31.1°C (304.2 K) and a critical pressure of 7.38 MP. Past the critical point, CO₂ is present as a supercritical fluid showing properties of both liquids and gases. In this state CO₂ can diffuse through solids like a gas and dissolve materials like a liquid. For CO₂ to be in this phase, its pressure must exceed the critical pressure, and its temperature must be above the critical temperature.
- When the temperature is higher than the critical temperature, increasing the pressure will not lead to forming liquid. Instead, the substance remains in a supercritical fluid state regardless of the pressure applied.
- When the pressure is greater than the critical pressure and the temperature is less than the critical temperature, CO₂ is in its liquid state. Additionally, the density of this liquid CO₂ increases as its temperature decreases (Dandekar 2006).
- Both triple point and critical point are located on vapour-liquid equilibrium line. This line separates the regions where a substance exists as a gas from where it exists as a liquid. The triple point is where solid, liquid, and gas phases can simultaneously exist, while the end of the vapour-liquid equilibrium line marks the critical point is, separate liquid and gas phases do not exist past this this point.
- Below the critical point, CO₂ can exist as a liquid at higher pressures and can transition between liquid and gas through evaporation and condensation.

2.3 CO₂ PHASES

Depending on temperature and pressure, the chemical compound CO₂ can exist in three main forms including solid (dry ice), liquid, or gas.

CO₂ in its solid phase, known as dry ice, undergoes sublimation at standard atmospheric pressure (101.3 kPa), transitioning directly from a solid to a gas at a temperature of -78.5 degrees Celsius. This unique property makes dry ice ideal for various applications like cooling, preservation, and even creating special effects.

CO₂ can exist as a liquid under high pressure conditions. At atmospheric pressure, CO₂ stays in the gas phase until its temperature drops to -56.6 degrees Celsius at which point it liquefies. Liquid CO₂ is utilised in different industrial processes, including chemical extraction, dry cleaning, and as a solvent in some applications.

CO₂ is most commonly encountered in its gaseous phase under normal atmospheric conditions. It is a colourless, odorless gas at room temperature and pressure (Trasatti 2007).

Figure 2 illustrates the phase diagram of CO₂ (Böttcher et al. 2012). This diagram maps out the conditions of temperature and pressure at which CO₂ exists as a solid (dry ice), liquid, or gas. The phase diagram is divided into regions representing each state of CO₂, with the boundaries indicating the particular conditions where CO₂ transitions between these phases. At high concentrations in the atmosphere, gaseous CO₂ acts as a greenhouse gas, contributing to global warming and climate change.

In the phase diagram, the region labelled as "gas" and "ideal gas" (in the lower part, under the supercritical and liquid regions) represents where CO₂ remains gaseous under various temperature and pressure conditions.

At the conditions simulated in the 3D model, CO₂ stays in the ideal gas region and in the gas phase. Since the simulation focuses on atmospheric conditions with relatively low pressures and moderate temperatures, CO₂ does not reach the conditions necessary for it to transition

into a liquid or solid state. Therefore, the use of the Ideal Gas EOS in this simulation is appropriate, as CO₂ will behave as an ideal gas throughout the study.

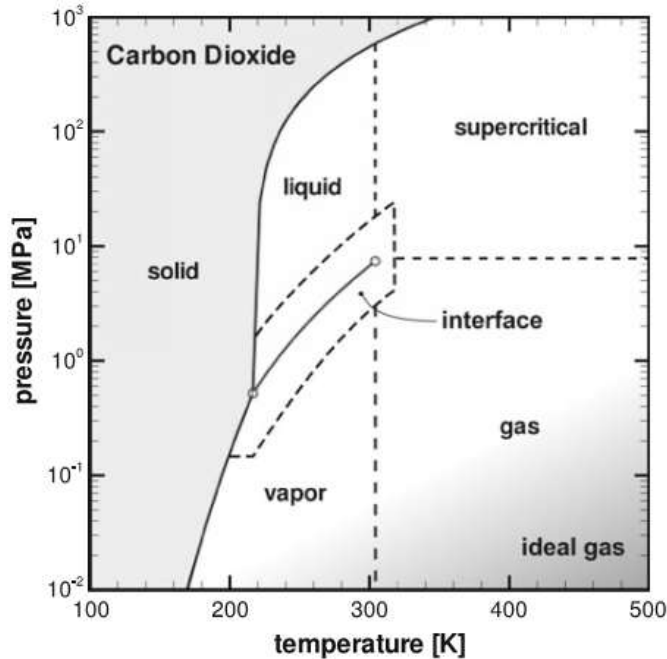


Figure 2 – phase diagram of CO₂ and its various phases across a range of pressures and temperatures.

2.4 CO₂ DECOMPRESSION

When a high pressure pipeline ruptures, the release of the substance can be broken down into three main stages: depressurisation, atmospheric expansion, and dispersion.

The decompression of CO₂ leads to a sudden drop of temperature as a result of the Joule-Thomson effect. Furthermore, at the release point an immediate choked flow occurs post pipeline rupture (Martynov et al. 2013). A decompression wave then forms and travels through the CO₂ within the pipeline towards the intact end. As this wave reaches different sections of the pipe, it accelerates the CO₂ in the opposite direction of the wave, ultimately

leading to a loss of containment from the system (Woolley, Fairweather, Wareing, Proust, et al. 2014).

The decompression wave speed is critical and is calculated by the deduction of the outflow velocity from the local speed of sound at that specific location (Cosham et al. 2012). Therefore, the accuracy of the equation of state used in the model has an important role in determining the velocity of the expansion wave.

$$W = c - u \quad (2.10)$$

In the above equation W is the wave speed, u is the outflow velocity and c is the local speed of sound (Botros et al. 2004).

A precise calculation of the wave speed is essential for two key reasons. Firstly, it allows us to calculate how quickly the pipeline is fully depressurized. Secondly, it helps assess the risk of a propagating fracture forming in the pipeline material (Flechas et al. 2020).

Figure 3 illustrates ductile fracture in a pipe and the formation of decompression waves.

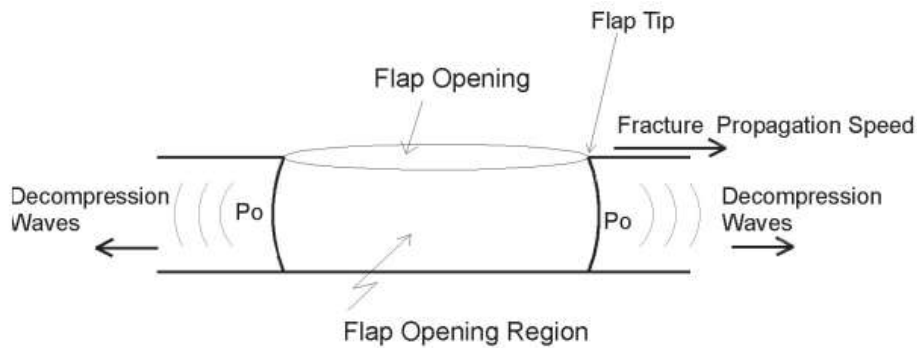


Figure 3 – ductile fracture and decompression waves (Botros et al. 2004)

As stated earlier, one of the major safety concerns during the sudden decompression of a pipeline safety is the risk of fractures propagating rapidly. Preventing or stopping these

fractures is crucial to pipeline integrity (Cosham & Eiber 2008). Even though there has been ongoing advancements, engineers often rely on the Battelle Two-Curve Model (BTCM) to assess fracture propagation in pipelines (Maxey et al. 1976). This model estimates a material's resistance to crack growth.

The BTCM uses two independent curves: fracture propagation (represented by a 'J-curve') fluid decompression wave velocities, both depending on pressure. For a schematic depiction of this model refer to Figure 4. The decompression curve's shape is influenced by the fluid state being either a single phase (green) or a two phase (red) fluid. These three J-curves reflect fracture speed trends for varying toughness levels. When the J-curve intersects the decompression curve, it suggests that the travelling speed of the decompression wave and fracture are equivalent. This creates a pressure plateau at the fracture tip, preventing further pressure drop. This plateau allows the fracture to propagate further. The BTCM predicts that the lowest required toughness to arrest a fracture that is expanding corresponds to the point where the decompression and J-curves meet (Elshahomi et al. 2015).

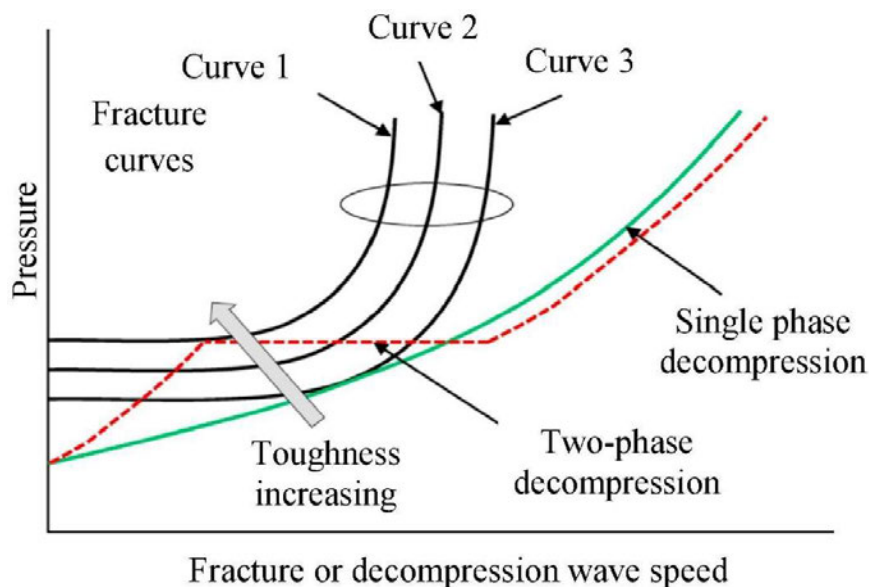


Figure 4 – diagram of the BCM model (Liu et al. 2018)

Preventing the propagation of ductile fractures is crucial for the safety of CO₂ pipelines. To prevent the propagation of fractures, a deep understanding of how CO₂ decompression behaves within the pipeline is needed. This includes analysing pressure and temperature changes, as well as the speed of the decompression wave. Given the significance of predicting the behaviour of CO₂ during decompression in pipelines, a numerous recent large-scale research projects focused on conducting rapid depressurization experiments. The valuable data obtained from these experimental programs is crucial for developing accurate decompression models (Teng et al. 2016).

BTCM recommends, a significant shift of the decompression wave speed curve (curve 1) displayed in Figure 4 to the left to prevent the occurrence of a running ductile fracture. Consequently, CO₂ pipelines require higher toughness levels. Additionally, anthropogenic CO₂ utilized in CCS projects typically is mixed with impurities. While these impurities may be present in small quantities, they can substantially alter the thermo-physical properties of the mixture in comparison to the pure CO₂. Subsequently, the changes in the phase envelope impacts the decompression behaviour of CO₂. Figure 5 illustrates the saturation line of the pure CO₂ alongside the phase envelopes of several CO₂ mixtures. The phase envelope for each mixture is made from two lines: these include 'bubble line' (located at the top) and 'dew line' (located at the bottom). In the area above the bubble line the gas is in its liquid phase, while in the area between these two lines, it resides in a two-phase region. This is absent in the case of pure CO₂. Lastly, the fluid exists in a vapor state in the area below the dew line. Notably, for a CO₂ mixture, the pressure at which the liquid starts to turn into gas (bubble line) is considerably higher compared to pure CO₂. This significantly affects how pure CO₂ and CO₂ mixtures behave during decompression. The presence of impurities also cause a considerable shift of the decompression wave speed curve (curve 1) towards the left. This

shift is due to a longer 'pressure plateau' within the two-phase zone. Due to this, the pressure doesn't drop as rapidly during decompression in mixtures compared to pure CO₂. Consequently, the BTCM suggests that pipelines carrying CO₂ mixtures require a higher toughness to prevent running fractures (Liu et al. 2018).

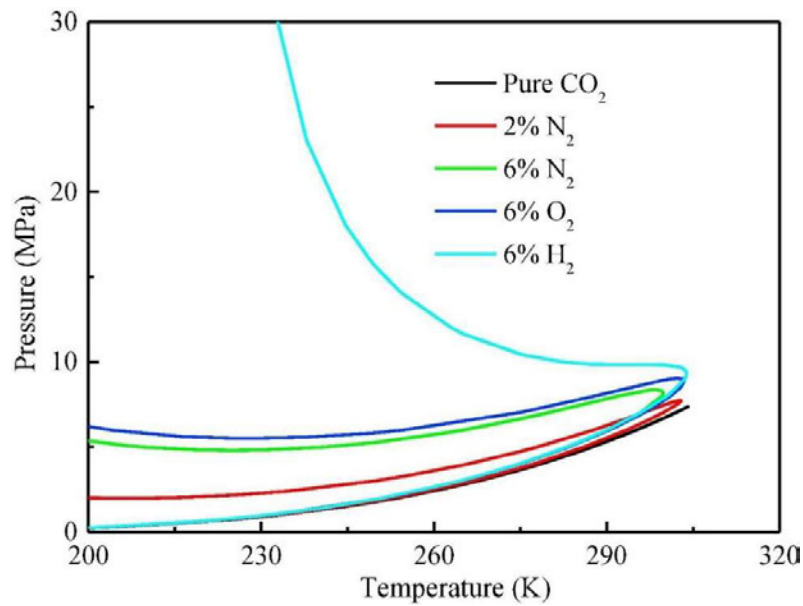


Figure 5 – saturated line of pure CO₂ and phase envelopes of CO₂ mixtures (Liu et al. 2018)

Led by DNV GL, the COSHER joint industry project conducted large-scale experiments to investigate how CO₂ behaves when rapidly released from pipelines (decompression) and how it disperses in the atmosphere. They designed and manufactured an industrial-scale depressurisation assembly which included a 219.1 millimetre diameter steel pipeline forming a 226-meter long loop. Over a duration of 204 seconds, a total of 136 tons of CO₂ was released to atmosphere. Researchers also recorded temperature readings, with a minimum of -17.8 degrees Celsius in the reservoir and the temperature of the fluid in the pipeline loop was recorded as -78 degrees Celsius (Ahmad et al. 2015).

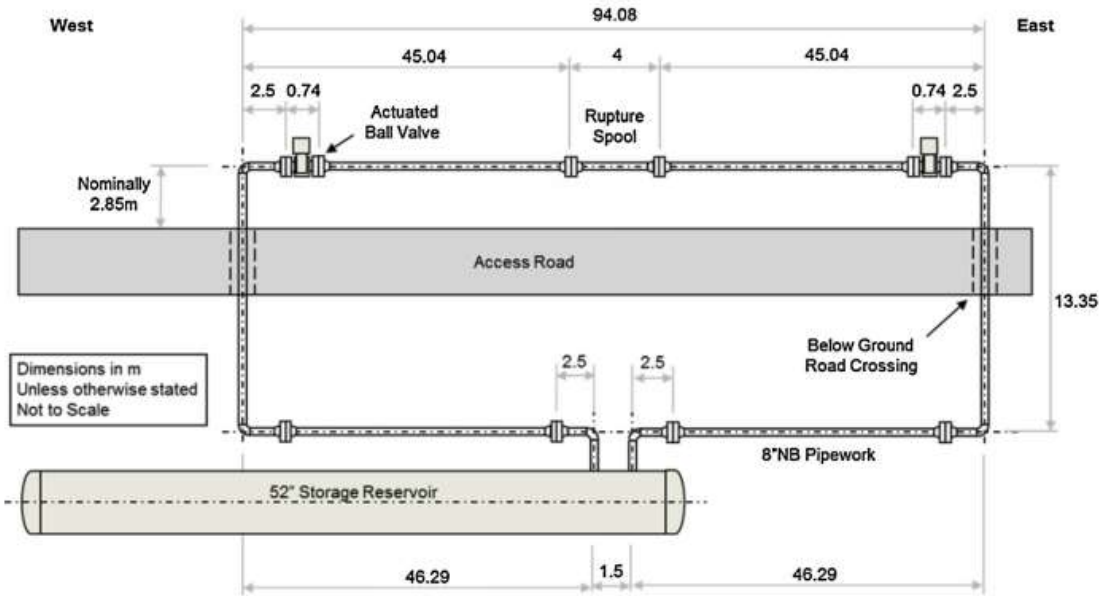


Figure 6 – schematic of the pipeline loop and the overall experiment setup (Ahmad et al. 2015).

Funded by National Grid, the COOLTRANS (Dense Phase Carbon Dioxide (CO₂) Pipeline Transportation) project was a major project that investigated how CO₂ mixtures behave under rapid pressure loss (decompression) in pipelines. This was achieved through shock tube tests and puncture experiments (Cosham et al. 2012).

The CO₂PipeHaz project was funded by the European Commission's FP7 Energy program. The aim of the project was to generate and validate mathematical models for assessing the risks associated with forthcoming CO₂ pipelines. To achieve this, the project designed a large-scale release experiment with a pipeline specifically built for the purpose. The pipeline used in the experiment had a diameter of 233 millimetres, 256 meters long, and had a wall thickness of 20 millimetres. The high operating pressure of 200 bar (20 MPa) allowed the project to conduct depressurization experiments with supercritical CO₂ (Woolley, Fairweather, Wareing, Falle, et al. 2014).



Figure 7 - CO₂PipeHaz project, a high-velocity CO₂ jet resulting from a complete rupture release test (Woolley, Fairweather, Wareing, Falle, et al. 2014).

Founded by N.V. Nederlandse Gasunie, the Dutch CCS research program (CATO2), investigated the behaviour of CO₂ during rapid depressurisation at various depressurisation rates. They conducted experiments using a 30-meter long, stainless steel tube with the diameter of 2 inch to determine the lowest temperature reached at different depressurisation rates (Vree et al. 2015). Additionally, they analysed the thermodynamic behaviour of CO₂ while releasing through nozzles of various sizes from a high pressure vessel (Ahmad et al. 2013).

The experimental setup for the CO₂PIPETRANS joint industry project (JIP), overseen by DNV GL, included a 257 meter long header pipeline, a 1meter long blasting device made up of dual-disc, a heating apparatus, and CO₂ inlets, as depicted in Figure 8. The setup had a maximum operating pressure of 16 MPa. Approximately 60 mm of rock wool was used to insulate the pipeline. The CO₂ release was facilitated through a blasting device made up of two plates at the outlet, while they were recording the temperature and pressure variations during release using a data recording equipment. High-frequency pressure sensors, integrated into the system, measured CO₂ pressures inside the pipeline. The experiments

involved three groups of CO₂ release scenarios, including gaseous, dense, and supercritical phases, with pressure measurements used to monitor pipeline rupture and decompression wave velocities calculated based on distance and travel time between measuring points (Guo et al. 2021).

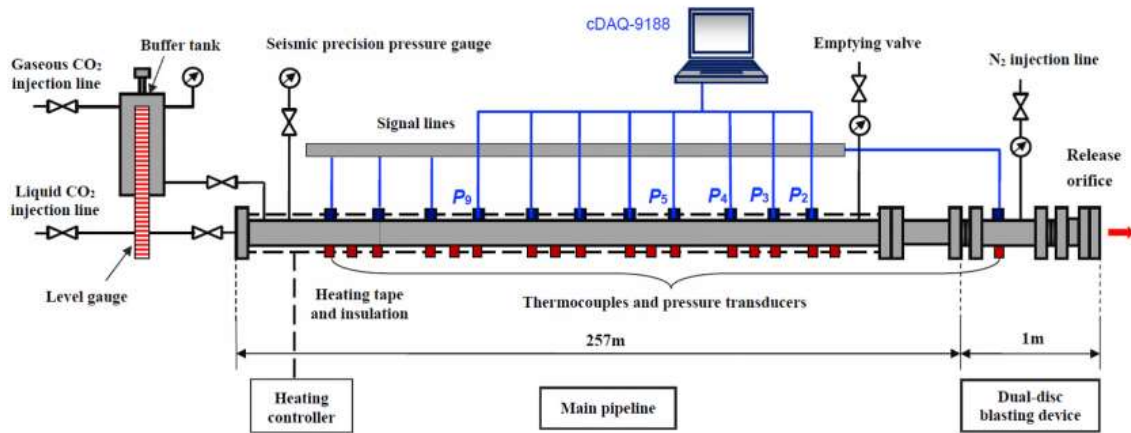


Figure 8 – CO₂ PIPETRANS joint industry project, test assembly (Guo et al. 2021)

These depressurization experiments on CO₂ pipelines have contributed to gathering valuable data for developing and improving mathematical models. These models help explain the observed phenomena during decompression and provide more accurate estimates of leakage hazards (Teng et al. 2016).

2.5 DECOMPRESSION MODELS

Gas decompression models play a key role in predicting the behaviour of gas mixtures during sudden decompression events, such as those occurring in pipeline leaks and ruptures. Amongst these models, GASDECOM is one of the most popular tools in natural gas pipeline safety studies and it excels at simulating the rapid decompression that occurs during a pipeline fracture. This helps engineers understand and predict how gas mixtures behave in the case of a sudden pressure drop (Jie et al. 2012).

Koornneef et al. (2010) in their study reviewed existing Quantitative Risk Assessments (QRAs) for CO₂ pipelines, identifying knowledge gaps and uncertainties that impact the accuracy of calculated risks. Their findings include uncertainties in failure rates, variance in maximum release rates, and the lack of knowledge about the vapour and dry ice fraction in releases. They also raised uncertainties from the absence of standardized exposure thresholds for CO₂. Mitigation strategies should focus on minimising the likelihood of large releases and reducing their potential consequences. They recommended validating the models, defining universal dose-effect relationships, reporting worst-case outcomes, and developing a guide for good practice for CO₂ pipelines.

Gas decompression models, like GASDECOM, are particularly accurate when the gas stays in a single-phase during decompression. Data from gas pipelines of pressures up to 10MPa was used to validate these models. Even with more recent tests involving richer gas mixtures, lower temperatures, and higher pressures, GASDECOM appears to still provide reliable predictions (Botros et al. 2007).

Recent investigations by Botros et al. (2004) into decompression wave speeds in gas mixtures, have shown alignments between experimental data and predictions from GASDECOM model, particularly in dry gas and two-phase regions. This experiment included conventional and rich gas compositions, using an expansion tube test-rig. However, the study highlights challenges in predicting phase change-related plateaus in wave speed, especially near the rupture location, emphasising the need to more enhancements in decompression models to be able to precisely assess the risks involved in pipeline rupture scenarios.

The success of natural gas pipeline safety and technology advancements relies heavily on assessing and comparing results from shock tube tests, burst tests, and computer simulation. Similarly, such assessments are crucial for developing CO₂ pipelines for Carbon Capture and Storage (CCS), especially for controlling the propagation of ductile fractures (Botros et al. 2004). Figure 9 illustrates a diagram of gas decompression pattern relevant to preventing ductile fracture propagation.

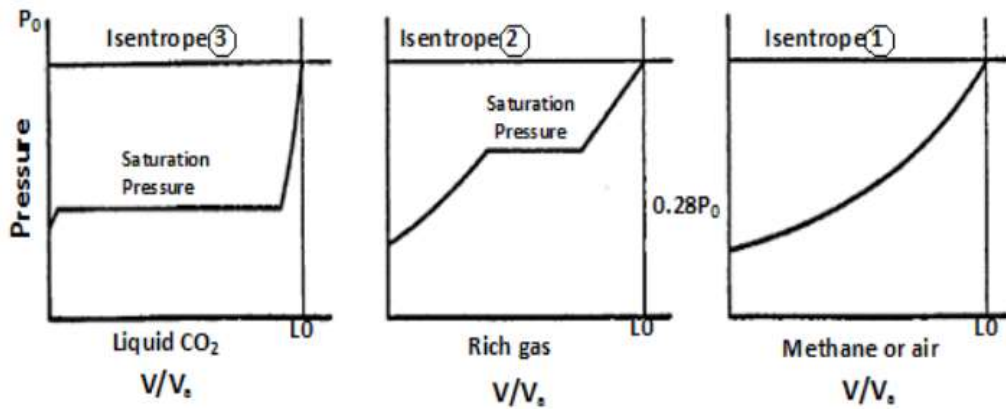


Figure 9 - gas decompression behavior for the assessment of ductile fracture propagation (Botros et al. 2004).

GASDECOM has been adopted by many models to study fracture propagation the only variation among these models lies in using various equation of state (Teng et al. 2016).

Bin et al. (2017) and Liu et al. (2018) suggested a 2-D multiphase equation on the basis of the mixture-model, implemented in the CFD software. This CFD model incorporates non-equilibrium phase change, while also integrating the GERG-2008 EOS for CO₂ and related mixtures. Despite displaying numerical stability issues, such as pronounced pressure fluctuations before stabilising at the pressure plateau, it provides a more realistic prediction of the decompression wave speed curve compared to generic equilibrium models.

Flechas et al. (2020) developed a comprehensive 2-D Computational Fluid Dynamics (CFD) model to simulate the transient decompression of carbon dioxide (CO₂) pipelines in the event of rupture. They studied the behaviour of pressurized liquefied CO₂ during rapid depressurization. Using ANSYS Fluent software, their model incorporated non-equilibrium phase transition phenomena. Notably, the paper compares two thermodynamic approaches the Peng-Robinson Equation of State and correlations based on the Span-Wagner Equation of State to evaluate their impact on decompression wave front arrival time and pressure plateau representation. The research results indicate that while both approaches effectively predict pressure plateaus, the Span-Wagner model yields more accurate predictions of the fast pressure drop region, attributed to its superior prediction of liquid speed of sound. Figure 10 illustrates a comparison of the experiment results Figure 10 –and CFD modelling using SW and PR EOS.

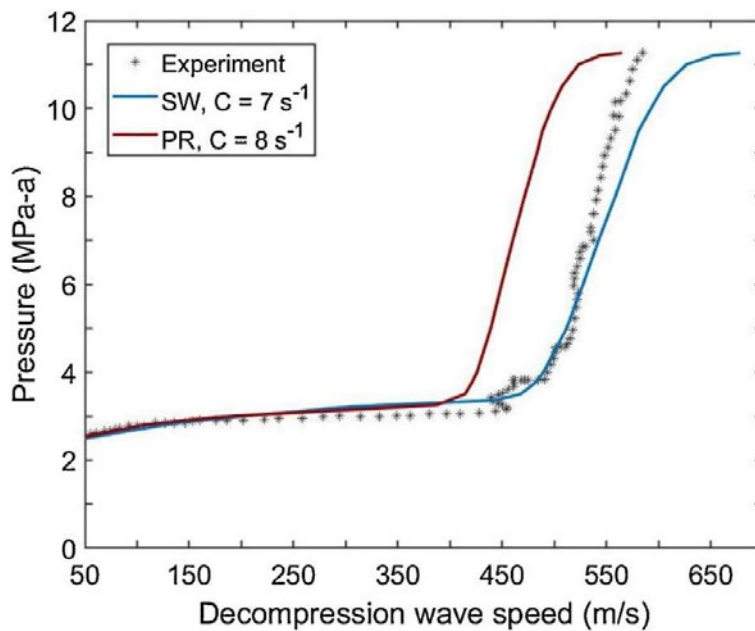


Figure 10 – average speed of decompression wave, PR EOS, SW EOS and Experimental data (Flechas et al. 2020)

In another study decompression wave was simulated using GERG-2008 Equation of State as well as Peng Robinson Equation of State. The findings indicate when comparing with experimental data, predictions by PR EOS generally showed greater difference than those from GERG-2008 EOS. This is mainly due to GERG-2008 EOS having better accuracy, within the liquid phase. As illustrated in Figure 11, the predicted stable pressure zone presented in graph tend to be greater than the experimental data (Botros et al. 2016).

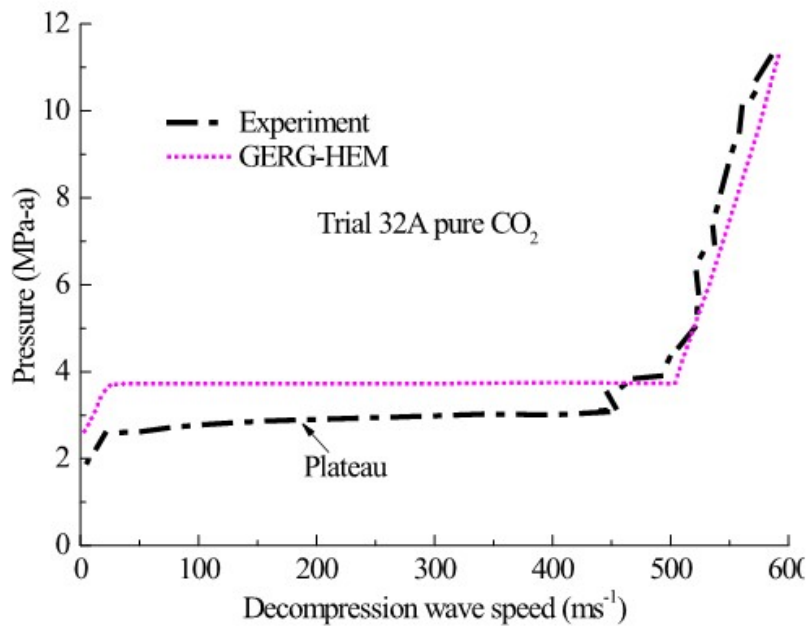


Figure 11 – Decompression wave speed from experiment vs modelling data (Botros et al. 2007)

2.6 CO₂ PHASE CHANGE DURING DECOMPRESSION

CO₂ can be released from pipelines or storage vessels in various phases, including gaseous, liquid, and dense phases. Within a Carbon Capture and Storage (CCS) system, depending on location and time the state of CO₂ may vary. Dispersion models used in such scenarios require accurate specification of source terms for the leak, containing parameters like temperature, leak rate, state (e.g., two-phase), source area and velocity. Typically, these

values are determined at the point where the jet expands and reaches the atmospheric pressure. Models for leak source terms must accommodate a comprehensive set of initial conditions including phase variations as the leak progresses. There are established expressions for leak rate exist of pure gaseous releases. However, in the dispersions that involve dense and liquid phases and when the initial conditions exceed the line of saturation, there will be a change of phase to vapor in the expansion process, known as "flashing." Only when we are dealing with a dense phase dispersion with initial conditions that are significantly greater than 31.1°C (critical temperature), result in purely vapor phase conditions at equilibrium. On the contrary, some releases that are in gaseous state in their initial conditions may reach a point so called sublimation, and this leads to a mixture involving solid and vapor refer to Leak number 6 in the diagram at Figure 12 (Hill et al. 2011).

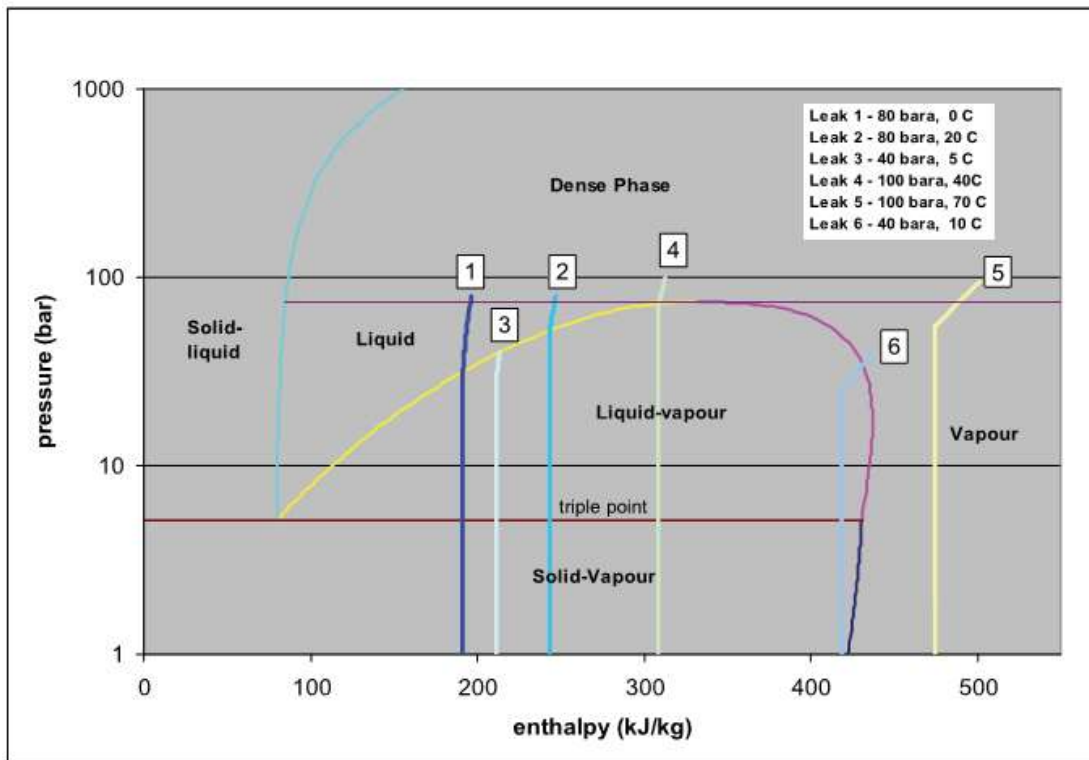


Figure 12- Various leak cases and their pressure-enthalpy paths (Hill et al. 2011).

2.7 COMPUTATIONAL FLOW DYNAMICS (CFD) DISPERSION MODELS

Theoretical modelling of gas dispersion involves both analytical and CFD approaches. One of the least complex models is the Gaussian model (Hanna et al. 2003), although initially not designed for the analysis of a heavier than air gas dispersion such as CO₂, it can predict the behaviours of CO₂ in small releases reasonably with some adjustments in the dispersion parameters (Liu et al. 2022). There are however other analytical models that better predict consequences of heavy gas dispersion, although more complex than the mentioned model, consists of DEGADIS , SLAB, Phast UDM, HEGADAS, among others. Analytical models offer the advantage of quick estimation with acceptable level of accuracy, and validation studies demonstrate their efficiency for small gas releases(Hanna & Chang 2001). However, their predictive capabilities for major-scale gas releases remain uncertain.

In contrast, CFD models, while considerably more complicated and require more time compared to those analytical models, are increasingly utilised in performing atmospheric dispersion simulations. The capability of CFD models to capture complicated physical phenomena, like turbulence in intricate geometries, drives this trend, alongside increased access to high-performance computing resources.

Mazzoldi et al. (2008) conducted a comparison between the performance of CFD and Gaussian models in simulating CO₂ dispersion through simulations of the KitFox experiment (Hanna & Chang 2001). The study revealed that CFD models outperformed Gaussian models.

Liu et al. (2019) integrated experimental investigation with simulations using CFD software to explore the dispersion behaviour of carbon dioxide post pipeline failure scenarios. The

CFD models that are verified against data from experiments, provide detailed insights into CO₂ dispersion patterns and evolution, crucial for risk assessment and safety planning. Notably, the simulations accurately predicted downwind concentrations and the influence of various factors such as wind speed and pipeline orientation on consequence distances. The study extended the CFD models to estimate consequence distances for longer pipelines under different wind conditions, shedding light on the influence of wind speed, and pipeline length on dispersion patterns. These findings highlight the importance of considering CFD analysis in assessing the safety implications of CO₂ pipeline failures and inform decisions regarding pipeline design, safety measures, and risk mitigation strategies.

2.8 SUMMARY

This literature review investigates the accidental release of high pressure CO₂ and the complex dynamics of CO₂ decompression, expansion, and dispersion, particularly in the relation to Carbon Capture Storage and utilisation (CCSU) systems. The design of CO₂ pipelines for such applications introduces some challenges, such as controlling ductile fracture propagation and accurately estimating hazardous distances in case of CO₂ dispersion. The review highlights some knowledge gaps in understanding these processes and highlights the need for further experimental and theoretical investigations.

While experiments provide valuable insights, their high cost and limited scope necessitate the study of theoretical predictions, particularly through Computational Fluid Dynamics (CFD) approaches. However, modelling multi-phase CO₂ decompression presents complexities, especially in simulating phase changes accurately. Previous models overpredicted the pressure plateaus in the curves for decompression wave speed, indicating the need for refinement.

The phase transition and having impurities in anthropogenic CO₂ further complicate decompression characteristics, underscoring the importance of efficient modelling tools for CO₂ mixtures. Yet, there remains a lack of studies on decompression of mixtures involving CO₂.

The study also acknowledges the impact that obstacles have and modelling of real-life terrain on heavy gas dispersion. However, research in this area is still growing, and there are some deviations between simulated and measured results and room for technical improvement. Overall, the literature highlights the need for comprehensive investigations and advancements in modelling techniques to enhance our understanding and management of CO₂ decompression and dispersion phenomena.

CHAPTER 3: METHODOLOGY

3.1 TWO-DIMENSIONAL (2D) SIMULATION OF CO₂ JET USING PENG-ROBINSON (PR) EQUATION OF STATE (EOS)

As discussed in the previous chapter, when a rupture occurs at a specific area along a CO₂ pipeline, a decompression wave, initiates and propagates in upstream and downstream directions along the length of the pipeline travelling opposite to the rupture location. Figure 3 illustrates this in detail. This wave results in the rapid discharge of gas from the pipeline into the surrounding environment due to the pressure in the pipeline being higher than the atmospheric pressure. If the initial pressure drop is significant, then it is possible that a choked flow develops and its speed increases to sonic speed at exit point. In this case, the decompression wave speed nearly reaches the speed of sound inside that fluid (Woolley, Fairweather, Wareing, Proust, et al. 2014).

Determining the velocity of the decompression wave (w) requires determining the speed of sound, pressure profile and outflow velocity. Noting that these variables will be dependent on time along the length of pipeline. This needs a comprehensive analysis of fluid composition, fluid dynamics and thermodynamic properties. Throughout the decompression process, partial condensation of the gas might occur due to the decrease in temperature. Therefore, the model needs to accurately consider phase changes and the thermodynamic behaviour of gases that are under these conditions.

Predicting the sudden release of pressurised CO₂ from a pipeline during rupture requires solving the governing equations including energy conservation, mass and momentum. These equations need to be solved in transient form using appropriate EOS. The technological advancements have recently improved computing capabilities, and this has resulted in more

accurate prediction of a fluid behaviour in the gas pipelines and while decompression is occurring.

This study uses a Computational Fluid Dynamics (CFD) software called Ansys Fluent to solve the governing equations and simulate the flow dynamics. The CFD technique has several advantages over other numerical approaches. Some of these advantages are as follows:

- CFD software such as Ansys can handle complex geometries compared to other simple analytical methods such as MATLAB. This results in realistic representations of real-world scenarios.
- CFD can be used to analyse different flow scenarios including gases, liquids, and multiphase mixtures.
- The program is capable of analysing different flow types including laminar, turbulent, compressible, transient, or steady-state conditions. Additionally, it facilitates the simulation of both ideal and real flows. The ability to simulate transient flows is especially beneficial for studying decompression waves.
- Detailed representation of flow properties such as velocity and pressure can be obtained from CFD software. Visualisation plays an important role in understanding the complex flow behaviour.
- User Defined Functions (UDFs) allow you to define boundary conditions and ANSYS simulations to meet specific needs of a project. For example, a power-law relation can be implemented through a UDF to calculate wind speeds at various elevations.
- CFD is capable of using precise real-gas EOS when we require accurate thermodynamic properties of flow mixtures.

3.1.1 Model Assumptions

The 2D CO₂ jet model was created based on the following assumptions:

- This study is limited to analysing the behaviour of gaseous CO₂.
- The CO₂ is assumed to be 100% pure, without any interference from other gases or impurities.
- 2D axisymmetric model to capture the key flow structures of CO₂ jets.
- 'no-slip' condition is assumed between the fluid and walls.
- To simplify the simulation, potential phase change during the release are not considered.
- CO₂ is assumed to enter the domain uniformly at a constant velocity and pressure, with no spatial variation across the inlet.

3.1.2 Creating the 2D geometry

The 2D geometry was created in the in-built ANSYS DesignModeler module. This feature-based, parametric software can either create complete parametric geometries from scratch or prepare existing CAD models for analysis. Since simulation requires specific modelling capabilities that typical CAD software does not support, DesignModeler fills this gap. As a module under the ANSYS Workbench, DesignModeler is both easy and efficient for preparing simple parametric models, particularly for 2-Dimensional simulations. These capabilities allow the creation of simulations such as the pipeline with a hole discussed in this study. ANSYS also offers another module called SpaceClaim, which is designed for creating more complex geometries with detailed shapes. This is useful for modelling aerodynamic shapes in race cars and similar applications.

Setting up the domain of the physical flow is a critical part of the simulation where you specify the domain where the computation will take place as well as the boundary conditions at which the analysis will initialise. These boundary conditions include several settings including but not limited to inlet, outlet, wall, fluid used and more. This simulation involves air flowing from a reservoir through a converging nozzle and into the atmosphere. The accuracy of the CFD model was validated using experiment completed by Eggins and Jackson (1970) where they studied air jets under high pressure. The computational domain is presented in Figure 14. In this experiment the diameter of the converging nozzle was 2.7mm, the operating pressure of the air was 6 atmosphere and the temperature of 20 degrees Celsius. They released air at the given pressure through a converging nozzle and measured the velocity of the air jet.

For turbulence modelling, k- ϵ model was used as it is suitable for this type of simulations. The Peng-Robinson EOS was utilised to determine the thermodynamic properties of air in real-time based on pressure and temperature. As presented in Figure 13, a plot of the experimental data on the velocity of air along the axis of the jet was compared against the simulated data. It needs to be noted that the plot of experimental data includes a small error of about 5-10%. In this study the pressure and temperature values from the experiment were used to initialise the simulation. The length of the converging nozzle was assumed to be 12mm as the exact length was not provided in the experimental setup. The experimental data show that the velocity reaches approximately 390 m/s at the exit of the nozzle. As the distance from nozzle exit increases, we can witness a steady increase in the velocity, and it reaches its highest value of 618 m/s at approximately 4.2 mm from the nozzle exit. Beyond this point, we can witness a sharp decrease and a continuous decline with distance. Although there are minor discrepancies, likely due to the assumed nozzle length, the overall trend and

the peak velocity are well-predicted by the simulation. This consistency in trend and peak velocity proves the reliability of the CFD model for simulating such high-speed jet flows, even with the assumption made regarding the nozzle length.

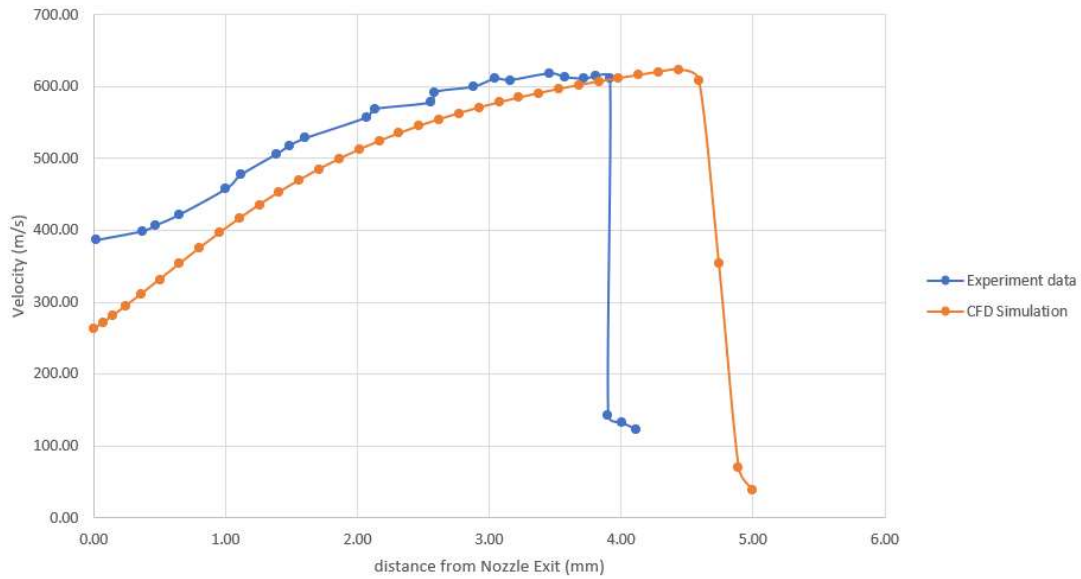


Figure 13 – Comparison of velocity profiles between CFD simulation and experimental data.

Given the relatively short duration of the process being studied, any impacts from heat transfer between CO₂ and ambient air as well as gravity can be neglected. Therefore, to simplify the simulation it is valid to produce a 2D axisymmetric domain and have less computational time. Also, as the air jet is symmetric an axisymmetric model was used to further reduce the computational time. Figure 14 presents the 2D computational domain used for the simulation.

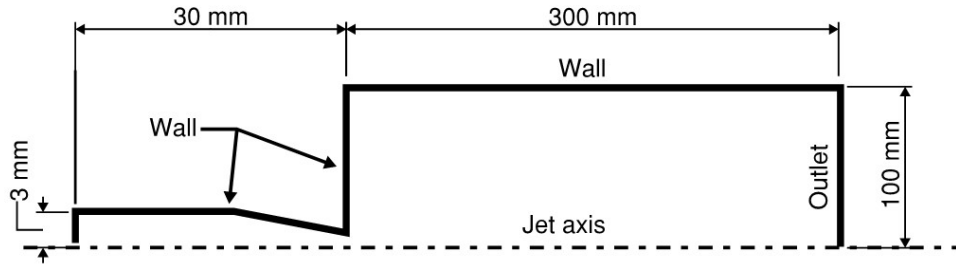


Figure 14 – Details of the 2D computational domain.

Figure 15 illustrates the meshing details at the converging nozzle. A total of 452,000 elements were included in the simulation domain.

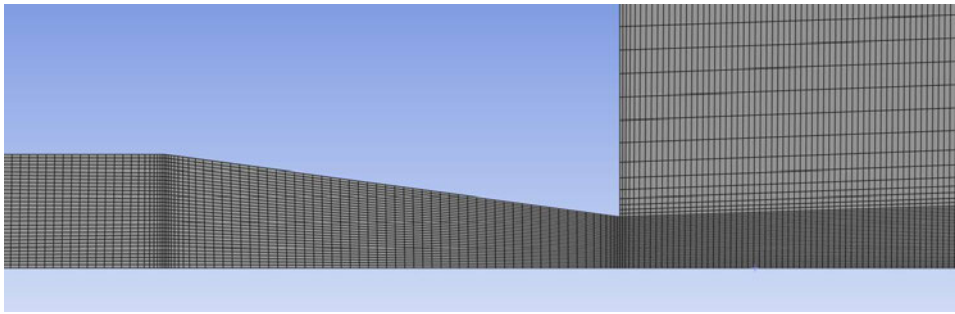


Figure 15 – Meshing configuration around the nozzle outlet.

Upon reaching a stable stage, the model transitioned to simulate the injection of CO₂ into the domain, replacing the previously simulated airflow.

3.1.3 Boundary Conditions

Solving the governing equations for fluid flow requires the definition of boundary conditions. These conditions serve as rules at the edges of the computational domain and they specify the behaviour of the fluid. Boundary conditions define details such as the flowrates entering and exiting the computational domain and the positioning of the inlet and outlet. Additionally, they specify factors such as the pressure of the fluid entering the domain or its velocity. The boundary conditions also specify the behaviour of the wall. The

computational domain for the simulation, as illustrated in Figure 16 consists of four segments, including an inlet, two walls typically specified as no-slip and an axis of symmetry. The axis of symmetry allows us to model only half of the geometry while capturing the entire flow pattern. This leads to a significant decrease in the number of cells and consequently computational time. Using these boundary conditions the process of CO₂ exiting through the converging nozzle will be analysed.

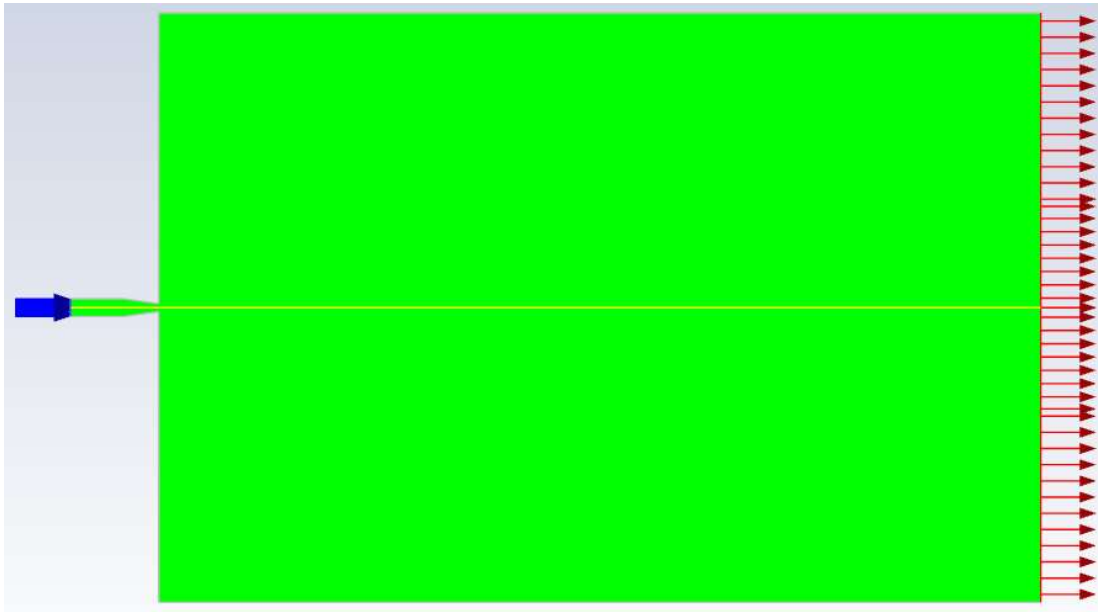


Figure 16 - Computational domain setup for the CO₂ jet simulation.

3.1.3.1 Inlet boundary condition

The inlet boundary is configured to model the CO₂ release through the converging nozzle and into the main domain where CO₂ will be exposed to air at atmospheric pressure of 101,325 Pa ($P_{\text{gauge}} = 0$ Pa) and the temperature of 20°C. The initial pressure is set to 6 atmosphere (506,625 Pa) being the pressure of the CO₂ reservoir/pipeline and the differential pressure between the reservoir pressure and atmosphere makes the CO₂ flow into the

atmosphere. The stagnation temperature of the CO₂ at the inlet is set to 20°C. Figure 17 depicts the inlet boundary condition setup in Ansys Fluent CFD software.

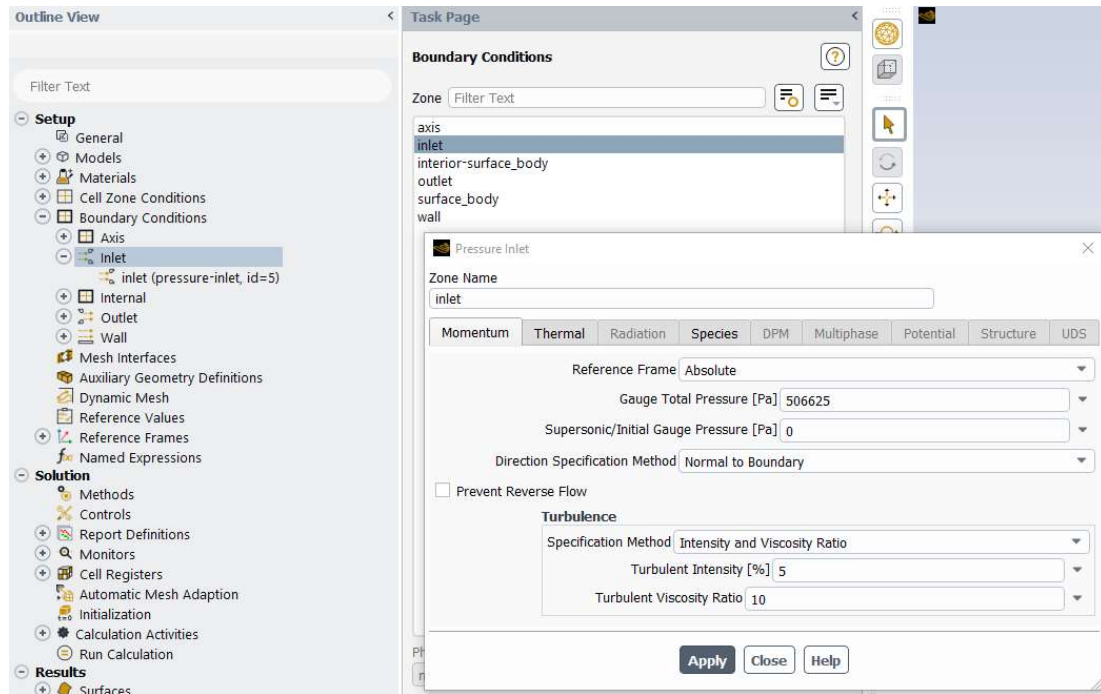


Figure 17 – ANSYS Fluent model settings for inlet boundary condition.

3.1.3.2 Wall Boundary Condition

As illustrated in Figure 14, wall boundary condition is applied to the top edge of the converging nozzle as well as the top and left edges of the computational domain. The wall roughness height is set to 0.005m and all wall boundaries are assigned the non-slip condition. This results in the velocity being zero at the interface between the interior cells and the wall boundaries, which is automatically applied by Ansys Fluent. Figure 18 presents the wall boundary condition setup in Ansys Fluent.

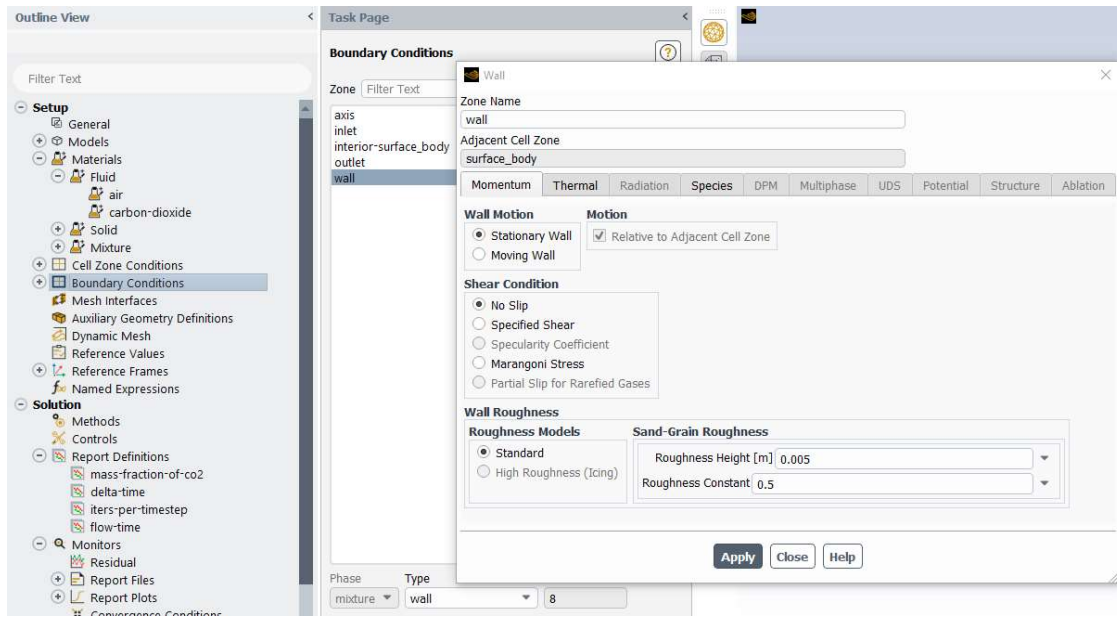


Figure 18 – ANSYS Fluent model settings for Wall boundary condition.

3.1.3.3 Axis of Symmetry Boundary Condition

The axis of symmetry is applied along the jet line, where flow and geometry are symmetric. This means the geometry and flow are mirrored around this axis, which reduces the computational domain to half, and so saves computational time and resources. Once the simulation is completed, the second half of the jet flow can be made visible in Ansys and presented in the results.

3.1.4 Mesh Details

Ansys Meshing module is accessible through the Ansys Workbench platform. Meshing provides the necessary resolution to accurately capture solution gradients. The module can be used on a range of geometries from simple to complex modes. As illustrated in Figure 19, a finer mesh was applied around the nozzle walls, injection point, and along the axis of symmetry to improve the resolution and accuracy of the velocity profile. This results in a

total of 452,560 elements. This refined mesh setup ensures that critical flow characteristics, especially at the symmetry axis, are captured with greater detail.

In ANSYS Fluent, the Finite Volume Method (FVM) is used to break down and solve the governing differential equations in discrete elements. Within these elements or volumes, the conservation equations for mass, momentum, and energy are integrated. This conversion process changes the partial differential equations that describe fluid flow into algebraic equations, which allows numerical solutions on a discrete mesh. The FVM can manage complex geometries and unstructured meshes that are often seen in fluid flow simulations.

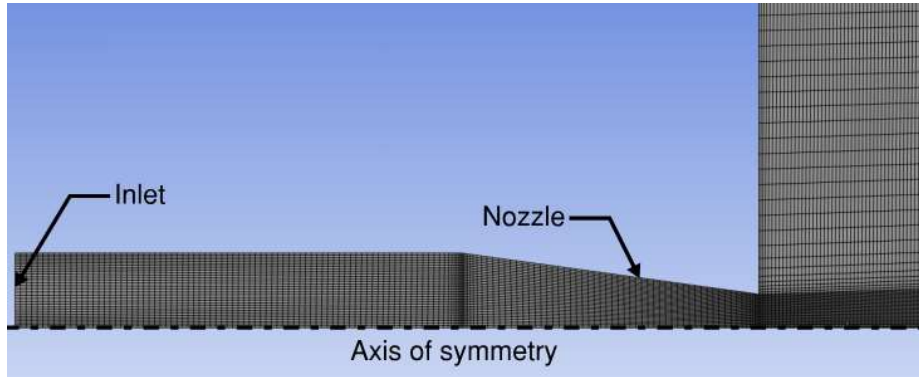


Figure 19 – Meshing around the inlet and nozzle.

3.1.5 Solver Type and Solution settings

The two solver types available in Ansys Fluent are pressure-based solver and density-based solver. The pressure-based solver is often used for incompressible or mildly compressible flows. The density-based solver however, is configured for solving all types of compressible, high speed flows where density is not constant (ANSYS Learning 2023).

The density-based solver in this context allows for the utilization of a real gas equation of state, such as the Peng Robinson EOS, which is based on the experimental data and offers high accuracy for addressing dispersion or leak problems like the one presented in this

research. Furthermore, allowing for density variations in scenarios involving high pressure leaks is essential. Therefore, the density-based solver is utilised to solve this simulation problem.

When it comes to solution formulation, Ansys Fluent offers two options: Explicit and Implicit. These formulations vary in how they linearise the coupled equations. The implicit formulation uses the following equation to discretise the volume equation.

$$\frac{\alpha_q^{n+1}\rho_q^{n+1}-\alpha_q^n\rho_q^n}{\Delta t}V+\sum_f\left(\rho_q^{n+1}U_f^{n+1}\alpha_{q,f}^{n+1}\right)=\left[S_{\alpha_q}+\sum_{p=1}^n(\dot{m}_{pq}-\dot{m}_{qp})\right]V \quad (3.1)$$

In this equation n+1 represents the index for the current time step, while n represents the index for the previous time step, α_q^{n+1} represents the value of the cell at time step n+1, α_q^n represents the value of the cell at time step n, $\alpha_{q,f}^{n+1}$ denotes the face value of the qth volume fraction at time step n+1, U_f^{n+1} represents the volume flux through the face at time step n+1 and V denotes the cell volume. The implicit method computes velocity, pressure and temperature over the entire mesh network concurrently, therefore requires substantial computing resources (ANSYS 2021).

The explicit formulation is time dependent uses the following equation to discretise the volume element.

$$\frac{\alpha_q^{n+1}\rho_q^{n+1}-\alpha_q^n\rho_q^n}{\Delta t}V+\sum_f\left(\rho_qU_f^n\alpha_{q,f}^n\right)=\left[\sum_{p=1}^n(\dot{m}_{pq}-\dot{m}_{qp})+S_{\alpha_q}\right]V \quad (3.2)$$

In this equation n+1 represents the index for the current time step, while n represents the index for the previous time step, $\alpha_{q,f}$ denotes the face value of the qth volume fraction, V denotes the cell volume and U_f represents the volume flux through the face, based on normal

velocity. The explicit method uses less computing resources as it imposes a limit on the time step size during the simulation process (ANSYS 2021). In this 2D simulation explicit method is used to reduce computing time and resources.

3.1.5.1 Spatial Discretization:

In this simulation, explicit formulation is selected for its suitability in handling high-speed, transient flows. The explicit approach allows the simulation to accurately capture rapid changes in flow variables, which are characteristic of high pressure jet releases. While it requires smaller time steps compared to implicit formulations, the explicit method is generally more stable for transient, shock-driven flows and can yield more precise results in such dynamic scenarios. This makes it a suitable option for analyzing decompression and turbulent jet dispersion.

The least squares cell based was used for gradient. This is an accurate method which is used for calculating variable gradients. It minimizes errors in the gradient approximation by using the least squares approach and it is suitable for complex or irregular mesh structures. The application of this method helps to ensure a more accurate and reliable solution is achieved. This technique provides better accuracy in comparison to alternative approaches including node based and cell based Green-Gauss.

As illustrated in Figure 20, the second order upwind system was used for flow, turbulent dissipation rate and kinetic energy, and due to having higher accuracy and reduced numerical diffusion compared to first order systems. It efficiently captures complex flow features and turbulence dynamics, to provide a more reliable and detailed solution. By considering a variety of cell shapes, it decreases approximation errors and improves the resolution of

gradients. Furthermore, this system is well-suited for simulations that involve complex flow trends.

The first order implicit scheme is selected for transient formulation due to its stability and computational efficiency. Although it is less accurate than higher-order schemes, it is capable of handling larger time steps without stability issues, and this makes it the suitable choice for many transient simulations. This method is useful for preliminary studies and where computational resources are limited.

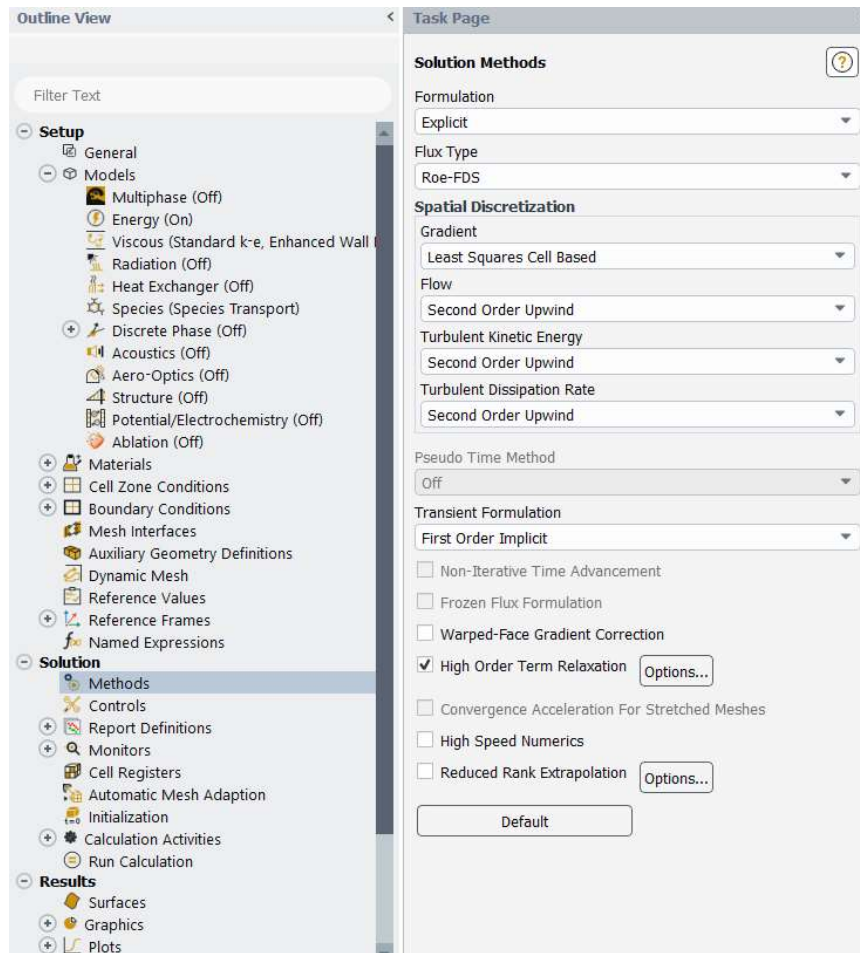


Figure 20 – ANSYS Fluent Solution Methods settings.

3.1.5.2 Turbulence Model

When a CO₂ pipeline ruptures or a leak initiates, the conditions at the leak point or rupture location changes from zero flow and zero Mach number prior to the leak initiation or rupture taking place to high velocity potentially sonic flow. In this scenario the flow becomes turbulent flow once Reynolds number reaches a specific value, making wall shear conditions within the pipeline a key parameter. Ansys Fluent provides several options for the accurate modelling of turbulence inside a pipeline. Amongst those k- ϵ is one of the most commonly used two equation models.

The k- ϵ model is selected for this simulation as it offers efficiency in computation and its accuracy is acceptable for turbulent flows. The selected model is a two-equation viscous model that solves two separate equations. It consists of an equation for the rate of dissipation of turbulent kinetic energy (ϵ) and a second equation for the turbulent kinetic energy (k). These equations consider the impacts of turbulence on the flow and are used for the calculation of turbulent viscosity. To maintain accuracy at areas adjacent to the wall, this turbulence model needs the incorporation of damping functions. These functions are crucial for guaranteeing the validity of the model extends into the viscous sublayer, restricting the performance of K and ϵ at the boundary (Blazek 2015b).

In Ansys there are three variations for the k- ϵ turbulence including standard k- ϵ model, the Realizable k- ϵ model, and the RNG k- ϵ model. It is worth noting that in flows where significant pressure variations are present the accuracy of the k- ϵ model reduces. Understanding the limitations of the k- ϵ model and its performance in different flow conditions is critical. Tang et al. (2023) performed a study that examined the influence of model parameters on accuracy across various pressure gradients.

3.1.5.3 Standard k-epsilon model:

- The standard k- ϵ turbulence model represents the original formula of this model.
- In this model a constant turbulent viscosity is assumed throughout the flow domain and is a popular model used due to its simplicity and computational efficiency.

3.1.5.4 RNG (Renormalization Group) k- ϵ model:

- The model includes a correction based on renormalization group theory to consider the near-wall behavior of turbulence and improve predictions in areas where pressure increases in the direction of flow leading to increased turbulence and more complex flow behavior (Sun et al. 2005).
- The RNG k- ϵ model tends to deliver accurate results, especially in complex flows near walls or regions with strong pressure gradients.

3.1.5.5 Realizable k- ϵ model:

- This model addresses some of the limitations that exist in the standard model by applying additional realizability constraints on the model coefficients, to ensure that the model simulations are physically meaningful.
- The model provides good turbulence predictions where the simulation involves flow behaviors around complex geometries and boundary conditions.

For this problem, standard k- ϵ model is utilised because of its simplicity, computational efficiency as well as the simple geometry being analysed. The enhanced wall treatment was turned on to improve the accuracy of turbulence modeling adjacent to the walls. This approach helps to better capture the effects of the areas near the wall on the overall flow, and to make the simulations more precise by improving the resolution and behavior of the

turbulence model near the boundaries. Figure 21 illustrates the Viscous Model settings of the simulation model.

Viscous Model

Model

- ☐ Inviscid
- ☐ Laminar
- ☐ Spalart-Allmaras (1 eqn)
- ☒ k-epsilon (2 eqn)
- ☐ k-omega (2 eqn)
- ☐ Transition k-k-omega (3 eqn)
- ☐ Transition SST (4 eqn)
- ☐ Reynolds Stress (5 eqn)
- ☐ Scale-Adaptive Simulation (SAS)
- ☐ Detached Eddy Simulation (DES)

k-epsilon Model

- ☒ Standard
- ☐ RNG
- ☐ Realizable

Near-Wall Treatment

- ☐ Standard Wall Functions
- ☐ Scalable Wall Functions
- ☐ Non-Equilibrium Wall Functions
- ☒ Enhanced Wall Treatment
- ☐ Menter-Lechner
- ☐ User-Defined Wall Functions

Enhanced Wall Treatment Options

- ☐ Pressure Gradient Effects
- ☐ Thermal Effects

Options

Buoyancy Effects: Only Turbulence Production

- ☒ Viscous Heating
- ☐ Compressibility Effects
- ☐ Production Kato-Launder
- ☐ Production Limiter

Model Constants

Cmu: 0.09

C1-Epsilon: 1.44

C2-Epsilon: 1.92

TKE Prandtl Number: 1

TDR Prandtl Number: 1.3

Energy Prandtl Number: 0.85

Wall Prandtl Number: 0.85

User-Defined Functions

Turbulent Viscosity: none

Prandtl and Schmidt Numbers

TKE Prandtl Number: none

TDR Prandtl Number: none

Energy Prandtl Number: none

Wall Prandtl Number: none

Turbulent Schmidt Number: none

Scale-Resolving Simulation Options

☐ Stress Blending (SBES) / Shielded DES

OK Cancel Help

Figure 21 - ANSYS Fluent Viscous Model settings for k-epsilon.

3.1.6 Equation of State implementation

In order to accurately simulate CO₂ behaviour during the decompression process, implementing a real-gas equation of state is a key (Wang et al. 2024). Several cubic equations of state are available in Ansys Fluent making it easy to implement a built-in EOS.

These EOSs include Soave-Redlich-Kwong (SRK), Redlich-Kwong (RK), and Peng-Robinson (PR).

The objective of this 2D simulation is to analyse the thermodynamic behaviour of gaseous CO₂ in its dense phase during release from a high pressure pipeline. To accurately represent this behaviour, it was determined to select the Peng-Robinson EOS for the simulation. The use of the PR EOS allows for a realistic simulation of CO₂ properties under high pressure conditions, and this provides an insight into the behaviour of CO₂ jets upon release. Figure 22 shows the CO₂ properties as modelled by the PR EOS for real gas conditions.

The screenshot displays the 'Create/Edit Materials' window in ANSYS Fluent. The material is named 'carbon-dioxide' with the chemical formula 'co2'. It is classified as a 'fluid' and 'Fluent Fluid Materials'. The equation of state (EOS) selected is 'real-gas-peng-robinson'. The 'Order Materials by' section shows 'Name' selected. The 'Properties' section lists various thermophysical properties with their units, models, and values:

Property	Unit	Model	Value
Density	[kg/m ³]	real-gas-peng-robinson	
Cp (Ideal Specific Heat)	[J/(kg K)]	piecewise-polynomial	
Thermal Conductivity	[W/(m K)]	constant	0.0145
Viscosity	[kg/(m s)]	power-law	
Molecular Weight	[kg/kmol]	constant	44.00995
Standard State Entropy	[J/(kgmol K)]	constant	213720.2
Reference Temperature	[C]	constant	25
Critical Temperature	[C]	constant	30.97
Critical Pressure	[Pa]	constant	7374000
Critical Specific Volume	[m ³ /kg]	constant	0.002137
Acentric Factor		constant	0.225

Figure 22 – Properties of CO₂ in ANSYS Fluent.

3.1.7 Miscellaneous Settings

3.1.7.1 Residuals:

Residuals are a measure of convergence in the iterative solution process of computational fluid dynamics (CFD) simulations. At each iteration they calculate the thermodynamic properties of the fluid and compare these with the exact values derived from the governing equations. Fundamentally, residuals represent the errors in approximating the solution (Blazek 2015a). For this study the convergence condition was specified as residuals must reach values equal or less than $1e-3$ as illustrated in Figure 23.

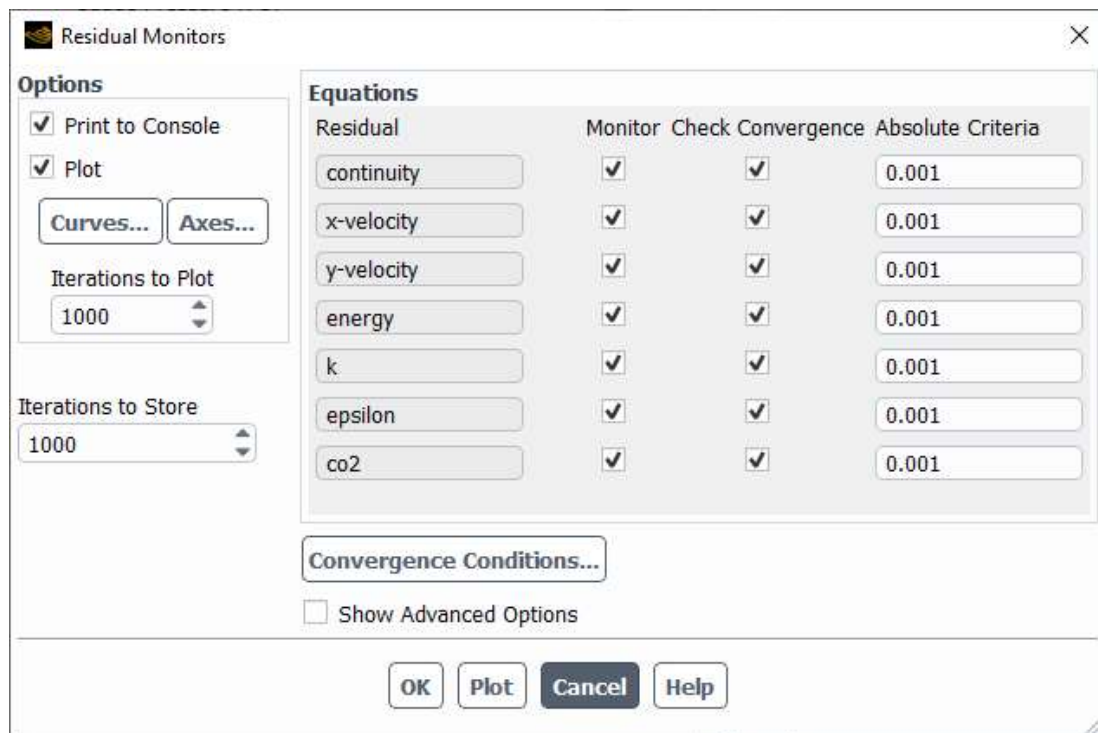


Figure 23 - ANSYS Fluent Residual Monitors.

3.1.7.2 Initialization:

Initialization is essentially a starting point for the iterative solver. The initial guess affects how efficiently and quickly the solver converges to the final solution. For this simulation

standard initialization was used with air being the primary fluid within the main domain to represent atmospheric conditions.

As presented in Figure 24, all initial values were set to zero, with the exception of temperature which was set to 20°C and the computation was performed across all zones.

Task Page

Solution Initialization

Initialization Methods

☐ Hybrid Initialization

☒ Standard Initialization

Compute from

All-zones

Reference Frame

☒ Relative to Cell Zone

☐ Absolute

Initial Values

U

Axial Velocity [m/s]

0

Radial Velocity [m/s]

0

Turbulent Kinetic Energy [m²/s²]

0

Turbulent Dissipation Rate [m²/s³]

0

co2

0

Temperature [C]

20

Initialize Reset Patch... Species

Reset DPM Sources Reset LWF Reset Statistics

VOF Check

Figure 24 – Initialization settings in ANSYS Fluent.

As shown on Figure 25, to represent the initial conditions more accurately, I patched the inlet region with CO₂ at the pressure of 6 atmosphere (506,625 Pa). The mass fraction of CO₂ was patched as one to indicate the inlet contains pure CO₂ only. This adjustment ensures

that the initial conditions of the inlet region are exactly defined and provides a realistic representation for the simulation analysis.

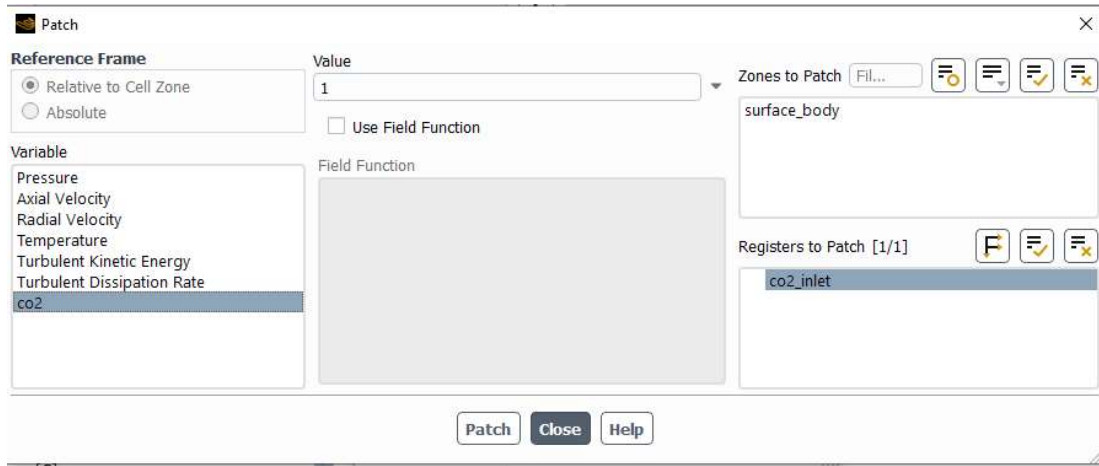


Figure 25 - ANSYS Fluent, patching the inlet conditions.

3.1.7.3 Run Calculation:

This dialog box is where the time advancement and calculation process for a transient simulation in ANSYS Fluent is configured and initiated. It provides options to set the time step size, the number of time steps, and the maximum number of iterations for each time step to achieve convergence. The time step size was defined as 1e-6 seconds. This controls the duration between each calculation in the simulation and allows for accurate modelling of changes in flow variables. The number of time steps was progressively increased to ensure the solution is refined and finer details are captured in the solution. The Max Iterations/Time Step parameter was set to 20 to ensure that the solution iteratively approaches convergence within each time step. For a transient high pressure CO₂ release simulation, the ‘number of time steps’ X ‘time step size’ represents the actual simulation time. For example, to simulate 4ms, you would set the number of time steps to 4000.

Additionally, the Reporting Interval and Profile Update Interval are set to 5 and 2, respectively to ensure that data is recorded and boundary conditions are updated at specified intervals. As illustrated in Figure 26, these settings are important for managing the accuracy and efficiency of the simulation process.

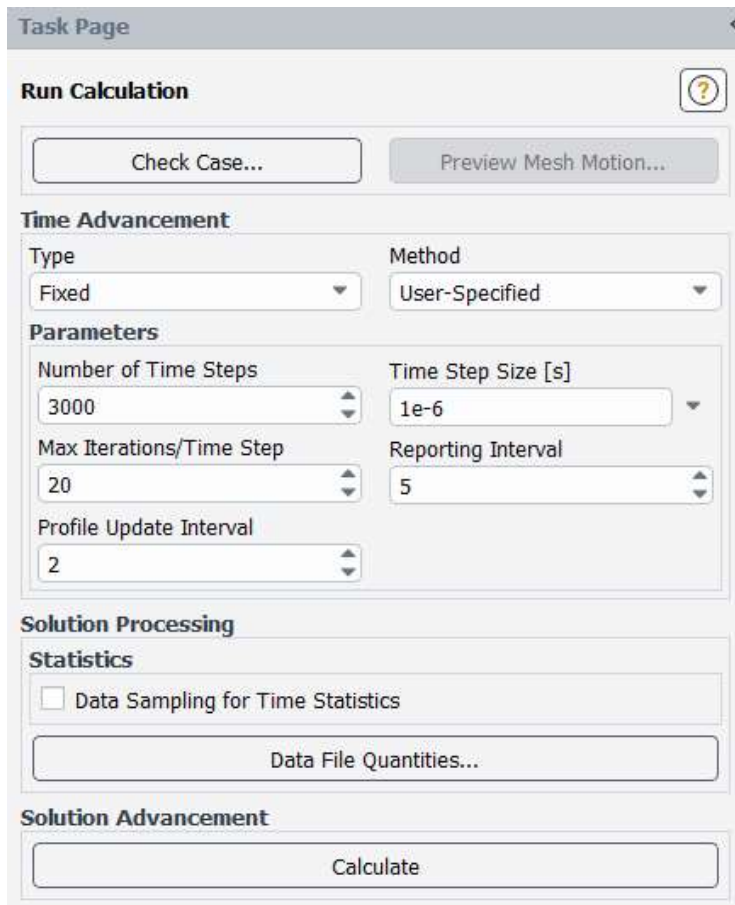


Figure 26 – ANSYS Fluent, run calculation settings.

3.1.7.4 Residuals Plot:

Figure 27 illustrates the convergence behaviour of various flow variables during the simulation. The plot tracks the residuals for velocity, continuity, energy, turbulence parameters, and CO₂ concentration over the number of iterations. The trends show how these variables approach a stable solution, with the residuals generally decreasing as the

simulation progresses. The goal is for the residuals to reach sufficiently low values, which indicates that the solution is converging and that the simulation results are reliable.

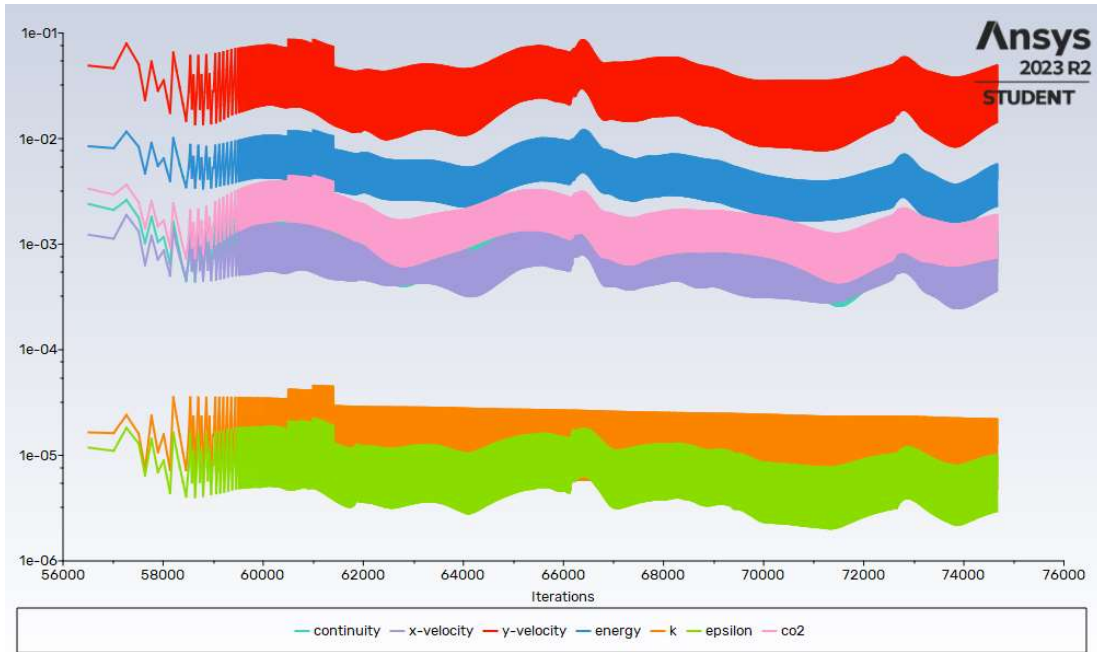


Figure 27 –Convergence behavior of various flow variables during the simulation.

3.2 CO₂ DISPERSION ANALYSIS IN A COMPLEX ENVIRONMENT

The computational domain, as shown in Figure 28, represents the details of the 3D domain which was modelled to simulate the dispersion of CO₂ within an environment where front and rear are subject to atmospheric conditions. The domain is modeled as a rectangular box with length of 15 meters, the width of 6.4 meters, and the height of 5.2 meters. This geometry is designed to capture the flow dynamics of CO₂ as it is released into the air and disperses within the space.

3.2.1 Model Assumptions

The current decompression model was produced on the basis of the following assumptions:

- This study is limited to analysing the behaviour of gaseous CO₂.
- The CO₂ is assumed to be 100% pure, without any interference from other gases or impurities.
- Simulation of CO₂ pipeline leak and release of fluid.
- 'no-slip' condition is assumed between the fluid and the ground.
- The leak is assumed to be vertical and originates at ground level.
- To simplify the simulation, potential phase change during the release are not considered.
- A power-law relationship is applied to model wind velocity changes with height, assuming a stable atmospheric boundary layer.

3.2.2 Purpose and Functionality of the Domain

The domain includes several surfaces, each representing different boundaries where specific conditions are applied. The front face of the domain includes two inlets: the CO₂ inlet and the air inlet. The CO₂ inlet is positioned at ground level, centerline of the domain and 1 meter from the front face and is modeled as a circular hole with a diameter of 20 mm. This inlet represents the point where CO₂ is introduced into the domain at various flowrates. The air inlet, located at the front, simulates the wind entering the domain at velocities calculated using a power law relation. This will allow the mixing and dispersion of the CO₂ towards the outlet in the rear.

The top wall and side wall boundaries are set up as symmetry to ensure there are no changes in velocity, pressure, or other variables across these boundaries. This setup prevents any flux such as mass or momentum across these walls, essentially mirroring the flow and ensuring the domain boundaries do not affect the flow field within the simulated area.

Two scenarios of CO₂ release will be simulated with flowrates of 10 m³/h and 12 m³/h. The size and shape of the domain are selected to allow adequate space for the CO₂ to interact with the incoming air and disperse. As shown in Figure 28, the 15 meter length of the domain was selected to ensure that the simulation can capture the full extent of the mixing of CO₂ with air over a realistic distance.

The inclusion of both CO₂ and air inlets allows for the study of various scenarios, such as the impact of airflow on CO₂ dispersion and the potential formation of hazardous concentrations of CO₂ within the domain. This setup is important for understanding the behavior of CO₂ leaks, which is critical for risk assessment and the development of safety protocols.

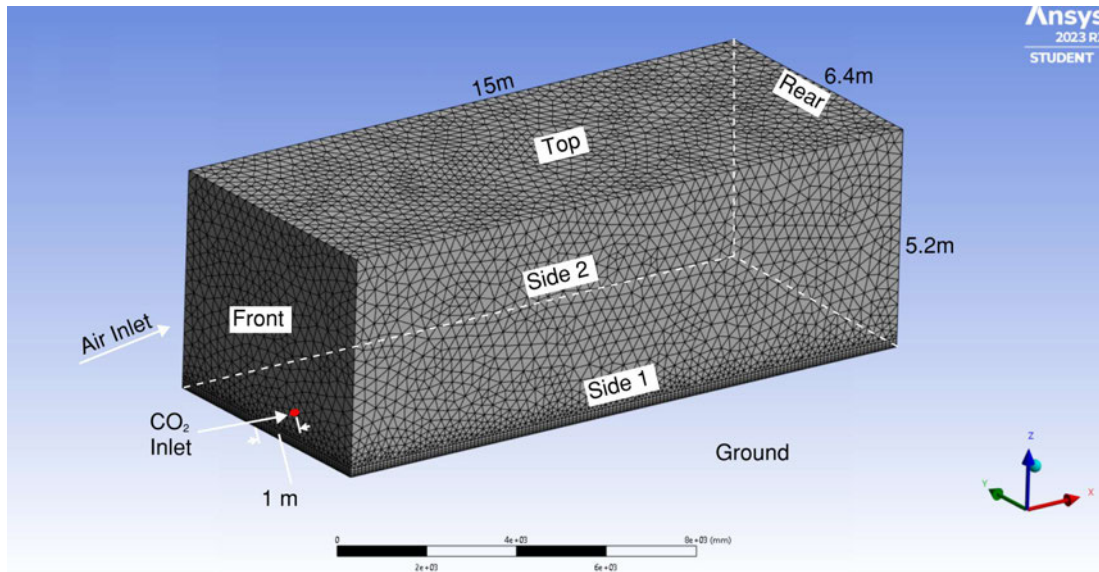


Figure 28 - Computational domain for CO₂ dispersion simulation.

3.2.3 Boundary Conditions for the 3D Simulation

The boundary conditions that are defined in the 3D simulation are summarized in Table 1. These conditions are important for modelling the behavior of CO₂ as it is released from the high pressure pipeline and interacts with the ambient air. Initially, the CO₂ is assumed to be 100% pure before it begins mixing with the air within the domain. This assumption ensures that the simulation focuses on the dispersion characteristics of pure CO₂ as it enters the environment.

Based on Figure 2 – phase diagram of CO₂, we know that CO₂ exists in the gaseous phase under the following conditions:

- Temperatures above 217 K (-56.4°C) and below 305.4 K (31.0°C), at pressures lower than the critical point of 7.38 MPa.
- In the ideal Gas Region, where CO₂ behaves like an ideal gas, typically at low pressures below 0.5 MPa and higher temperatures above 300 K.

3.2.3.1 CO₂ Inlet Boundary Condition

The boundary conditions are selected to guarantee that CO₂ remains in the gaseous phase and within the ideal gas region throughout the simulation. By controlling both the temperature and pressure within specific ranges, keeping the temperature between 217 K (-56.4°C) and 305.4 K (31.0°C) and maintaining the pressure at atmospheric pressure, below the critical point of 7.38 MPa. This is to ensure that CO₂ does not transition to a liquid or solid state. Additionally, by operating in the ideal gas region at low pressures (below 0.5 MPa) and higher temperatures (above 300 K), CO₂ will behave as an ideal gas within the system.

Using the ideal gas formula, the behavior of CO₂ after dispersion can be predicted. Since CO₂ has a molar weight of 44 g/mol compared to molar weight of air 29 g/mol, it is considerably heavier. As a result, CO₂ will tend to sink and stay closer to the ground compared to lighter gases. The temperature difference between CO₂ and the surrounding air can also influence buoyancy forces. In this simulation CO₂ is cooler than the ambient air, and so it will tend to stay closer to the ground due to negative buoyancy. Conversely, if it is warmer, it might rise more quickly. In the simulation, CO₂ is introduced into the domain with a wind speed calculated using power law. The wind will carry the CO₂ horizontally, but its vertical motion will depend on its density relative to the surrounding air and any thermal effects. The temperature of CO₂ directly affects its density through the ideal gas law:

$$\rho = \frac{p}{RT} \quad (3.3)$$

In this equation:

- ρ represents density
- p represents pressure

- R represents specific gas constant
- T represents temperature in Kelvin

The CO₂ source is represented by a 20 mm diameter inlet and is also modeled as a velocity inlet, with CO₂ introduced at a temperature of 277K and at the flow rates of 10 m³/h and 12 m³/h, corresponding to approximate velocities of 8.8 m/s for 10 m³/h and 10.6 m/s for 12 m³/h flowrates.

As illustrated in Figure 29 velocity magnitude is applied, which represents the initial speed of the CO₂ as it releases and enters the domain. The "Magnitude, Normal to Boundary" specification ensures that the CO₂ flow aligns perpendicularly to the boundary.

The CO₂ temperature is set to 277 K, approximating the expected temperature of the CO₂ during release. This temperature helps simulate realistic thermal interactions between the CO₂ and the ambient air. Furthermore, the species boundary condition specifies a CO₂ mass fraction of 1.0, which indicates that pure CO₂ enters the domain through this boundary without any air or other gases. This setup allows for clear tracking of CO₂ dispersion patterns in the simulation.

The default turbulence settings remain unchanged. These are set to improve the simulation accuracy in capturing the CO₂ spread and mixing behavior. Using an "Intensity and Viscosity Ratio" method, a viscosity ratio of 10 and a turbulent intensity of 5% are defined.

Velocity Inlet

Zone Name
inlet_co2

Momentum Thermal Radiation Species DPM Multiphase Potential Structure UDS

Velocity Specification Method: Magnitude, Normal to Boundary

Reference Frame: Absolute

Velocity Magnitude [m/s]: 8.8

Supersonic/Initial Gauge Pressure [Pa]: 0

Outflow Gauge Pressure [Pa]: 0

Turbulence

Specification Method: Intensity and Viscosity Ratio

Turbulent Intensity [%]: 5

Turbulent Viscosity Ratio: 10

Apply Close Help

Figure 29 - Model settings for CO₂ inlet boundary condition.

3.2.3.2 Air Inlet Boundary Condition

Wind velocity is a critical factor in the study of heavy gas dispersion, as it directly influences how gases like CO₂ disperse in the atmosphere. In outdoor environments, wind rarely flows uniformly due to factors like surface friction, obstacles, and terrain. To model this more accurately, a power-law profile is often applied to represent the difference of wind velocity with height increase in the boundary layer. This approach has been used by several researchers, including (Xing et al. 2013), and (Liu et al. 2014), to model the impact of wind on the dispersion of gas.

The wind velocity at different heights (U_z) is expressed as a function of a reference wind speed (U_1) at a specific height (Z_1), with the stability exponent (p) which accounts for atmospheric stability effects. This approach allows for a more realistic simulation of wind

behavior, especially for studies involving ground-level releases like CO₂ leaks from pipelines or gas facilities (Xing et al. 2013).

$$U_z = U_1 * \left(\frac{Z}{Z_1}\right)^P \quad (3.4)$$

Xing et al. (2013) in their study, calculated a wind speed of 0.6 m/s based on field measurements of 0.37 m/s at 2 meters above ground level, with a stability class "F" which indicates highly stable atmospheric conditions. Such conditions are typical in suburban or rural areas at night, when stable air layers prevent mixing, causing gases to stay closer to the ground. This slow wind speed, combined with the atmospheric stability, helps accurately simulate CO₂ behavior under similar conditions, such as low wind velocities resulting in limited dispersion, which creates potential risk zones around the release site.

As shown in Figure 30, I developed a User-Defined Function (UDF) in ANSYS Fluent to implement the wind velocity profile in the CFD model. The UDF calculates and assigns wind velocity based on height, using the power-law relation discussed earlier for boundary layer flow. This will allow a realistic wind profile in the CFD simulation. This custom function helped to capture the influence of wind on CO₂ dispersion with higher accuracy.

```

#include "udf.h"

/* Define the power-law velocity profile for wind */
DEFINE_PROFILE(wind_velocity_profile, thread, nv)
{
    real z;          // Height coordinate
    real z_r = 2.0;  // Reference height in meters
    real u_r = 0.6;  // Reference velocity at height z_r (in m/s)
    real alpha = 0.3; // Wind shear exponent
    real velocity;    // Calculated velocity
    real xyz[ND_ND];  // Array to hold the centroid coordinates

    face_t f; // Loop over each face in the boundary

    begin_f_loop(f, thread)
    {
        F_CENTROID(xyz, f, thread); // Get the coordinates of the face centroid
        z = xyz[2]; // Z-coordinate (assuming 3D model)

        if (z > 0.0) {
            velocity = u_r * pow((z / z_r), alpha); // Power-law equation
            F_PROFILE(f, thread, nv) = velocity; // Assign the calculated velocity
        }
        // Do nothing if z <= 0.0 and let Fluent's default wall condition (no-slip) apply.
    }
    end_f_loop(f, thread)
}

```

Figure 30 – UDF script to define a power-law velocity profile for wind.

The front surface of the domain is defined as a velocity inlet for air. This will ensure a consistent flow of air into the simulation space. The air temperature at the inlet is set to 293K (approximately 20°C), representing typical ambient conditions. This temperature setting helps create realistic thermal interactions between the CO₂ and surrounding air which allows the simulation to more accurately reflect how CO₂ disperses in typical outdoor environments. Additionally, the species boundary condition is set with a CO₂ mass fraction of 0.0, and this indicates that only pure air enters through this boundary.

To capture the natural turbulence of the incoming air, the default turbulence settings remain unchanged. These settings reflect realistic atmospheric conditions. Figure 31 shows the air inlet settings.

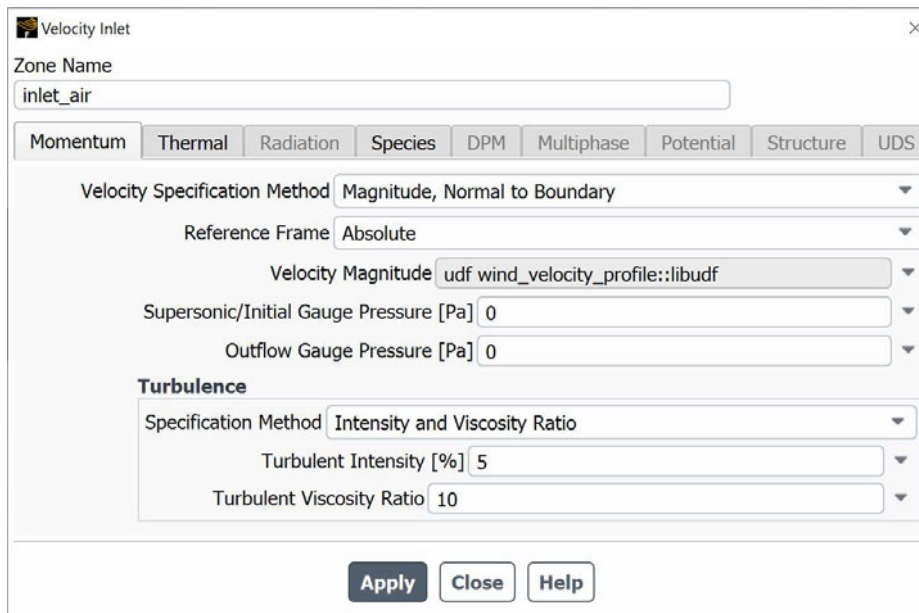


Figure 31 - Model settings for Air inlet boundary condition.

3.2.3.3 Wall Boundary Condition

The ground boundary is defined as wall with no-slip enabled to simulate the frictional interaction with a solid surface. This boundary condition is important in capturing realistic flow dynamics, particularly because CO₂ is heavier than air. As a result, CO₂ tends to accumulate near the ground when released, which influences the dispersion pattern as it spreads horizontally and mixes with air. The no-slip condition on the ground simulates how the CO₂ interacts with the surface and slowing down due to friction and creating a grounded layer of gas that behaves similarly to real-world conditions.

As displayed in Figure 32, a roughness model is applied with a roughness height of 0.005 m and a roughness constant of 0.5 to simulate realistic ground interaction effects.

The ground wall temperature is set to 293 K (20°C), assuming it remains constant throughout the simulation. The ground surface is modeled with soil properties, which influence the thermal behavior and interaction between CO₂ and the ground.

Wall

Zone Name
wall_ground

Adjacent Cell Zone
domain

Momentum Thermal Radiation Species DPM Multiphase UDS Potential Structure Ablation

Wall Motion

☒ Stationary Wall
☐ Moving Wall

Motion
☒ Relative to Adjacent Cell Zone

Shear Condition

☒ No Slip
☐ Specified Shear
☐ Specularity Coefficient
☐ Marangoni Stress
☐ Partial Slip for Rarefied Gases

Wall Roughness

Roughness Models
☒ Standard
☐ High Roughness (Icing)

Sand-Grain Roughness
Roughness Height [m] 0.005
Roughness Constant 0.5

Apply Close Help

Figure 32 - Model settings for Wall boundary condition.

3.2.3.4 Symmetry Boundary Condition

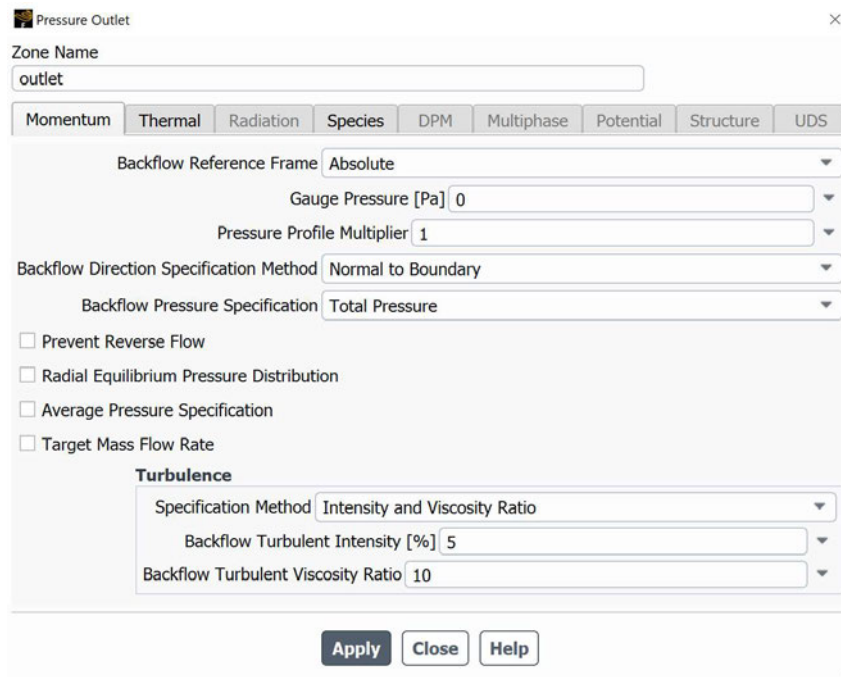
The top, left and right surfaces of the domain are defined as symmetry. In ANSYS Fluent, boundaries defined as symmetry mean that variables have no normal velocity and no gradient, which essentially makes them impermeable. This setup simulates an idealized open environment and allows the CO₂ flow to reflect symmetrically without any influence from external factors beyond the simulation domain.

3.2.3.5 Outlet Boundary Condition

In the 3D domain, the rear surface is defined as a pressure outlet, and the pressure is at atmospheric pressure. This will allow for the free exit of gases from the domain, which is important for maintaining realistic flow dynamics throughout the simulation.

The "Total Pressure" setting ensures that the pressure distribution across the outlet remains consistent with natural atmospheric conditions, to simulate an open environment for the CO₂ to disperse.

To account for any backflow conditions that may arise, the temperature is set at 293 K (20°C), which represents the ambient air temperature. The species mass fraction for CO₂ is set to 0 at the outlet, which indicates that only ambient air is expected to flow back if there is any reverse flow. As per other boundary conditions, the turbulence settings remain unchanged. Figure 33 shows the outlet boundary configuration for the simulation.



The screenshot shows the 'Pressure Outlet' dialog box with the following settings:

- Zone Name:** outlet
- Backflow Reference Frame:** Absolute
- Gauge Pressure [Pa]:** 0
- Pressure Profile Multiplier:** 1
- Backflow Direction Specification Method:** Normal to Boundary
- Backflow Pressure Specification:** Total Pressure
- ☐ Prevent Reverse Flow
- ☐ Radial Equilibrium Pressure Distribution
- ☐ Average Pressure Specification
- ☐ Target Mass Flow Rate
- Turbulence:**
 - Specification Method:** Intensity and Viscosity Ratio
 - Backflow Turbulent Intensity [%]:** 5
 - Backflow Turbulent Viscosity Ratio:** 10

Buttons at the bottom: Apply, Close, Help.

Figure 33 - Model settings for outlet boundary condition.

Table 1 illustrated the boundary and initial conditions for this complex 3D simulation setup, and it details the parameters and their respective configurations for air and CO₂ inlets, wall roughness, pressure outlets, and temperature settings.

Table 1 –Boundary conditions

Parameters	Setup
Top, side 1 and side 2 surfaces	Symmetry
Front surface	Velocity inlet (air)
Bottom (ground)	Wall
CO ₂ Inlet	Velocity inlet
Rear Surface	Pressure outlet
Temperature of air	293 K (~ 20 °C)
Temperature of CO ₂	277 K (~ 4 °C)
CO ₂ flowrates (converted velocity)	10 m ³ / h (8.85 m/s), 12 m ³ / h (10.6 m/s)

3.2.4 Mesh Details

The computational domain was discretised using a tetrahedral mesh, as shown in Figure 34. This type of mesh was selected due to its ability to model complex geometries and flow patterns effectively. To improve accuracy in critical areas, particularly around the CO₂ inlet and near the ground, a finer mesh resolution was applied. Additionally, inflation layers were

incorporated to gradually refine the mesh near the ground surface. This refinement allows for a more precise capture of CO₂ concentration and velocity behaviour at ground level and downstream of the inlet, where higher concentrations and velocities are expected. Accurate simulation of the mixing between CO₂ and air in these regions is critical for this study. The updated mesh consists of 93,011 nodes and 294,716 elements, to produce a detailed representation of the flow domain and achieve consistent simulation results.

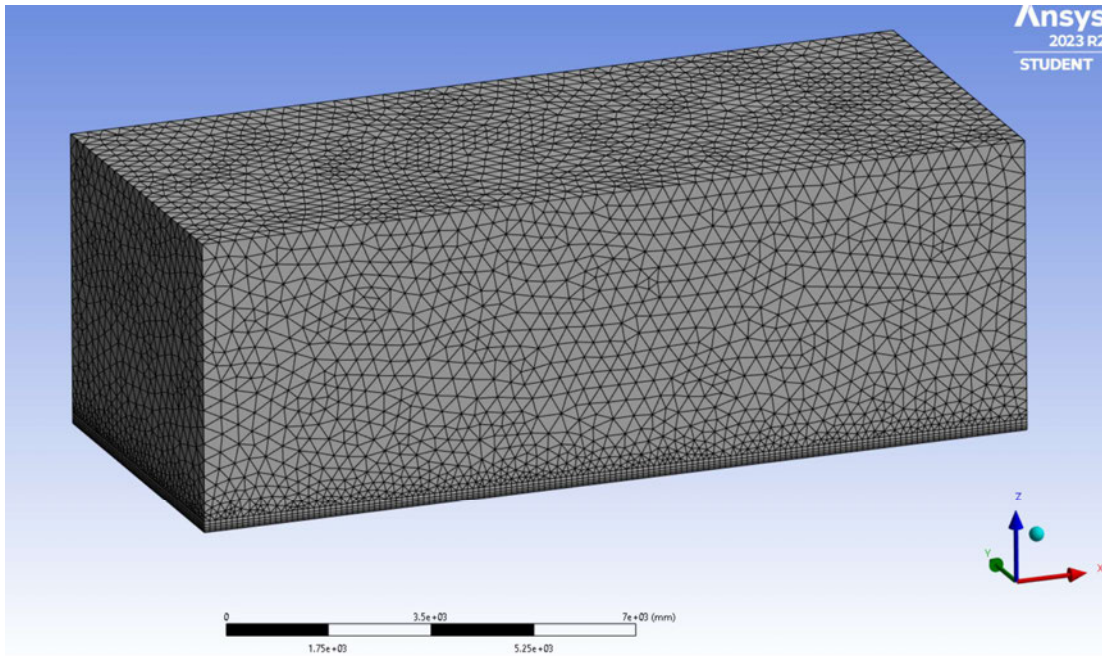


Figure 34 – mesh details for the 3D dispersion model

3.2.5 Solver Type and Solution settings

In this 3D simulation, the same density-based solver which was implemented in the 2D simulation was selected. Furthermore, for this 3D simulation, the implicit solver was chosen due to its stability and ability to accept larger time step sizes compared to the explicit method. Although the implicit solver requires more computational resources, it computes velocity, pressure, and temperature across the entire mesh in parallel, to have a more stable

solution for transient simulations with high-speed flows like CO₂ dispersion. The implicit method also allows for faster convergence and better handling of the rapid pressure and temperature changes associated with CO₂ releases.

3.2.5.1 Spatial Discretization:

In the 3D simulation, spatial discretization plays a key role in accurately solving the governing equations for CO₂ dispersion. As illustrated in Figure 35, for flow variables the second order upwind was used, including velocity, turbulent kinetic energy, and specific dissipation rate. For high speed flows it is important to take this approach, as it provides better accuracy in capturing changes in flow and ensures the stability of the solution.

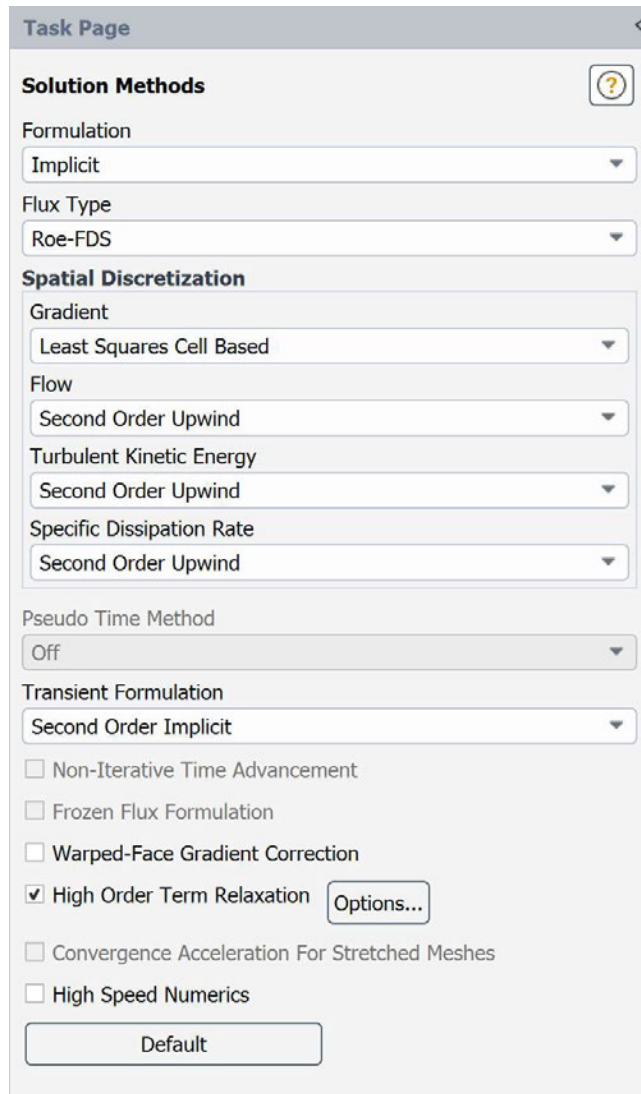


Figure 35 – ANSYS Fluent Solution Methods settings.

3.2.5.2 Turbulence Model

In CO₂ release scenarios, such as a pipeline leak, the flow transitions from zero velocity to high-speed. As the flow velocity increases, the Reynolds number rises, making turbulence modelling critical for accurate simulation. For the 3D simulation, it was decided to use the k-omega ($k-\omega$) SST turbulence model as it offers better accuracy in predicting flows with strong significant pressure changes, near-wall behaviour, and complicated boundary layer dynamics, which are important in such CO₂ dispersion simulations (Blazek 2015b).

The $k-\omega$ model consist of two-equations that calculates turbulent kinetic energy (k) and dissipation rate (ω), which accounts for the scale of turbulence. This model shows better performance near walls and where flow separation occurs. This makes the $k-\omega$ model suitable for this scenario where CO_2 is released from an inlet and interacts with the surrounding air.

In particular, in this simulation it was determined to use the SST (Shear Stress Transport) $k-\omega$ model. The SST formulation has the benefits of both $k-\epsilon$ model and $k-\omega$ model by mixing them. Near the walls, $k-\omega$ model provides accurate predictions, and the $k-\epsilon$ formulation is used in the main flow stream, and this improves the overall accuracy and stability for high-speed flow simulations such as the 2D simulation of CO_2 jet.

To further refine the accuracy of the turbulence model, viscous heating was enabled, which considers the additional heating effects due to viscosity at high velocities. Production Limiter was also activated to avoid over-prediction of turbulence production in regions of strong gradients.

Near-wall treatment was set to correlation-based wall functions, which enhances the model's ability to handle boundary layer effects in the region where CO_2 interacts with the walls and ground. Figure 36Figure 43 shows the 3D simulation settings under viscous model.

Viscous Model

Model

- ☐ Inviscid
- ☐ Laminar
- ☐ Spalart-Allmaras (1 eqn)
- ☐ k-epsilon (2 eqn)
- ☒ k-omega (2 eqn)
- ☐ Transition k-kl-omega (3 eqn)
- ☐ Transition SST (4 eqn)
- ☐ Reynolds Stress (7 eqn)
- ☐ Scale-Adaptive Simulation (SAS)
- ☐ Detached Eddy Simulation (DES)
- ☐ Large Eddy Simulation (LES)

k-omega Model

- ☐ Standard
- ☐ GEKO
- ☐ BSL
- ☒ SST

k-omega Options

☐ Low-Re Corrections

Near-Wall Treatment

correlation

Options

Buoyancy Effects: Only Turbulence Production

- ☒ Viscous Heating
- ☐ Curvature Correction
- ☐ Corner Flow Correction
- ☐ Production Kato-Launder
- ☒ Production Limiter

Transition Options

Transition Model: none

Model Constants

Alpha*_inf: 1

Alpha_inf: 0.52

Beta*_inf: 0.09

a1: 0.31

Beta_i (Inner): 0.075

Beta_i (Outer): 0.0828

TKE (Inner) Prandtl #: 1.176

User-Defined Functions

Turbulent Viscosity: none

Prandtl and Schmidt Numbers

Energy Prandtl Number: none

Wall Prandtl Number: none

Turbulent Schmidt Number: none

Scale-Resolving Simulation Options

☐ Stress Blending (SBES) / Shielded DES

OK Cancel Help

Figure 36 - Viscous Model properties for k-omega.

3.2.6 Equation of State implementation

The is modeling of CO₂ dispersion is critical in understanding how far and in what concentration CO₂ may spread following a high pressure release. The simulation provides

understanding of the behavior of CO₂ when treated as an ideal gas, and it considers interactions with environmental factors such as atmospheric pressure, ambient temperature, and wind velocity. Additionally, operational conditions such as the pipeline's initial pressure and temperature also influence the dispersion characteristics. These variables play a key role in determining the extent and risk areas surrounding a potential CO₂ leak, which are essential for effective safety assessments and mitigation strategies.

For the purposes of this study, an incompressible ideal gas model was used for both air and CO₂ to simplify the representation of CO₂. However, more complex EOS alternatives such as Peng-Robinson (PR), Soave-Redlich-Kwong (SRK), or Redlich-Kwong (RK) can often be implemented to predict the behavior of real gas, the incompressible ideal gas assumption is sufficient for this simulation given the specific flow characteristics and the conditions being analysed. The CO₂ properties for incompressible ideal gas are illustrated in Figure 37.

The screenshot shows the 'Create/Edit Materials' dialog box in Ansys Fluent. The 'Name' field is 'carbon-dioxide' and the 'Chemical Formula' is 'co2'. The 'Material Type' is set to 'fluid', and the 'Fluent Fluid Materials' dropdown is set to 'carbon-dioxide (co2)'. The 'Mixture' dropdown is set to 'none'. The 'Order Materials by' section has 'Name' selected. The 'Properties' section shows the following values:

Property	Value
Density [kg/m ³]	incompressible-ideal-gas
Cp (Specific Heat) [J/(kg K)]	constant
Thermal Conductivity [W/(m K)]	constant
Viscosity [kg/(m s)]	constant
Molecular Weight [kg/kmol]	constant

The values for the constant properties are: Cp = 840.37, Thermal Conductivity = 0.0145, Viscosity = 1.37e-05, and Molecular Weight = 44.00995. The dialog box includes buttons for 'Change/Create', 'Delete', 'Close', and 'Help'.

Figure 37 – properties of CO₂ in Ansys Fluent

3.2.7 Miscellaneous Settings

3.2.7.1 Residuals:

Residuals are a measure of convergence in the iterative solution process of computational fluid dynamics (CFD) simulations. For this 3D simulation the convergence condition was specified as residuals must reach values equal or less than $1e-4$ as illustrated in Figure 38.

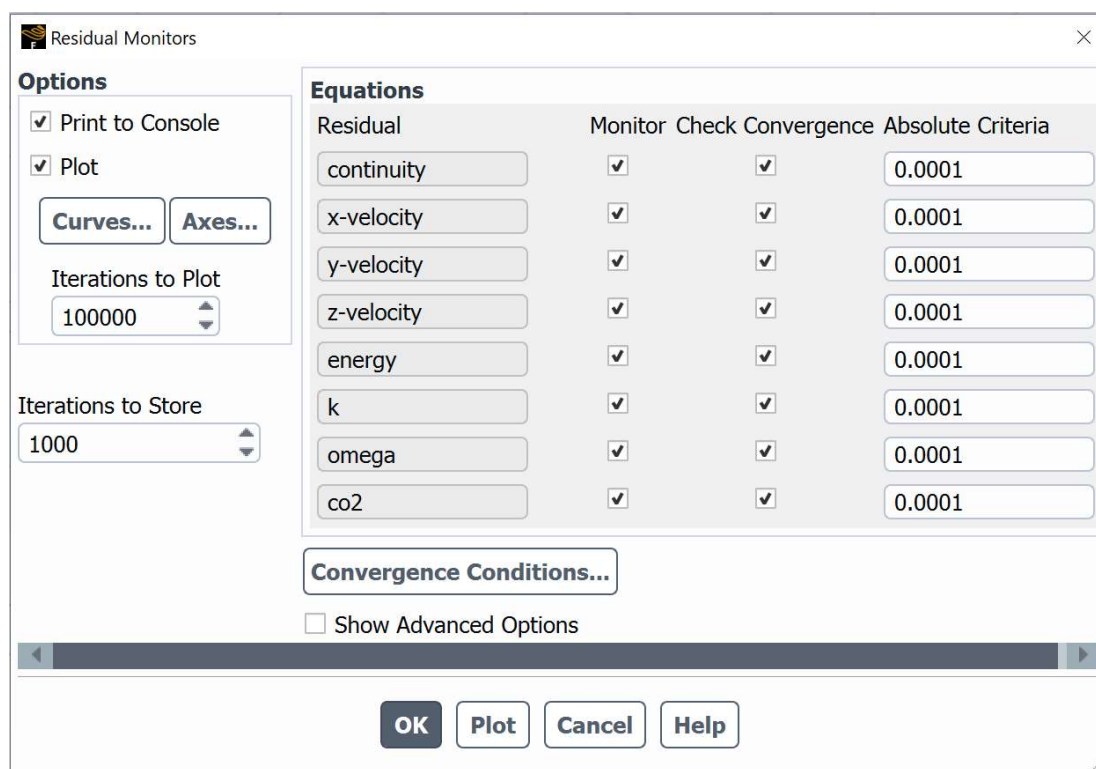


Figure 38 - ANSYS Fluent Residual Monitors.

3.2.7.2 Initialization:

In this 3D simulation standard initialization was selected with air being the primary fluid within the main domain to represent atmospheric conditions. The CO₂ inlet was set with a lower temperature of 277K, while the rest of the domain was initialized to the atmospheric temperature of 293K.

This ensures that the domain is at the atmospheric temperature and allows the simulation to capture the effect of the lower temperature CO₂ entering from the inlet. As presented in Figure 39, all initial values were set to zero, with the exception of temperature which was set to 293K and the computation was performed across all zones. The CO₂ inlet conditions were then patched into the inlet region.

Task Page

Solution Initialization

Initialization Methods

☐ Hybrid Initialization

☒ Standard Initialization

Compute from

Reference Frame

☒ Relative to Cell Zone

☐ Absolute

Initial Values

Y Velocity [m/s]

Z Velocity [m/s]

Turbulent Kinetic Energy [m²/s²]

Specific Dissipation Rate [s⁻¹]

co2

Temperature [K]

Figure 39 – Initialization settings in ANSYS Fluent.

As shown in Figure 40Figure 44, to represent the initial conditions more accurately, I patched the CO₂ inlet region with CO₂ at the Z velocity in accordance with the flowrate and the temperature of 277K. The mass fraction of CO₂ was patched as one to indicate the inlet contains CO₂.

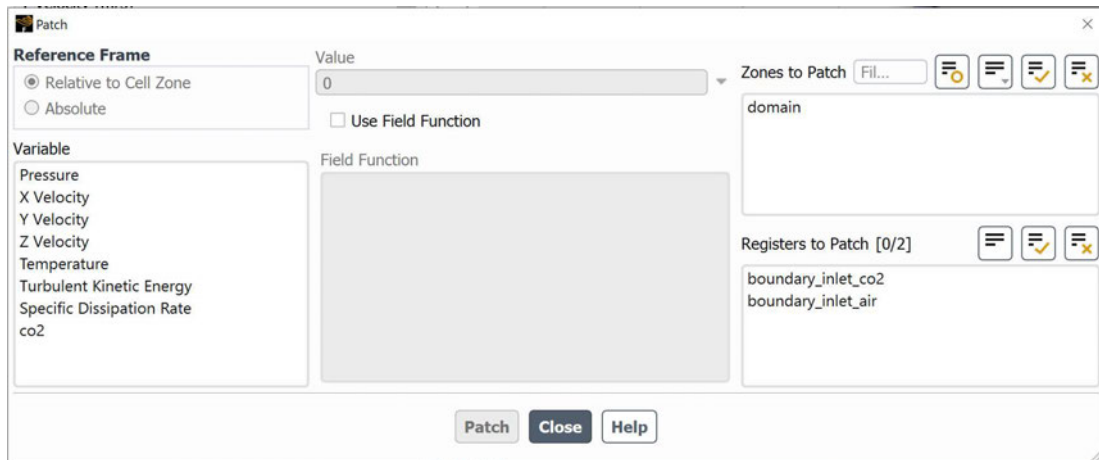


Figure 40 - ANSYS Fluent, patching the inlet conditions.

3.2.7.3 Run Calculation:

For the 3D simulation, the time advancement type selected is fixed, meaning the size of time step is constant throughout this simulation. As shown in Figure 41, time step size was set to 0.003 seconds, to ensure that the solver updates the flow field at stages for every small time advancement.

For this simulation, the total of 34,000 time steps were simulated. This number of time steps, combined with the size of time step, defines the total simulation time. Each step represents 0.003 seconds, the total simulation time equals 102 seconds of real-time flow. This duration is sufficient to observe the development and dissipation of the CO₂ jet as it disperses through the domain.

Initially, each time step had 20 iterations, which after the initial simulation time was reduced to 15. This allows the solver to converge iteratively within each time increment before advancing to the next step.

Task Page <

Run Calculation ?

Check Case... Preview Mesh Motion...

Time Advancement

Type: Fixed Method: User-Specified

Parameters

Number of Time Steps: 5000 Time Step Size [s]: 0.003

Max Iterations/Time Step: 20 Reporting Interval: 1

Profile Update Interval: 1

Options

☐ Extrapolate Variables

☐ Report Simulation Status

Solution Processing

Statistics

☐ Data Sampling for Time Statistics

Data File Quantities...

Solution Advancement

Calculate

Figure 41 – ANSYS Fluent, run calculation settings.

CHAPTER 4: RESULT AND DISCUSSION

4.1 TWO-DIMENSIONAL (2D) SIMULATION OF CO₂ JET USING PENG-ROBINSON EOS

4.1.1. Velocity Profile Along the Axis

Figure 42 illustrates the velocity magnitude alongside the axis of the CO₂ jet as it exits the high pressure reservoir and expands into the surrounding environment. At the nozzle exit, the velocity increases sharply, which shows the acceleration of CO₂ as it is forced through the nozzle. The velocity rapidly increases to approximately 539 m/s at around 35 millimetres from the nozzle, which is common for a supersonic jet exiting into the atmospheric condition. This sharp peak corresponds to the region just before the flow encounters the Mach disk.

Just after this peak, the velocity drops suddenly, which is a sign of the normal shock wave at the Mach disk. At this point, the flow decelerates from supersonic to subsonic speeds. The sharp decline in velocity, is a key property of the Mach disk and it comes with a significant reduction in velocity, down to about 18 m/s at the exact position of the Mach disk.

The velocity increases slightly on the downstream of Mach disk due to the expansion waves that occur after the shock, and this leads to a series of oscillations in the velocity profile. These fluctuations are characteristic of the downstream jet flow, where the flow undergoes multiple expansions and compressions as it adjusts to the ambient pressure. As the distance from the nozzle increases, the velocity reduces slowly, which is expected as the jet disperses and the flow energy dissipates into the surrounding environment.

Overall, this velocity profile shows the behaviour of the CO₂ jet as it exits the nozzle, interacts with the Mach disk, and continues to expand. Understanding this velocity

distribution is crucial for predicting the spread and impact of CO₂ leaks from high pressure pipelines, particularly in terms of how far the gas will travel and the potential areas affected by the leak. This information is essential for effective risk assessment and the development of safety measures to mitigate the impact of such leaks.

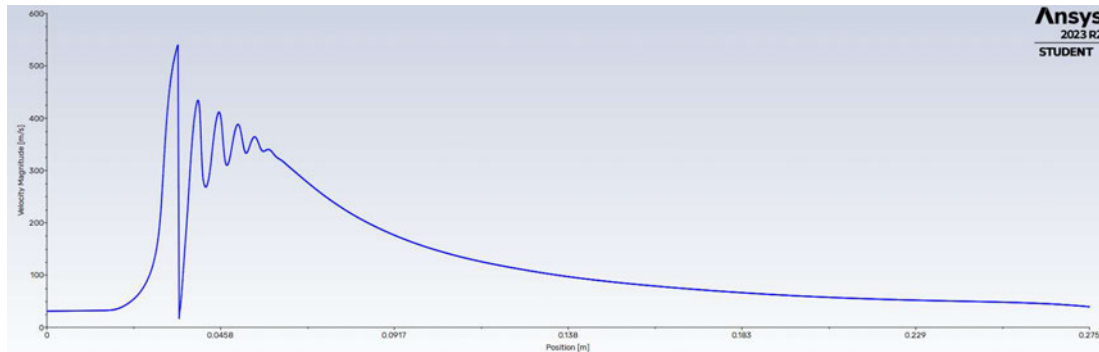


Figure 42 – Prediction of velocity along the axis of CO₂ jet.

4.1.2. Temperature Distribution Around Nozzle Outlet

The temperature distribution in high-speed jet flows, particularly around the nozzle outlet and Mach disk, is critical for understanding the thermal behaviour and energy exchange in the flow field. The formation of shock waves, including the Mach disk, impacts the temperature profile, and this results in variations that are important for accurate analysis of the simulated flow.

Figure 43Figure 44 illustrates the temperature contour plot of the CO₂ jet flow at the nozzle depicting the distribution of temperature throughout the flow field. The colour scale on the left represents the temperature in Kelvin (K). The flow emerges from the nozzle at a high temperature, indicated by the red and orange regions near the nozzle exit. As the CO₂ expands into the surrounding environment, the temperature decreases significantly, as shown by the transition from red to green and blue colours.

The Mach disk is visible in the contour plot where the temperature drops sharply. The minimum temperature is the dark blue area in the centre of the flow, reaching as low as 114.6K. This drop in temperature occurs due to the sudden deceleration and compression of the flow as it encounters the Mach disk, which is a characteristic shock wave formed in supersonic flow conditions. Downstream of the Mach disk, the flow undergoes a series of expansions and compressions, resulting in alternating temperature bands that fades away as the flow progresses further from the nozzle.

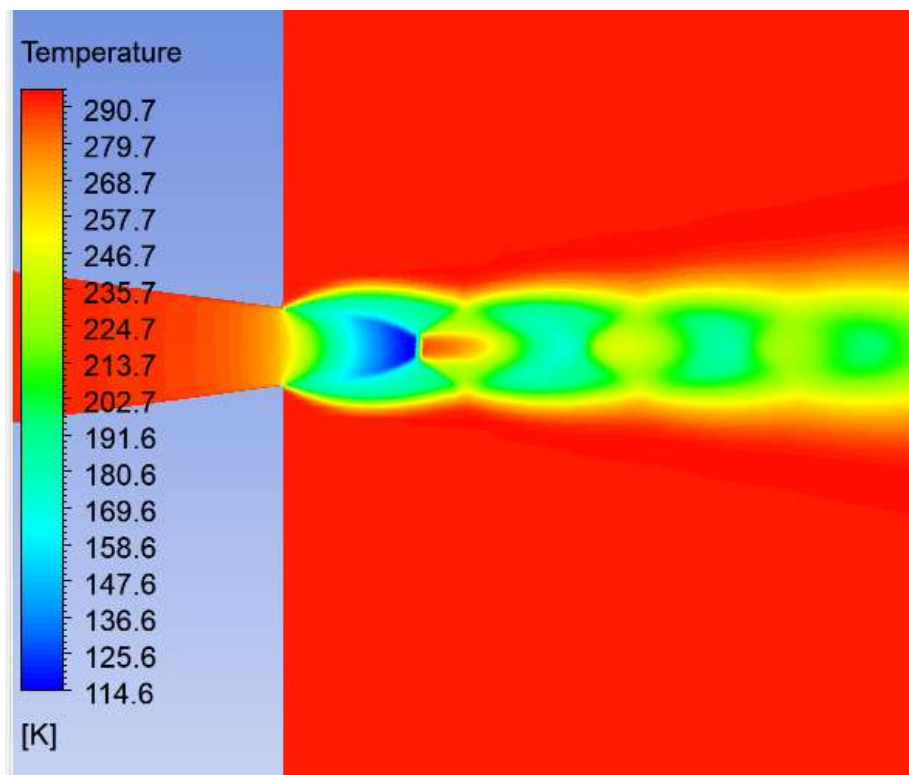


Figure 43 - Temperature contour plot of CO₂ jet flow.

4.1.3. Pressure Distribution Around Nozzle Outlet

The pressure distribution in high-speed jet flows is an important aspect of understanding the behaviour of supersonic jets, particularly in the vicinity of the nozzle outlet and the Mach disk. The pressure variations within the flow field influence the formation of shock waves,

and the overall stability of the jet. In this study, the focus was on capturing the complex details of pressure changes as the CO₂ jet expands and dissipates in the ambient environment.

Figure 44 presents the pressure contour plot of the CO₂ jet flow, showing the distribution of pressure, particularly around the nozzle exit and the downstream region where the Mach disk forms. On the left side of the figure there is a colour scale showing the pressure values in Pascals (Pa), ranging from approximately -92,080 Pa to 483,900 Pa.

As shown in the plot, the flow exits the nozzle at a high pressure, indicated by the red and orange regions near the nozzle exit, which corresponds to a pressure of around 231,908.6 Pa. This high pressure zone is a result of the compressed CO₂ within the nozzle being released into the domain environment which is at atmospheric pressure of 101,325 Pa. The pressure decreases sharply as the flow accelerates and expands into the surrounding atmosphere. This leads to the formation of the Mach disk, which is indicated by a significant drop in pressure.

The Mach disk is visible in the contour as a region where the pressure decreases abruptly and it transitions from orange/red to blue, which corresponds to a lower pressure region. It can be observed that downstream of the Mach disk, the pressure continues to oscillate, and it forms a series of expansion and compression waves that gradually fade away in intensity as the flow moves further from the nozzle.

The pressure contour plot visualizes the shock structures and the resulting pressure fluctuations within the flow, providing insight into the complex dynamics of high-speed CO₂ jets. The interaction of the jet with the environment, as depicted by pressure distribution, is essential for understanding the behaviour of the flow in practical applications that involve supersonic jets and gas dispersion in open environments.

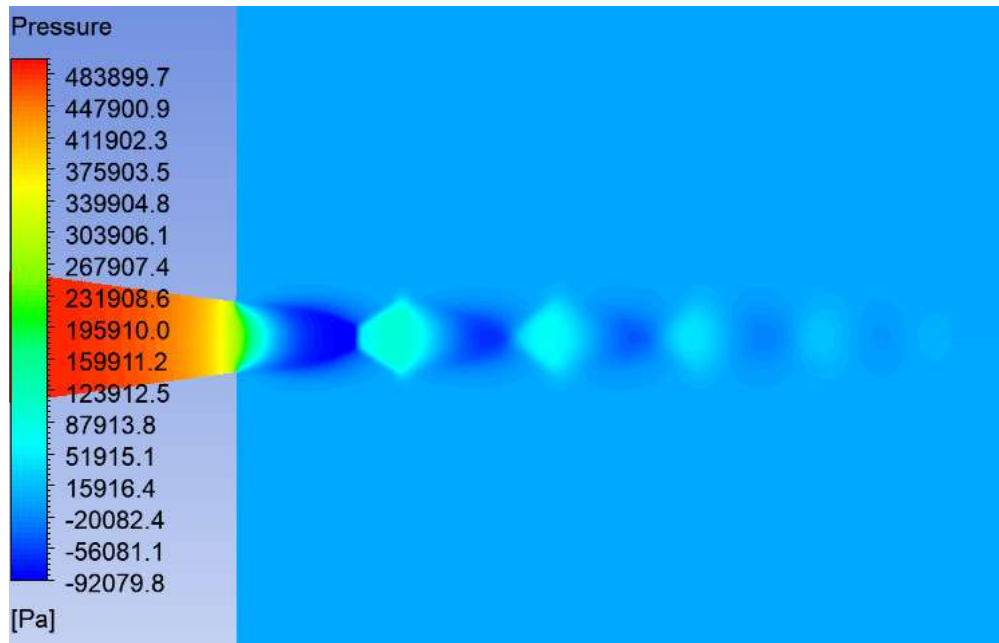


Figure 44 - Pressure contour plot of CO₂ jet

4.1.4. Velocity Distribution Around Nozzle Outlet and Mach Disk

The velocity distribution in a supersonic jet flow provides valuable insight into the flow dynamics, particularly at the nozzle outlet and Mach disk. The profile of velocity is influenced by the expansion and compression processes occurring within the flow, which assist in understanding the behavior of high-speed jets. In this study, the velocity distribution was analysed to capture the detailed velocity changes as the CO₂ jet expands and interacts with the ambient environment.

Figure 45 is the contour plot representation of the CO₂ jet velocity, highlighting the distribution of velocity along the flow field, near the outlet of the nozzle and downstream where the formation of the Mach disk is observed. On the left side of the figure there is a colour scale showing the velocity values in meters per second (m/s), ranging from 0 to 523.1 m/s.

As shown in the plot, the flow exits the nozzle at a high velocity, indicated by the red and orange regions near the nozzle exit, where the velocity reaches approximately 326.9 m/s. This high velocity is due to CO₂ expanding as it transits from a high pressure environment into the lower pressure environment. As the flow progresses downstream, the velocity continues to increase, reaching a peak in the areas just before the Mach disk, where the flow undergoes rapid acceleration.

The Mach disk is a critical feature in the flow and is identified in the contour as a region where the velocity decreases sharply, transitioning from the high-velocity red/orange regions to lower-velocity green and blue regions. This decrease in velocity is a result of the shockwave formed at the Mach disk, where the supersonic flow slows down and compresses abruptly. Beyond the Mach disk, the velocity continues to fluctuate, with alternating regions of acceleration and deceleration. This corresponds to the series of shock waves and expansion fans downstream.

This velocity contour plot shows the visualization of the flow dynamics in good details, and it shows how the velocity changes in reaction to the expansion and compression within the jet. Understanding these velocity variations is crucial for analyzing the performance of supersonic jets and the impact of such flows in practical applications, such as gas leaks in open environments.

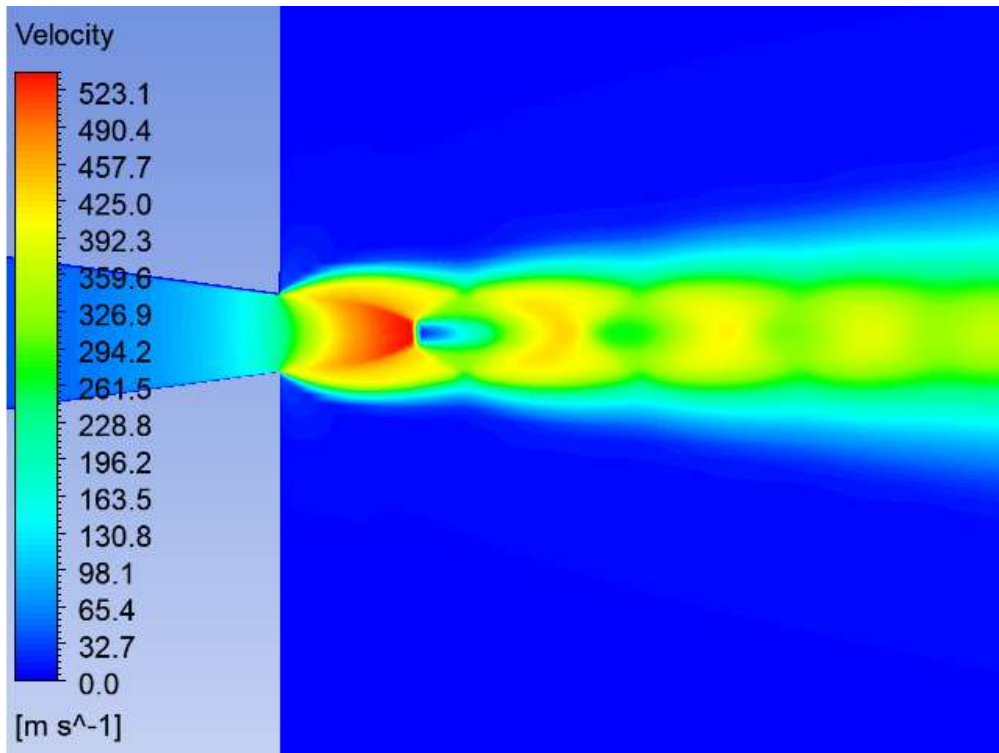


Figure 45 - Velocity contour plot of the CO₂ jet flow at outlet and downstream of nozzle.

4.1.5. Mach Number

Figure 46 illustrates the Mach number contour plot of the CO₂ jet flow. On the left side of the figure there is a colour scale showing the variation of the Mach number, between 0 and 3.3. As shown in the plot, the flow exits the nozzle with a Mach number just above 1.0, which is indicated by the transition from blue to green. It represents the flow as it just reaches and slightly exceeds the speed of sound. As the flow continues to expand and accelerate downstream, the Mach number increases, with the regions just before the Mach disk reaching values above Mach 2.0.

The Mach disk is a key feature of supersonic jets and is visible in the contour as a region where the Mach number drops abruptly, transitioning from high Mach numbers (red) to values around Mach 1.0 (blue). This drop occurs due to the formation of Mach disk, and

change of flow type as supersonic flow is suddenly decelerated to subsonic speeds. Mach number continues to fluctuate, downstream of the Mach disk, with area of acceleration and deceleration.

This Mach number contour plot offers a valuable visualization of the supersonic flow dynamics, and it highlights the variations in flow speed relative to the speed of sound as the CO₂ jet interacts with its surroundings. The ability to capture these Mach number variations is critical for understanding the behaviour of supersonic jets, particularly in applications where precise control of shock wave structures and flow speeds is required.

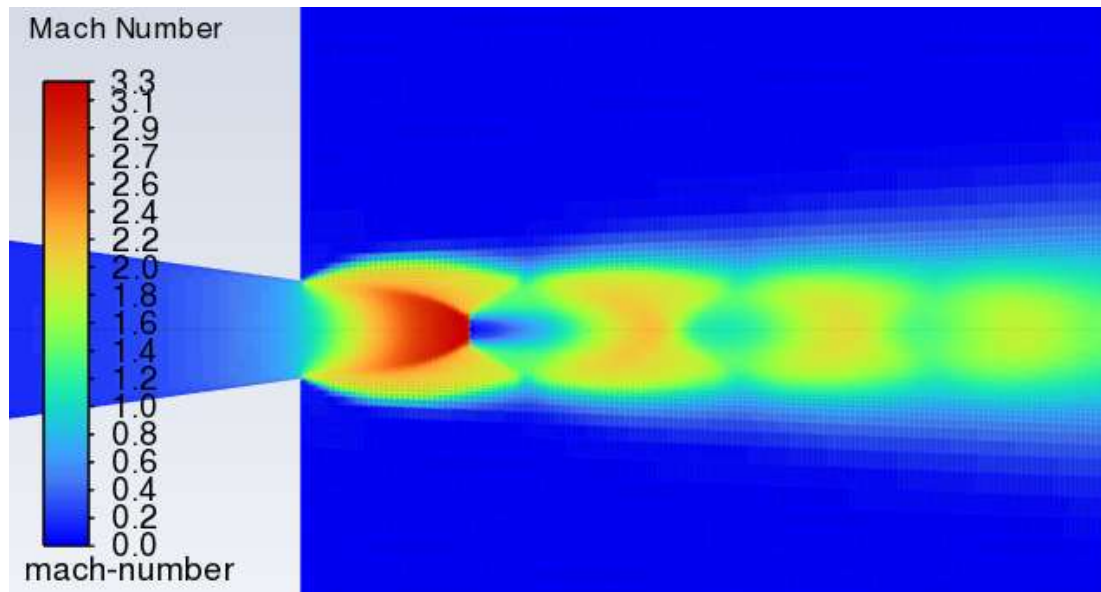


Figure 46 - Mach number contour plot.

Figure 47 illustrates the shadowgraph image (Liu et al. 2014) alongside the flow structure of the CO₂ jet which was simulated utilising the k-epsilon ($k-\epsilon$) model. Generally, the experimental shadowgraph and the flow structure of the simulated model are in good agreement. It is observed that the key features of the flow structure are accurately simulated and present in both the shadowgraph image and contour plot. Notably, the normal shock wave, identified as the Mach disk, is clearly depicted in both images, and this demonstrates

the simulation's ability to replicate the complex flow dynamics observed in the experimental setup. The alignment of these features validates the effectiveness of the simulation model in predicting the behaviour of high-speed jets and their associated shock structures.

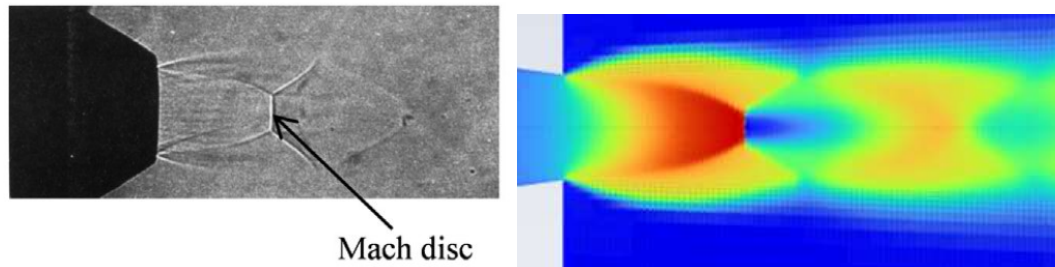


Figure 47- shadowgraph image alongside the simulated velocity.

4.1.6. Distribution of CO₂ in the domain

Figure 48 illustrates the mass fraction distribution of the CO₂ as it exits the nozzle and disperses into the surrounding environment. This plot provides insights into how the CO₂ concentration varies throughout the flow field, which is essential for understanding the behaviour of the CO₂ jet as it releases from a high pressure pipeline into the atmosphere.

On the left side of the figure there is a colour scale showing the CO₂ mass fraction, varying between 0.0 (blue) and 1.0 (red). A mass fraction of 1.0 indicates pure CO₂, while lower values represent a mixture of CO₂ with the surrounding air.

At the nozzle exit, the CO₂ mass fraction is highest, shown in red, indicating that the jet is composed almost entirely of CO₂. As the jet travels away from the outlet of nozzle, the mass fraction decreases, transitioning from red to green, yellow, and eventually blue as the CO₂ mixes with the surrounding air. This mixing process leads to a quick dilution of CO₂, which is shown by the gradual fading of colour intensity from the nozzle exit to the far field.

The plot also highlights the core of the jet, where the CO₂ concentration remains relatively high before it starts to disperse. This region is characterized by a higher mass fraction, indicated by the green to yellow transition, which extends from the nozzle before significant mixing with the ambient air occurs.

Understanding the distribution of CO₂ mass fraction is crucial for assessing the potential hazards associated with a CO₂ leak. Areas with higher CO₂ concentrations, closer to the nozzle, represent regions where the risk of asphyxiation or other health hazards may be significant. As the CO₂ disperses, the concentration decreases, reducing the immediate risk but potentially affecting a larger area.

This plot is also essential for validating the effectiveness of dispersion models used in risk assessments. By assessing the mixing behaviour of CO₂ with air, the simulation assists with predicting the concentration levels at various distances from the leak. This allows for the design of appropriate safety measures and emergency response strategies.

In summary, the CO₂ mass fraction plot provides a good visualization of how the gas disperses into the environment, and it highlights the areas of highest concentration and showing how quickly the gas mixes with air.

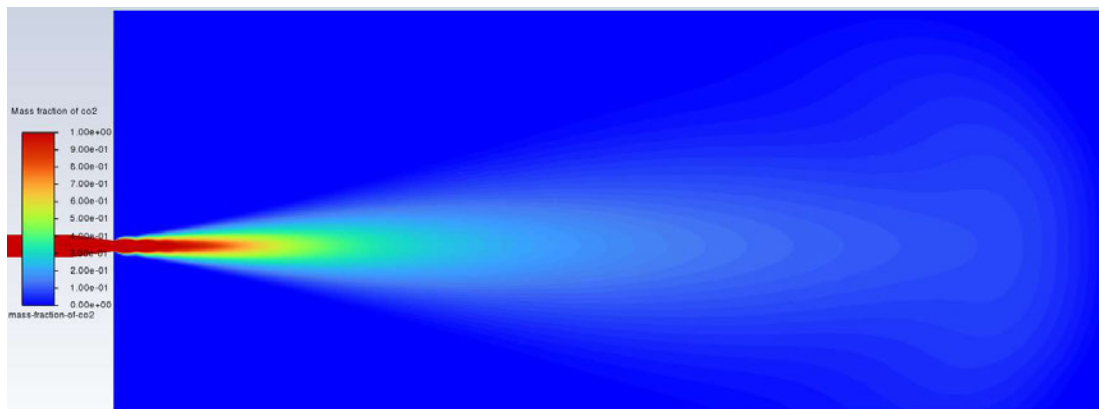


Figure 48 – CO₂ mass fraction distribution plot

4.2 CO₂ DISPERSION ANALYSIS IN A COMPLEX ENVIRONMENT

4.2.1 CO₂ Concentration Over Time at 10 m³/h

Figure 49 illustrates the plot of the CO₂ concentration at a sensor located at coordinates (4, 1.5, 0) for the 10 m³/h flowrate. This graph validates the 3D simulation results against the scaled CO₂ release experiment completed by Xing et al. (2013), where CO₂ behaviour was studied following a release through a 20mm diameter hole located one meter away from the front vertically into a box shaped domain at a few different flowrates over a period of 100 seconds.

In the first 10 seconds, both the experimental and simulation data show a rapid increase in CO₂ concentration. The simulation results show a sharper rise, and it picks at around 2.5% CO₂, while the experiment reaches a peak concentration of approximately 1.1% CO₂, showing an overestimation in the initial rise.

After the initial peak, the experimental data stabilizes at around 1% CO₂ with small fluctuations, whereas the simulation data presents a more dynamic behaviour, and it fluctuates around 0.8% – 1.2% for the remainder of the simulation.

The overall trend in both datasets is aligned, as both show a rapid rise followed by stabilization. This comparison validates the simulation to a good extent, though further refinement might be necessary to improve accuracy, particularly during the initial phase and in capturing fluctuations.

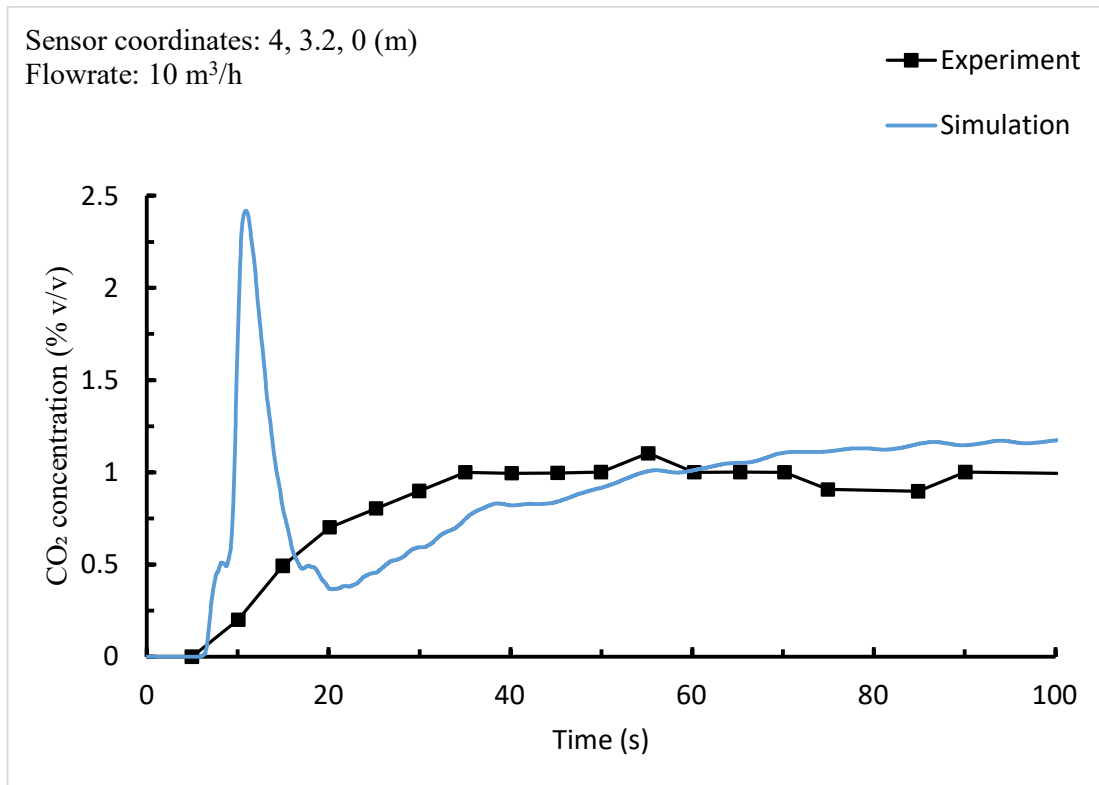


Figure 49 – CO₂ concentration over time at the given coordinates and 12m³/h flowrate.

The contour plot in Figure 50 presents the combined iso-surface and contour plot of CO₂ mass fraction dispersion at a flow rate of 10 m³/h captured at 102s. The plot highlights the concentration distribution of CO₂ after being released from the inlet. The contour lines indicate different levels of concentration, with the highest concentration near the release point, which gradually decreases as the gas disperses downstream.

The 1% CO₂ concentration region is visible as the contour follows the dispersion of CO₂ through the domain. This region is concentrated closer to the release point but spreads horizontally and vertically as it interacts with the ambient air. The pattern of CO₂ distribution suggests that the denser gas settles near the ground, and it gradually disperses over time. The highest concentration levels remain concentrated closer to the release point, with a significant amount of CO₂ settling near the ground.

In addition, the consequence distance, identified as 8 meters from the release point, marks the extent within which CO₂ concentrations may pose potential hazards. This consequence distance provides a valuable insight for assessing safety boundaries around potential CO₂ release sites.

This visualization is important for understanding how CO₂ behaves when released into the atmosphere under specific conditions. This information allows for more accurate predictions of potential hazardous zones around pipelines or gas facilities and is valuable in evaluating the safety and environmental impact of accidental or managed CO₂ releases.

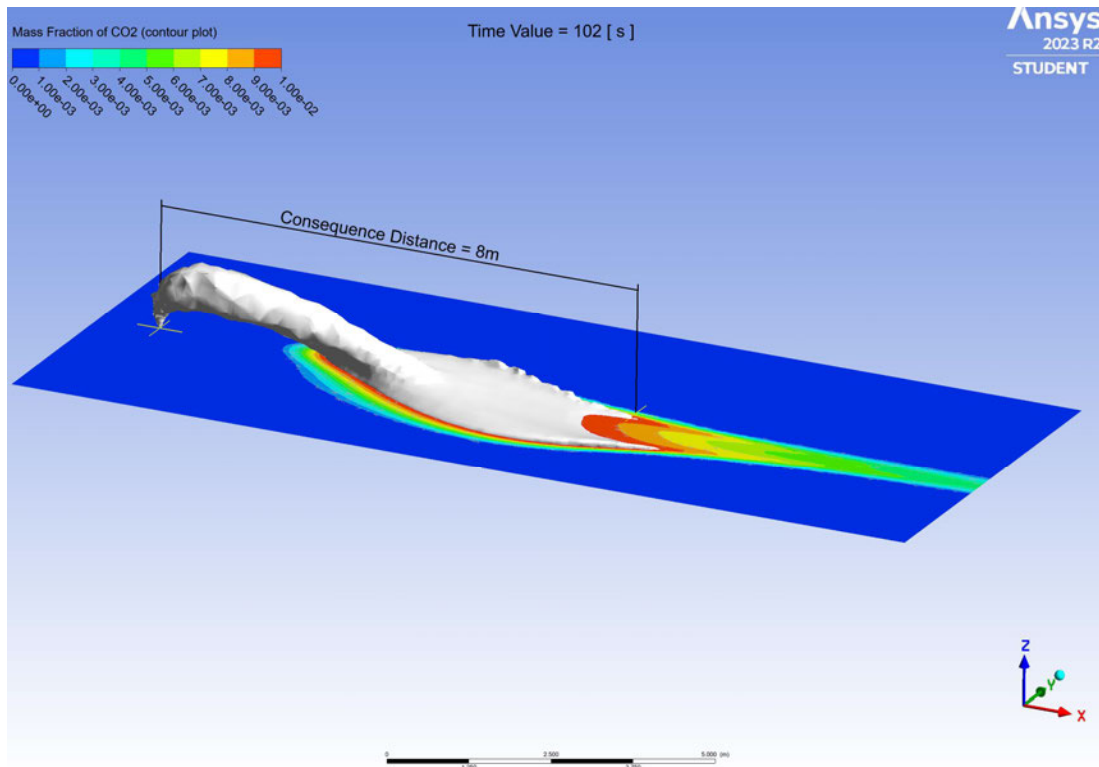


Figure 50 - Contour plot showing the dispersion of CO₂ mass fraction at 10 m³/h flowrate, with emphasis on 1% concentration level.

4.2.2 CO₂ Concentration Over Time at 12 m³/h

Figure 51 presents the plot of CO₂ concentration at a sensor located at coordinates (4, 1.5, 0) for the 12 m³/h flowrate. This graph compares the 3D simulation results with the scaled CO₂ release experiment conducted by Xing et al. (2013).

In the first 10 seconds, the simulation results display a sharp increase in CO₂ concentration, reaching a peak of around 1.8% CO₂, while the experimental data shows a more gradual rise, peaking at approximately 1.3% CO₂. Similar to the 10 m³/h case, the simulation overestimates the initial rise in concentration in comparison with the experimental data.

After the initial peak, the experimental data stabilizes around 1.1% CO₂, with minor fluctuations. On the other hand, the simulation results fluctuate between 0.5% and 0.8% CO₂ for the remainder of the simulation. Despite these differences, the overall trend is consistent. Both datasets show a rapid increase followed by a period of stabilization. While the comparison validates the general behavior captured in the simulation, further refinement could enhance the accuracy during the early stages and in capturing post-peak fluctuations.

In conclusion, the simulation data is in good agreement with the experimental results. Both datasets show a similar trend in CO₂ concentration over time. While there are minor discrepancies, particularly during the initial rise and post-peak fluctuations, the overall alignment between the experimental and the simulated data confirms the validity of the CFD model to predict CO₂ dispersion at the given flow rate. This consistency indicates that the CFD simulation provides a reliable representation of the CO₂ release behaviour observed in the experiment.

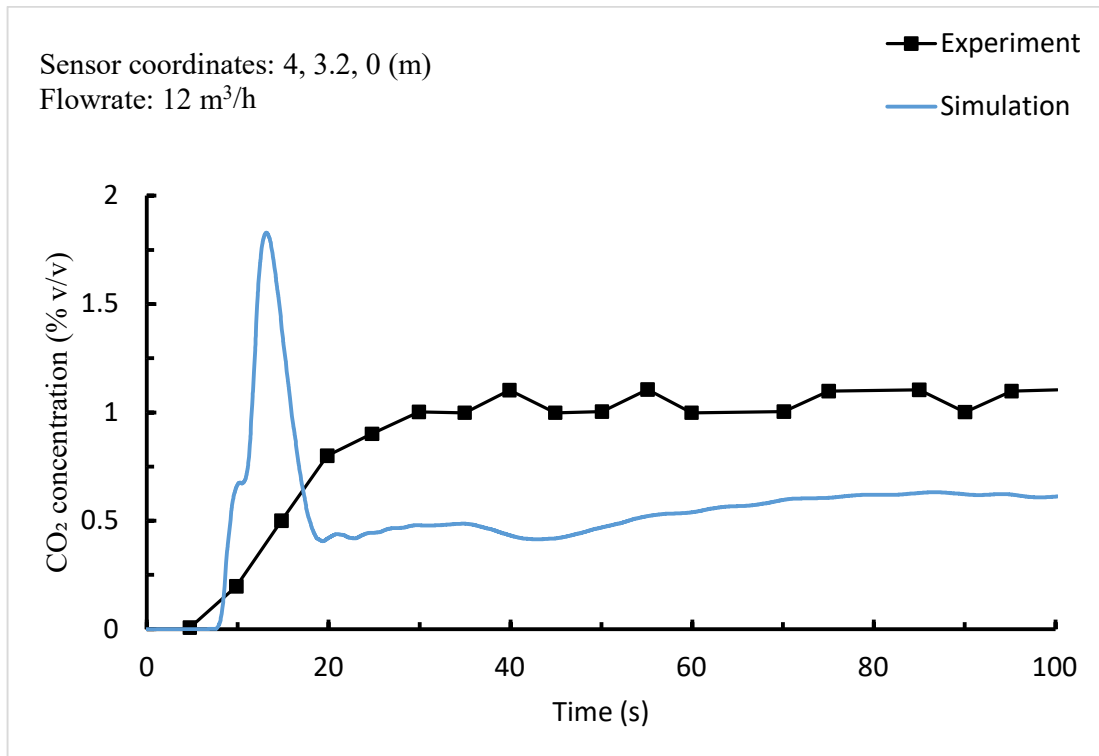


Figure 51 - CO₂ concentration over time at the given coordinates and 12m³/h flowrate.

Figure 52 presents the combined iso-surface and contour plot of CO₂ mass fraction dispersion at a flow rate of 12 m³/h captured at 102s. The contour illustrates the concentration levels of CO₂ as it disperses in the downstream direction from the release point due to wind, with an emphasis on the 1% concentration level. The highest concentrations are observed near the release point, gradually diminishing as the CO₂ disperses further downwind.

The 1% concentration level is represented by the red-yellow contour near the lower region of the flow domain. The plot shows as CO₂ moves further away from the source the concentration reduces. The dispersion pattern reflects the influence of wind and ground surface interaction, with the CO₂ settling on the ground as it travels downwind, demonstrating the expected behavior for heavier than air gases like CO₂.

Furthermore, the consequence distance, determined as 10.5 meters from the release point, marks the distance within which CO₂ concentrations could reach levels of concern. This consequence distance is critical for assessing the potential impact zone around CO₂ release sites and for informing safety measures.

This contour plot provides a visual representation of the concentration field that complements the sensor data. The plot indicates a consistent dispersion trend in line with experimental observations.

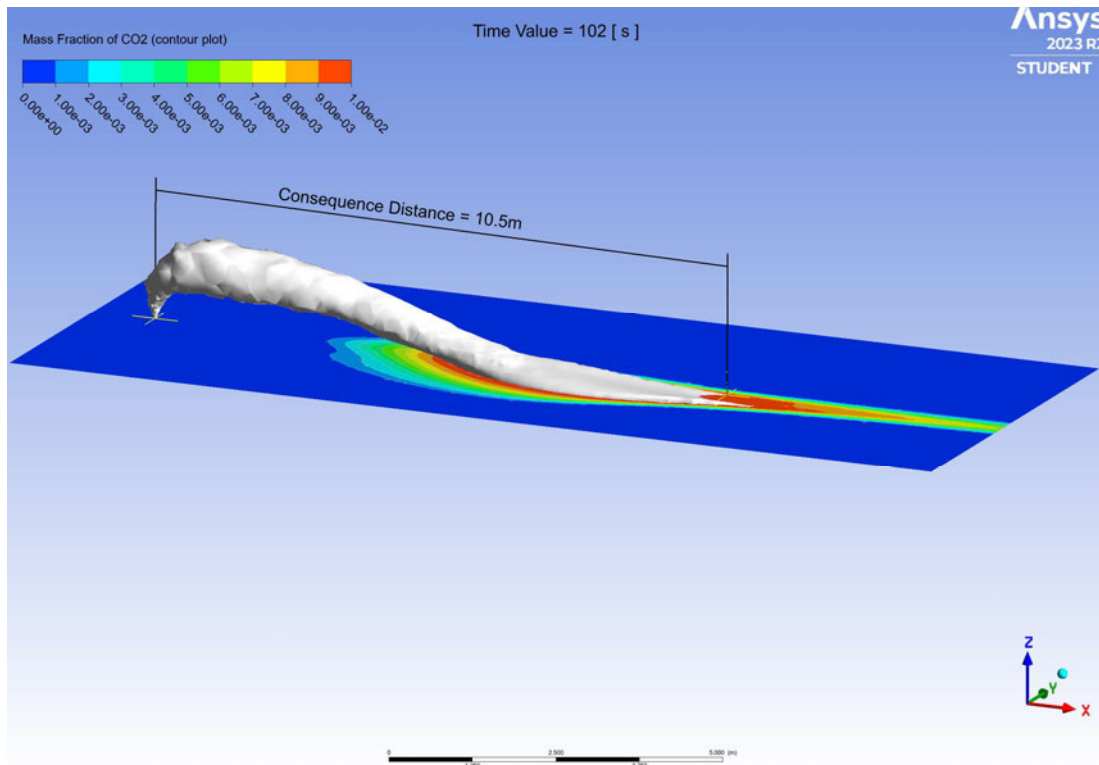


Figure 52 - Contour plot showing the dispersion of CO₂ mass fraction at 12 m³/h flowrate, with emphasis on 1% concentration level.

Figure 53 shows the iso-surface visualisation of the CO₂ envelope from the 3D simulation of CO₂ dispersion. The figure reflects the general behaviour of CO₂ for both flow rates analysed, and it demonstrates key features of the gas dispersion.

At the release point, CO₂ is released into the domain and is then dispersed into the surrounding environment. The CO₂ envelope shows the outline of the spread of the gas cloud. The highest concentrations are near the source and it gradually decreases as it moves downwind. The direction of the wind, indicated by the arrow, plays a critical role in shaping the dispersion pattern. As the wind flows from left to right, it drives the CO₂ cloud downwind, which leads to an elongated plume that disperses further as it moves away from the source.

I observed from this simulation that a wide CO₂ envelope is formed as it disperses. The cloud expands and thins out as it moves further from the release point, and the highest concentration is near the source. The maximum extent of the CO₂ cloud is defined as consequence distance and is determined based on critical concentration levels, such as the 1% level previously discussed. This distance is important for evaluating the potential risk zone surrounding CO₂ pipelines or facilities, particularly in case of leaks or ruptures.

Additionally, the image shows the role of wind in driving the dispersion of CO₂. The wind pushes the gas cloud downwind, and it forms the characteristic elongated shape of the gas plume. The interaction between the wind and the ground creates an accumulation of CO₂ near the surface, as shown in the lower part of the CO₂ envelope. This is typical behaviour for heavier than air gases like CO₂, which tend to stay close to the ground and pose a hazard in those areas.

The consequence distance and CO₂ envelope shape are important factors to consider when defining hazardous zones around pipelines or facilities handling CO₂.

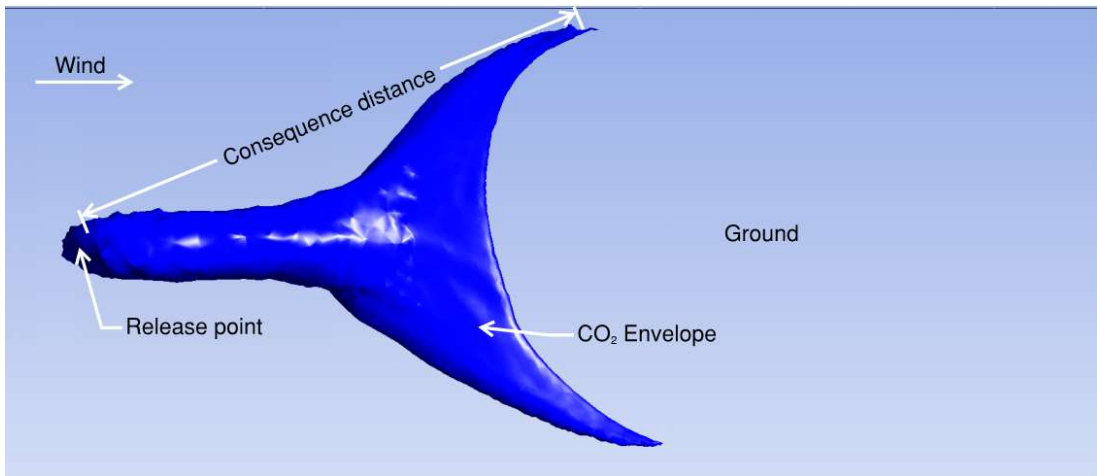


Figure 53 - Iso-surface visualization of CO₂ showing the release point, CO₂ envelope, consequence distance, and wind direction.

CHAPTER 5: CONCLUSIONS AND FUTURE WORK

5.1 SIMULATION OF CO₂ JET USING PENG-ROBINSON EOS

The detailed analysis of temperature, pressure, velocity, and Mach number distributions provided by the contour plots is critical in understanding the behavior of CO₂ release from a high pressure reservoir. These plots offer a detailed view of the flow dynamics that occur when CO₂ is released into the atmosphere, especially under conditions where the flow transitions from supersonic to subsonic speeds due to shock waves, such as those represented by Mach disks.

The temperature distribution plot shows the thermal variations present in the CO₂ jet as it exits the nozzle. Understanding these temperature variations is important because they directly affect the dispersion behavior of CO₂. Cold CO₂ jets can lead to localized areas of very low temperature, which might cause cryogenic effects such as freezing of surrounding structures or ground surfaces. In risk assessments, this information is vital for determining safe distances from the leak point to avoid potential hazards like frostbite or structural damage due to extreme cold.

Furthermore, the pressure distribution plot shows how the pressure changes as CO₂ expands from a high pressure state within the pipeline to the ambient pressure of the surrounding environment. This plot is essential for assessing the potential impact of a CO₂ leak, particularly in terms of overpressure effects. High pressure jets can cause significant damage to nearby structures and pose risks to human safety. By analyzing pressure distribution, engineers can determine the potential blast radius and establish exclusion zones or protective measures to mitigate these risks.

The velocity distribution plot provides insight into the speed at which CO₂ is ejected from the pipeline and how it changes as the flow moves downstream. High-velocity jets can transport CO₂ over large distances quickly, increasing the area affected by the leak. This information is crucial for emergency response planning, as it helps predict how quickly CO₂ can spread and what areas might be impacted. It also informs the design of mitigation plans, such as the placement of barriers or the use of dispersion models to protect sensitive locations.

The Mach number distribution plot highlights the regions where the flow is supersonic and where it decelerates to subsonic speeds, particularly at the Mach disk. It is important to understand the formation and location of shock waves to predict the behavior of the CO₂ plume. Supersonic jets can carry CO₂ further before it disperses, and this potentially affects a larger area. The presence of shock waves can also lead to complex flow patterns that may cause unpredictable dispersion of the gas. By analyzing the Mach number distribution, risk assessors can better predict the spread of CO₂ and create more accurate emergency response protocols.

Together, these plots provide a detailed picture of the physical phenomena associated with a CO₂ leak from a high pressure pipeline. They allow engineers and safety professionals to understanding how CO₂ behaves as it exits the pipeline, risk assessors can predict where the gas will travel, and which areas are at risk of exposure. Also, the data on temperature, pressure, and velocity help determine safe distances from the leak point, where the risk of high concentration, harm from cold exposure, overpressure, or high-velocity impacts is minimized.

The ability to model and predict the outcomes of a CO₂ leak help with becoming compliance with safety regulations and standards and ensuring that pipelines are operated within safe limits and that adequate precautions are in place.

In summary, the detailed analysis provided by this simulation is a critical part of risk assessments for CO₂ pipelines. They provide a valuable insight and raises awareness of the potential hazards followed by an accidental CO₂ leak and provide the required data to develop effective safety and mitigation strategies.

5.2 CO₂ DISPERSION ANALYSIS IN A COMPLEX ENVIRONMENT

This research aimed to model and analyse the dispersion of carbon dioxide (CO₂) due to a pipeline leak. The focus of the research was on understanding the thermodynamic behaviour and safety implications of pipeline leaks. By using Computational Fluid Dynamics (CFD) simulations, this study captured critical aspects of CO₂ behaviour in 3D models. The aim was to provide insights that are critical for risk assessment and safety planning around carbon capture, utilization, and storage (CCUS) infrastructures. The 3D simulations demonstrated the dispersion patterns and concentration profiles of CO₂. There was a good agreement between the simulation results and experimental results from Xing et al. (2013). This simulation demonstrates the power and accuracy of CFD tools in predicting CO₂ dispersion.

In particular, this analysis highlighted the impact of environmental conditions like wind direction, and ground interactions on CO₂ spread. Contour plots and iso-surface visualizations demonstrated that dispersion distance and concentration levels near the ground are significantly influenced by these conditions, which are crucial in determining areas where CO₂ accumulation can pose serious health risks to humans.

The analysis showed how high CO₂ concentrations could potentially accumulate close to the ground due to the higher density of the gas compared to air, and this highlights the need for safety measures and clear demarcation of hazardous zones around CO₂ pipelines.

The boundary conditions applied to the 3D simulations, provided a realistic representation of CO₂ spread in an open environment, and this allowed the model to be applicable to real-world scenarios.

Furthermore, the use of user-defined function (UDF) for wind velocity profiles allowed for a more accurate simulation of atmospheric conditions. The good alignment of the simulation results with experimental data validates the accuracy of the model. This indicates CFD's potential as a reliable tool for future safety assessments and decision-making in CO₂ transportation and storage.

Overall, the study proves the feasibility of using CFD modelling to improve the safety and efficiency of CCUS projects by providing detailed predictions of CO₂ dispersion under accidental release scenarios. By simulating dispersion patterns, this model can assist in defining safe boundaries around CO₂ pipelines and optimise pipeline placement, and refine emergency response strategies. This contributes to the mitigation of risks associated with CO₂ handling and storage.

To extend the findings of this study and improve the accuracy of the model and applicability, several opportunities for future research are recommended:

- Future work could include a comparison of additional turbulence models, such as RNG k- ϵ , and standard k- ϵ , to find the most suitable model for capturing CO₂ jet dispersion under various atmospheric and release conditions. This comparison would help understand how turbulence affects CO₂ spread and could improve the accuracy of the model.
- Extending the model to include factors such as temperature fluctuations, humidity levels, and more complex terrain features (e.g., hills, vegetation, buildings) will improve the practicality and applicability of the model. These modifications would allow for a more complete assessment of how changing atmospheric conditions influence CO₂ behaviour.

- In the current study, CO₂ was assumed to remain in the gaseous state. However, incorporating phase changes (solid, liquid, and supercritical CO₂) into the model could provide a more accurate representation of CO₂ under different pressure and temperature conditions, especially during rapid decompression events such as pipeline ruptures. Modelling phase changes could discover additional safety risks, such as dry ice formation near the release point.
- Expanding the validation process by comparing simulation results with experimental data across a wider range of CO₂ concentrations, flow rates, and atmospheric conditions would improve the adaptability of the model. This wider validation will make the model more reliable under various circumstances.

In conclusion, this study highlights the importance of advanced CFD modelling in understanding and managing the risks associated with CO₂ transportation and storage, which is a critical element of the global fight against climate change. As the CCUS industry grows in Australia, accurate dispersion models will become more important for safeguarding public safety and environmental protection. Through constant development and validation, the findings and methodologies from such research can support creating good industry standards and best practices for CO₂ infrastructure.

REFERENCES

Abdulkadirova, KS, Peters, CJ, Sengers, JV & Anisimov, MA 2010, 'An isomorphic Peng–Robinson equation for phase-equilibria properties of hydrocarbon mixtures in the critical region', *The Journal of Supercritical Fluids*, vol. 55, no. 2, pp. 594-602.

Ahmad, M, Osch, MB-v, Buit, L, Florisson, O, Hulsbosch-Dam, C, Spruijt, M & Davolio, F 2013, 'Study of the thermohydraulics of CO₂ discharge from a high pressure reservoir', *International Journal of Greenhouse Gas Control*, vol. 19, pp. 63-73.

Ahmad, M, Lowesmith, B, De Koeijer, G, Nilsen, S, Tonda, H, Spinelli, C, Cooper, R, Clausen, S, Mendes, R & Florisson, O 2015, 'COSHER joint industry project: Large scale pipeline rupture tests to study CO₂ release and dispersion', *International Journal of Greenhouse Gas Control*, vol. 37, pp. 340-53.

ANSYS 2021, *Ansys Fluent Theory Guide*.

Solver Setup in Ansys Fluent — Lesson 2 2023, Created by ANSYS Learning, viewed 15/03/2023,

<https://www.google.com/search?q=ansys+fluent+solver+type&rlz=1C1ONGR_en-GBAU971AU971&oq=ansys+fluent+solver+type&gs_lcrp=EgZjaHJvbWUyCggAEEUYFhgeGDkyDQgBEAAyhgMYgAQYigUyDQgCEAAyhgMYgAQYigUyDQgDEAAyhgMYgAQYigUyDQgEEAAyhgMYgAQYigUyCggFEAAygaAQYogQyCggGEAAygaAQYogTSAQg0NzE4ajBqNKgCALACAQ&sourceid=chrome&ie=UTF-8#fpstate=ive&vld=cid:178bcb2f,vid:TCEcRLAUtXE,st:0>.

Bin, L, Xiong, L, Cheng, L, Ajit, RG, Guillaume, M & Anh Kiet, T 2017, 'Multi-phase decompression modeling of CO₂ pipelines: Original Research Article: Multi-phase decompression modeling of CO₂ pipelines', *Greenhouse Gases: Science and Technology*, vol. 7, pp. 665-79.

Blazek, J 2015a, 'Chapter 3 - Principles of Solution of the Governing Equations', in J Blazek (ed.), *Computational Fluid Dynamics: Principles and Applications (Third Edition)*, Butterworth-Heinemann, Oxford, pp. 29-72.

Blazek, J 2015b, 'Chapter 7 - Turbulence Modeling', in J Blazek (ed.), *Computational Fluid Dynamics: Principles and Applications (Third Edition)*, Butterworth-Heinemann, Oxford, pp. 213-52.

Botros, KK, Studzinski, W, Geerligs, J & Glover, A 2004, 'Determination of Decompression Wave Speed in Rich Gas Mixtures', *Canadian journal of chemical engineering*, vol. 82, no. 5, pp. 880-91.

Botros, KK, Geerligs, J, Zhou, J & Glover, A 2007, 'Measurements of flow parameters and decompression wave speed following rupture of rich gas pipelines, and comparison with

GASDECOM', *International Journal of Pressure Vessels and Piping*, vol. 84, no. 6, pp. 358-67.

Botros, KK, Geerligs, J, Rothwell, B & Robinson, T 2016, 'Measurements of Decompression Wave Speed in Pure Carbon Dioxide and Comparison With Predictions by Equation of State', *Journal of pressure vessel technology*, vol. 138, no. 3.

Böttcher, N, Taron, J, Kolditz, O, Park, C-H & Liedl, R 2012, 'Evaluation of thermal equations of state for CO₂ in numerical simulations', *Environmental earth sciences*, vol. 67, no. 2, pp. 481-95.

Cosham, A & Eiber, RJ 2008, 'Fracture propagation in CO₂ pipelines', *Journal of Pipeline Engineering*, vol. 7, no. 4.

Cosham, A, Jones, DG, Armstrong, K, Allason, D & Barnett, J 2012, 'The Decompression Behaviour of Carbon Dioxide in the Dense Phase', *Proceedings of the* pp. 447-64.

Dandekar, AY 2006, *Petroleum Reservoir Rock and Fluid Properties*, 1st edn, CRC Press, Boca Raton, viewed 4/09/2024, <.

Dilay, GW & Heidemann, RA 1986, 'Calculation of Joule-Thomson inversion curves from equations of state', *Industrial & Engineering Chemistry Fundamentals*, vol. 25, no. 1, pp. 152-8.

Elshahomi, A, Lu, C, Michal, G, Liu, X, Godbole, A & Venton, P 2015, 'Decompression wave speed in CO₂ mixtures: CFD modelling with the GERG-2008 equation of state', *Applied Energy*, vol. 140, pp. 20-32.

Flechas, T, Laboureur, DM & Glover, CJ 2020, 'A 2-D CFD model for the decompression of carbon dioxide pipelines using the Peng-Robinson and the Span-Wagner equation of state', *Process Safety and Environmental Protection*, vol. 140, pp. 299-313.

Guo, X, Xu, S, Chen, G, Yan, X & Cao, Q 2021, 'Fracture criterion and control plan on CO₂ pipelines: Theory analysis and full-bore rupture (FBR) experimental study', *Journal of Loss Prevention in the Process Industries*, vol. 69, p. 104394.

Hanna, SR & Chang, JC 2001, 'Use of the Kit Fox field data to analyze dense gas dispersion modeling issues', *Atmospheric Environment*, vol. 35, no. 13, pp. 2231-42.

Hanna, SR, Britter, R & Franzese, P 2003, 'A baseline urban dispersion model evaluated with Salt Lake City and Los Angeles tracer data', *Atmospheric Environment*, vol. 37, no. 36, pp. 5069-82.

Hekmatmehr, H, Esmaeili, A, Pourmahdi, M, Atashrouz, S, Abedi, A, Ali Abuswer, M, Nedeljkovic, D, Latifi, M, Farag, S & Mohaddespour, A 2024, 'Carbon capture technologies: A review on technology readiness level', *Fuel*, vol. 363, p. 130898.

Hill, TA, Fackrell, JE, Dubal, MR & Stiff, SM 2011, 'Understanding the consequences of CO₂ leakage downstream of the capture plant', *Energy Procedia*, vol. 4, pp. 2230-7.

Huffaker, RM 1970, 'Laser Doppler Detection Systems for Gas Velocity Measurement', *Applied Optics*, vol. 9, no. 5, pp. 1026-39.

Jie, H, Xu, B, Wen, J, Cooper, R & Barnett, J 2012, *Predicting the Decompression Characteristics of Carbon Dioxide Using Computational Fluid Dynamics*, vol. 3.

Koornneef, J, Spruijt, M, Molag, M, Ramírez, A, Turkenburg, W & Faaij, A 2010, 'Quantitative risk assessment of CO₂ transport by pipelines—A review of uncertainties and their impacts', *Journal of Hazardous Materials*, vol. 177, no. 1, pp. 12-27.

Kunz, O & Wagner, W 2012, 'The GERG-2008 Wide-Range Equation of State for Natural Gases and Other Mixtures: An Expansion of GERG-2004', *Journal of Chemical & Engineering Data*, vol. 57, no. 11, pp. 3032-91.

Li, C-Y, Marquez, JAD, Hu, P & Wang, Q 2023, 'CO₂ pipelines release and dispersion: A review', *Journal of Loss Prevention in the Process Industries*, vol. 85, p. 105177.

Li, H & Yan, J 2009, 'Evaluating cubic equations of state for calculation of vapor–liquid equilibrium of CO₂ and CO₂-mixtures for CO₂ capture and storage processes', *Applied Energy*, vol. 86, no. 6, pp. 826-36.

Liu, B, Liu, X, Lu, C, Godbole, A, Michal, G & Tieu, AK 2018, 'A CFD decompression model for CO₂ mixture and the influence of non-equilibrium phase transition', *Applied Energy*, vol. 227, pp. 516-24.

Liu, C, Zhou, R, Su, T & Jiang, J 2022, 'Gas diffusion model based on an improved Gaussian plume model for inverse calculations of the source strength', *Journal of Loss Prevention in the Process Industries*, vol. 75, p. 104677.

Liu, X, Godbole, A, Lu, C, Michal, G & Venton, P 2014, 'Source strength and dispersion of CO₂ releases from high-pressure pipelines: CFD model using real gas equation of state', *Applied Energy*, vol. 126, pp. 56-68.

Liu, X, Godbole, A, Lu, C, Michal, G & Linton, V 2019, 'Investigation of the consequence of high-pressure CO₂ pipeline failure through experimental and numerical studies', *Applied Energy*, vol. 250, pp. 32-47.

Luo, Z, Wu, P, Wen, H, Wang, Y, Liu, C, Du, X & Liu, L 2024, 'Effect of source strength on the simulation of jet dispersion and hazard distances during accidental release of liquid CO₂', *Process Safety and Environmental Protection*.

Martynov, S, Brown, S, Mahgerefteh, H & Sundara, V 2013, 'Modelling choked flow for CO₂ from the dense phase to below the triple point', *International Journal of Greenhouse Gas Control*, vol. 19, pp. 552-8.

Maxey, WA, Kiefner, JF & Eiber, RJ 1976, *Ductile fracture arrest in gas pipelines*, American Gas Association, Arlington, VA, United States.

Mazzoldi, A, Hill, T & Colls, JJ 2008, 'CFD and Gaussian atmospheric dispersion models: A comparison for leak from carbon dioxide transportation and storage facilities', *Atmospheric Environment*, vol. 42, no. 34, pp. 8046-54.

Onyebuchi, VE, Kolios, A, Hanak, DP, Biliyok, C & Manovic, V 2018, 'A systematic review of key challenges of CO₂ transport via pipelines', *Renewable and Sustainable Energy Reviews*, vol. 81, pp. 2563-83.

Rowland, D, Hughes, TJ & May, EF 2016, 'Extending the GERG-2008 equation of state: Improved departure function and interaction parameters for (methane+butane)', *The Journal of Chemical Thermodynamics*, vol. 97, pp. 206-13.

Shalom, E, Ajoy, G & Heinrich, H 2002, *Fundamentals Of Equations Of State*, World Scientific Publishing Company, Singapore, SINGAPORE.

Soepyan, FB, Habib, M, Zhang, Z, Nemetz, LR, Haque, ME, Esquino, AM, Rivero, JR, Bhattacharyya, D, Lipscomb, GG, Matuszewski, MS & Hornbostel, KM 2024, 'Optimization of a Natural Gas Power Plant with Membrane and Solid Sorbent Carbon Capture Systems', *Carbon Capture Science & Technology*, vol. 10, p. 100165.

Sun, L, Zhao, H, Kiselev, SB & McCabe, C 2005, 'Predicting Mixture Phase Equilibria and Critical Behavior Using the SAFT-VRX Approach', *The Journal of Physical Chemistry B*, vol. 109, no. 18, pp. 9047-58.

Tang, D, Li, J, Zeng, F, Li, Y & Yan, C 2023, 'Bayesian parameter estimation of SST model for shock wave-boundary layer interaction flows with different strengths', *Chinese Journal of Aeronautics*, vol. 36, no. 4, pp. 217-36.

Taylor, BN & Cohen, ER 1990, 'Recommended values of the fundamental physical constants: a status report', *Journal of research of the National Institute of Standards and Technology*, vol. 95, no. 5, pp. 497-523.

Teng, L, Li, Y, Zhao, Q, Wang, W, Hu, Q, Ye, X & Zhang, D 2016, 'Decompression characteristics of CO₂ pipelines following rupture', *Journal of Natural Gas Science and Engineering*, vol. 36, pp. 213-23.

Trasatti, S 2007, *P. Atkins J. De Paula Atkins' Physical Chemistry 8th ed. 2006 Oxford University Press Oxford, UK ISBN: 0198700725*, Elsevier Ltd, 0013-4686.

Vianello, C, Macchietto, S & Maschio, G 2012, 'Conceptual models for CO₂ release and risk assessment: a review', *Chemical Engineering*, vol. 26, no. 1, pp. 573-8.

Vitali, M, Leporini, M, Masi, O, Speranza, A, Corvaro, F & Marchetti, B 2023, 'Net zero Flow Assurance - Validation of various equations of state for the prediction of VLE and density of CO₂-rich mixtures for CCUS applications', *International Journal of Greenhouse Gas Control*, vol. 125, p. 103877.

Vree, B, Ahmad, M, Buit, L & Florisson, O 2015, 'Rapid depressurization of a CO₂ pipeline – an experimental study', *International Journal of Greenhouse Gas Control*, vol. 41, pp. 41-9.

Wang, J, Yan, L, Xiao, C, Zhang, Z, Liu, D, Yao, S & Lu, Z 2024, 'Experimental study of near-field characteristics of high-pressure CO₂ pipeline leakage', *International Journal of Greenhouse Gas Control*, vol. 137, p. 104205.

Woolley, RM, Fairweather, M, Wareing, CJ, Proust, C, Hebrard, J, Jamois, D, Narasimhamurthy, VD, Storvik, IE, Skjold, T, Falle, SAEG, Brown, S, Mahgerefteh, H, Martynov, S, Gant, SE, Tsangaris, DM, Economou, IG, Boulougouris, GC & Diamantonis, NI 2014, 'An integrated, multi-scale modelling approach for the simulation of multiphase dispersion from accidental CO₂ pipeline releases in realistic terrain', *International Journal of Greenhouse Gas Control*, vol. 27, pp. 221-38.

Woolley, RM, Fairweather, M, Wareing, C, Falle, S, Mahgerefteh, H, Martynov, S, Brown, S, Narasimhamurthy, V, Storvik, I, Sælen, L, Skjold, T, Economou, I, Tsangaris, D, Boulougouris, G, Diamantonis, N, Cusco, L, Wardman, M, Gant, S, Wilday, J & Jamois, D 2014, 'CO₂PipeHaz: Quantitative Hazard Assessment for Next Generation CO₂ Pipelines', *Energy Procedia*, vol. 63, pp. 2510-29.

Xing, J, Liu, Z, Huang, P, Feng, C, Zhou, Y, Zhang, D & Wang, F 2013, 'Experimental and numerical study of the dispersion of carbon dioxide plume', *Journal of Hazardous Materials*, vol. 256-257, pp. 40-8.